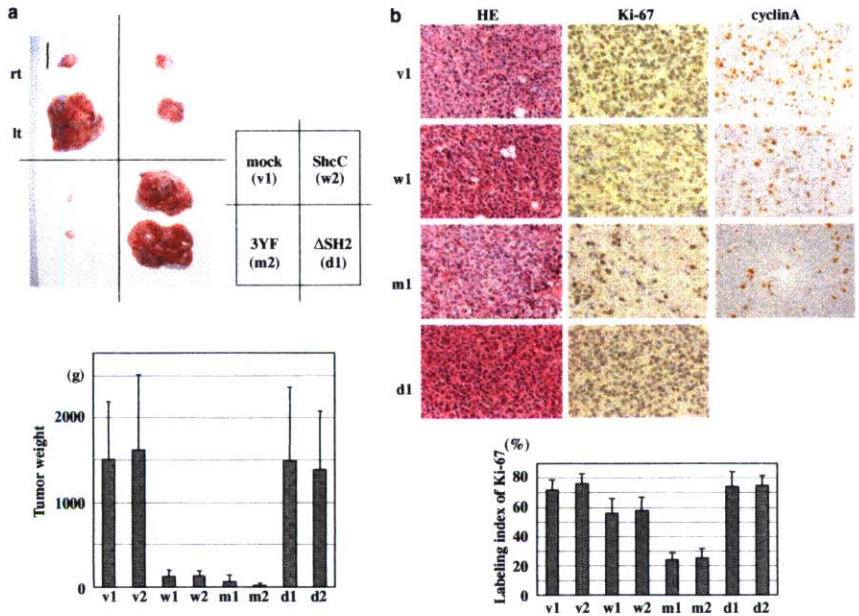

Figure 7 Nude mouse tumors derived from ShcC mutant cells. (**a**) Photographs of tumors from nude mice at three weeks after subcutaneous injection of ShcC mutant cells (upper panel). Tumorigenicity shown by the average weight (±s.d.) of the eight tumors derived from each clone (lower panel). Two independent clones are analysed for each ShcC mutant. Bar: 10 mm (**b**) Photographs of a cross-section of each tumor tissue using a microscope at a magnification of ×400. HE: tumor tissues stained with hematoxylin and eosin; Ki-67 and cyclin-A: tumor tissues immunostained against Ki-67 and cyclin-A, respectively (upper panels). The proliferating activity of each tumor was defined as the labeling index of Ki-67 by counting the positive stained cells per 1000 tumor cells. The data show the average scores ± s.d. of the positive cells in three different areas of each slide (lower panel). NB-39-nu clones are described as: v1 and v2 (control), w1 and w2 (expressing ShcC-wt), m1 and m2 (expressing 3YF-ShcC), d1 and d2 (expressing ΔSH2-ShcC)

of ShcC (Miyake *et al*., 2002) might indicate additive effects of hyperphosphorylation and downregulation of ShcC on phenotype of neuroblastoma. There is the possibility that an unknown mechanism causes downregulation of ShcC, which is hyperphosphorylated by receptor stimulation, and eventually induces malignant transition of tumors.

We have shown in this study that hyperphosphorylated ShcC in neuroblastoma cells plays an essential role in regulating cellular proliferation, survival, migration and transformation, and each domain of ShcC might differentially regulate these physiological functions. Controlling these domain-mediated signals could be a target in restricting the progression and metastasis of neuroblastoma cells.

Materials and methods

Plasmid constructions

The full-length human ShcC cDNA for transfection was donated by Dr T Nakamura (Nakamura *et al*., 1996b), and inserted into a mammalian expression vector pcDNA3.1. Tyrosine-to-phenylalanine mutations were introduced in the ShcC cDNAs by *in vitro* site-directed mutagenesis, which changed Y221/222 and Y304 to three phenylalanines (3YF-ShcC). The SH2 domain (amino acid 379–472)-deleted form of ShcC (ΔSH2-ShcC) was also generated. All parts amplified by PCR were verified by sequencing.

Cell culture, transfection

NB-39-nu cells were used in our previous report (Miyake *et al*., 2002). The stable expression of ShcC mutants, the full-length of ShcC (ShcC-wt), 3YF-ShcC and ΔSH2-ShcC in NB-39-nu cells were obtained by transfection using Fugene™ 6 transfection reagent (Roche Molecular Biochemicals) according to the manufacturer's instructions. Then, cell clones were obtained from individual G418-resistent colonies and subjected to Western blot screening using the T7 tag antibody (Novagen). These cells were cultured in an RPMI 1640 medium with 10% FCS (Sigma) at 37°C in 5% CO_2. A suspension culture of the cells was essentially performed according to a previously published procedure (Folkman and Moscona, 1978; Frisch and Francis, 1994; Wang and Sheibani, 2002). In this study, LOW-CELL-BINDING 90 mm-Petri dishes treated with 2-Methacryloxyethyl Phosphorylcholine (MPC) (Nalge Nunc International) were used instead of poly-HEMA-coated dishes.

The cells were grown to confluence in tissue culture dishes, and were then trypsinized and plated at a concentration of 1×10^6 cells/90 mm dish into MPC-treated Petri dishes and cultured for 0–48 h. The cells were then collected by pipetting, washed by PBS and extracted with PLC-lysis buffer (Rozakis-Adcock *et al*., 1993) for the Western analysis.

Preparation of specific antibodies, cell stimulation, immunoprecipitation and immunoblotting

The polyclonal antibodies against the CH1 domains of ShcC (amino acid 306–371) and against Cas protein (αCas) were prepared as described (Sakai *et al*., 1994, 2000). A phospho specific polyclonal antibody against Cas (αP-Cas460Y) was generated by immunizing rabbits with a synthetic peptide, CAEDV(pY)DVP, which is a representative of the repetitive tyrosine-containing motifs in the substrate domain of Cas, after being conjugated with thyroglobulin. Other antibodies were purchased as follows: anti-phosphotyrosine antibody (4G10) (Upstate Biotechnology, Inc), anti-p44/42 MAPK (ERK1/2) and anti-phospho-p44/42 MAPK (phospho-ERK1/2) antibodies (BioLabs), anti-Akt and anti-phospho-Akt (Ser473) antibodies (Cell Signaling), anti-c-Src antibody (Upstate Biotechnology, Inc.), anti-phospho Src family (Tyr416) antibody (Cell Signaling), anti-Fyn antibody and anti-pan-Src antibody (SRC2) (SantaCruz Biotechnology, Inc.). As secondary antibodies, horseradish peroxidase (HRP)-conjugated anti-rabbit and anti-mouse Ig (Amersham) were used. Cell-stimulation analysis with epidermal growth factor (EGF; Wako) was performed as described. The cells were starved for 24 h and treated for 5 min with EGF (100 ng/ml) (Miyake *et al*., 2002). As for stimulation with fibronectin, cultured cells were starved for 24 h then trypsinized without FCS and after the suspending condition for 30 min, seeded onto fibronectin (10 μg/ml)-coated dishes and harvested after 1 h using PLC lysis buffer. Control cells were harvested before the attachment on the fibronectin-coated surface. The immunoprecipitation and Western analysis were performed using the procedure described in the previous report (Miyake *et al*., 2002).

Evaluation of tendency to form cell aggregations on dish surface

Cells were seeded onto plastic dishes (1×10^6 cells per 100-mm diameter dish). After 5 days, distinctive colonies of cell aggregations proliferated independently of the attachment to the dish surface, and each of them consisted of more than 10 cells per dish. The data were obtained from three independent experiments.

Soft agar colony-formation assay

Anchorage-independent growth was determined by assaying colony formation in soft agar as described in the previous report (Honda *et al*., 1998). Briefly, 10^5 trypsinized cells were resuspended in DMEM containing 10% FCS and 0.4% Sea Plaque GTG agarose (Bioproduct) and poured onto bottom agar containing 10% FCS and 0.53% agarose in 6-cm culture dishes. The cells were then incubated at 37°C with 5% CO_2. After 14 days, colonies containing more than five cells were counted under the microscope.

Wound-healing assay

A wound-healing assay was performed according to the method used previously (Honda *et al*., 1999). Briefly, cells were grown to confluence in Matrigel-coated plastic culture dishes, and a wound was made using a sterile micropipette tip. Cell movement was assessed 24 and 48 h after wounding under the microscope at a magnification of ×100.

Cell migration and invasion assay

Cell invasion was analysed according to the procedure of the Boyden chamber cell migration assay with some modification (Honda *et al*., 1999), using a FALCON™ Cell Culture Insert, a chamber with a pore size of 8 μm (Becton Dickinson Labware) whose interior was filled with a plug of 10 μg Matrigel (IWAKI) per filter. A total of 1×10^5 cells in 200 μl of serum-free medium were plated in the Matrigel chamber, and a serum-free medium containing 50 μg/ml of fibronectin was placed in the 24-well plate as a lower chamber, then incubated for 12 h at 37°C in 5% CO_2. The number of cells migrated through the Matrigel to the underside of the filter was counted under the microscope. The same procedure was performed without Matrigel coating for the analysis of cell migration.

*Apoptosis of neuroblastoma cells induced by all-*trans *RA*

Cells, were seeded into 24-well tissue culture plates at a density of 5×10^4 cm^{-2} and cultured in the presence of the indicated concentration of RA (all-*trans* form; Sigma) dissolved in 70% ethanol. Control cultures were treated with the same concentration of ethanol. To identify RA-induced apoptotic reaction, TUNEL (TdT-mediated dUTP-biotin nick end labeling) was performed according to the manufacturer's instructions (In Situ Cell Death Detection, POD: Roche) as described by Gavrieli *et al*. (1992). The cells were counterstained with hematoxylin-eosin.

[^{3}H]thymidyne incorporation assay

This was performed essentially as described previously (McNeil *et al*., 1985). A total of 2×10^4 cells were seeded onto 24-well dishes and cultured for 48 h and shifted to a serum-free medium, and then 24 h later were followed by overnight stimulation with 100 ng/ml EGF. [^{3}H]thymidine (1 μCi/ml) was added for the last 4 h of incubation. The amount of incorporated [^{3}H]thymidine radioactivity was measured by liquid scintillation counting. Results are expressed as disintegrations per minute of incorporated [^{3}H]thymidine per well.

Generation of tissue samples and histological evaluation

Nude mouse tumors were obtained by independent injections of 5×10^6 ShcC mutant cells into the bilateral subcutaneous tissues of each mouse. Tumor tissues were fixed in formalin at 4°C, transferred to 70% ethanol, and blocked in paraffin. Sections were stained with hematoxylin and eosin.

Immunohistochemistry

The sections of the tumor tissues from ShcC mutant cells were immunostained with anti-Ki-67 antibody (DAKO) and anti-cyclin-A antibody (Novocastra Laboratories) using the labeled streptavidin biotin (LSAB) methods according to the manufacturer's instructions of the LSAB kit (Dako). All the primary antigens were used at a 1 : 100 dilution. Peroxidase activity was visualized with 3, 3′-diaminobebenzidine (DAB).

Acknowledgements
This study was supported by the Program for Promotion of Fundamental Studies in Health Sciences of Organization for Pharmaceutical Safety and Research of Japan, and was also supported by a grant from SBS, Inc. Izumi Miyake is the recipient of Research Resident Fellowships from the Japan Health Sciences Foundation.

References

Andrechek ER, Hardy WR, Siegel PM, Rudnicki MA, Cardiff RD and Muller WJ: (2000). *Proc. Natl. Acad. Sci. USA*, **97**, 3444–3449.
Collins LR, Ricketts WA, Yeh L and Cheresh D. (1999). *J. Cell Biol.*, **147**, 1561–1568.
Folkman J and Moscona A. (1978). *Nature*, **273**, 345–349.
Freedman VH and Shin SI. (1974). *Cell*, **3**, 355–359.
Frisch SM and Francis H. (1994). *J. Cell Biol.*, **124**, 619–626.
Gavrieli Y, Sherman Y and Ben-Sasson SA. (1992). *J. Cell Biol.*, **119**, 493–501.
Giancotti FG. (1997). *Curr. Opin. Cell. Biol.*, **9**, 691–700.
Gu J, Tamura M, Pankov R, Danen EH, Takino T, Matsumoto K and Yamada KM. (1999). *J. Cell Biol.*, **146**, 389–403.
Honda H, Nakamoto T, Sakai R and Hirai H. (1999). *Biochem. Biophys. Res. Commun.*, **262**, 25–30.
Honda H, Oda H, Nakamoto T, Honda Z, Sakai R, Suzuki T, Saito T, Nakamura K, Nakao K, Ishikawa T, Katsuki M, Yazaki Y and Hirai H. (1998). *Nat. Genet.*, **19**, 361–365.
Iwahara T, Fujimoto J, Wen D, Cupples R, Bucay N, Arakawa T, Mori S, Ratzkin B and Yamamoto T. (1997). *Oncogene*, **14**, 439–449.
Kumar CC. (1998). *Oncogene*, **17**, 1365–1373.
McNeil PL, McKenna MP and Taylor DL. (1985). *J. Cell Biol.*, **101**, 372–379.
Miyake I, Hakomori Y, Shinohara A, Gamou T, Saito M, Iwamatsu A and Sakai R. (2002). *Oncogene*, **21**, 5823–5834.
Morris SW, Naeve C, Mathew P, James PL, Kirstein MN, Cui X and Witte DP. (1997). *Oncogene*, **14**, 2175–2188.
Nakamura N, Chin H, Miyasaka N and Miura O. (1996a). *J. Biol. Chem.*, **271**, 19483–19488.
Nakamura T, Sanokawa R, Sasaki Y, Ayusawa D, Oishi M and Mori N. (1996b). *Oncogene*, **13**, 1111–1121.
O'Bryan JP, Martin CB, Songyang Z, Cantley LC and Der CJ. (1996a). *J. Biol. Chem.*, **271**, 11787–11791.
O'Bryan JP, Songyang Z, Cantley L, Der CJ and Pawson T. (1996b). *Proc. Natl. Acad. Sci. USA*, **93**, 2729–2734.
Parsons JT and Weber MJ. (1989). *Curr. Top. Microbiol. Immunol.*, **147**, 79–127.
Pawson T, Gish GD and Nash P. (2001). *Trends Cell Biol.*, **11**, 504–511.
Pelicci G, Dente L, De Giuseppe A, Verducci-Galletti B, Giuli S, Mele S, Vetriani C, Giorgio M, Pandolfi PP, Cesareni G and Pelicci PG. (1996). *Oncogene*, **13**, 633–641.
Pelicci G, Lanfrancone L, Grignani F, McGlade J, Cavallo F, Forni G, Nicoletti I, Pawson T and Pelicci PG. (1992). *Cell*, **70**, 93–104.
Pelicci G, Troglio F, Bodini A, Melillo RM, Pettirossi V, Coda L, De Giuseppe A, Santoro M and Pelicci PG. (2002). *Mol. Cell. Biol.*, **22**, 7351–7363.
Rozakis-Adcock M, Fernley R, Wade J, Pawson T and Bowtell D. (1993). *Nature*, **363**, 83–85.
Sakai R, Henderson JT, O'Bryan JP, Elia AJ, Saxton TM and Pawson T. (2000). *Neuron*, **28**, 819–833.
Sakai R, Iwamatsu A, Hirano N, Ogawa S, Tanaka T, Mano H, Yazaki Y and Hirai H. (1994). *EMBO J.*, **13**, 3748–3756.
Sidell N, Altman A, Haussler MR and Seeger RC. (1983). *Exp. Cell Res.*, **148**, 21–30.
Stevenson LE, Ravichandran KS and Frackelton Jr AR. (1999). *Cell Growth Differ.*, **10**, 61–71.
Thomas D and Bradshaw RA. (1997). *J. Biol. Chem.*, **272**, 22293–22299.
van der Geer P, Wiley S, Gish GD and Pawson T. (1996). *Curr. Biol.*, **6**, 1435–1444.
van der Geer P, Wiley S, Lai VK, Olivier JP, Gish GD, Stephens R, Kaplan D, Shoelson S and Pawson T. (1995). *Curr. Biol.*, **5**, 404–412.
Wang Y and Sheibani N. (2002). *J. Cell. Biochem.*, **87**, 424–438.
Wary KK, Mainiero F, Isakoff SJ, Marcantonio EE and Giancotti FG. (1996). *Cell*, **87**, 733–743.
Wary KK, Mariotti A, Zurzolo C and Giancotti FG. (1998). *Cell*, **94**, 625–634.
Wei L, Yang Y, Zhang X and Yu Q. (2002). *J. Cell. Biochem.*, **87**, 439–449.
Weng Z, Thomas SM, Rickles RJ, Taylor JA, Brauer AW, Seidel-Dugan C, Michael WM, Dreyfuss G and Brugge JS. (1994). *Mol. Cell. Biol.*, **14**, 4509–4521.
Windham TC, Parikh NU, Siwak DR, Summy JM, McConkey DJ, Kraker AJ and Gallick GE. (2002). *Oncogene*, **21**, 7797–7807.

Supplementary Information accompanies the paper on Oncogene website (http://www.nature.com/onc)

American Journal of Pathology, Vol. 167, No. 1, July 2005

Tumorigenesis and Neoplastic Progression

Biological Role of Anaplastic Lymphoma Kinase in Neuroblastoma

Yuko Osajima-Hakomori,*¶‖ Izumi Miyake,*† Miki Ohira,‡ Akira Nakagawara,‡ Atsuko Nakagawa,§ and Ryuichi Sakai*

From the Growth Factor Division, National Cancer Center Research Institute, Chuo-ku, Tokyo; St. Marianna University School of Medicine,¶ Kawasaki-shi, Kanagawa; Tokyo Metropolitan Geriatric Hospital,‖ Itabashi-ku, Tokyo; the Department of Pediatrics,† Kitasato University School of Medicine, Sagamihara-shi, Kanagawa; the Division of Biochemistry,‡ Chiba Cancer Center Research Institute, Cyuo-ku, Chiba; and the Department of Pathology,§ Aichi Medical University, Aichi-gun, Aichi, Japan*

Anaplastic lymphoma kinase (ALK) is a tyrosine kinase receptor originally identified as part of the chimeric nucleophosmin-ALK protein in the t(2;5) chromosomal rearrangement associated with anaplastic large cell lymphoma. We recently demonstrated that the ALK kinase is constitutively activated by gene amplification at the ALK locus in several neuroblastoma cell lines. Forming a stable complex with hyperphosphorylated ShcC, activated ALK modifies the responsiveness of the mitogen-activated protein kinase pathway to growth factors. In the present study, the biological role of activated ALK was examined by suppressing the expression of ALK kinase in neuroblastoma cell lines using an RNA interference technique. The suppression of activated ALK in neuroblastoma cells by RNA interference significantly reduced the phosphorylation of ShcC, mitogen-activated protein kinases, and Akt, inducing rapid apoptosis in the cells. By immunohistochemical analysis, the cytoplasmic expression of ALK was detected in most of the samples of neuroblastoma tissues regardless of the stage of the tumor, whereas significant amplification of ALK was observed in only 1 of 85 cases of human neuroblastoma samples. These data demonstrate the limited frequency of ALK activation in the real progression of neuroblastoma. *(Am J Pathol 2005, 167:213–222)*

Receptor tyrosine kinases (RTKs) play an important role in regulating diverse cellular processes, such as proliferation, differentiation, survival, motility, and malignant transformation. The activation of RTKs typically requires ligand-induced receptor oligomerization, which results in tyrosine autophosphorylation of the receptors at tyrosine residues.[1–3] By recruiting specific sets of signal transducer molecules in a phosphorylation-dependent manner, each RTK is capable of inducing individual, specific cellular responses.[4] On the other hand, activation of RTKs by either mutations or overexpression is frequently found in various human malignancies.[3,5]

Anaplastic lymphoma kinase (ALK) is a 200-kd tyrosine kinase encoded by the *ALK* gene on chromosome 2p23. ALK was first identified as part of an oncogenic fusion tyrosine kinase, nucleophosmin-ALK, which is associated with anaplastic large cell lymphoma.[6,7] It was also found as a form of fusion protein with a clathrin heavy chain (CTCL) in myofibroblastic tumors.[8] Full-length ALK has the typical structure of an RTK, with a large extracellular domain, a lipophilic transmembrane segment, and a cytoplasmic tyrosine kinase domain.[9,10] ALK is highly homologous to leukocyte tyrosine kinase (LTK) and is further classified into the insulin receptor superfamily. The *LTK* gene is mainly expressed in pre-B lymphocytes and neuronal tissues,[11–13] whereas expression of the normal *ALK* gene in hematopoietic tissues has not been detected. Instead, it is dominantly expressed in the neural system.[14,15] In the developing brains of mice, specific expression of *ALK* was seen in the thalamus, mid-brain, olfactory bulb, and selected cranial regions, as well as the dorsal root, the ganglia of mice,[9,10,16] suggesting a specific role in the development of the embryonic nervous system. Currently, however, the function of ALK in adult normal tissue or carcinogenesis remains an open question. Several studies have recently indicated pleiotrophin or midkine as possible ligands for ALK.[17,18] Although they appeared to induce the functional activa-

Supported by the Program for the Promotion of Fundamental Studies in Health Science of the Organization for Pharmaceutical Safety and Research of Japan. Y.O-H. is the recipient of a Research Resident Fellowship from the Foundation for Promotion of Cancer Research, Japan.

Accepted for publication March 23, 2005.

Address reprint requests to Ryuichi Sakai, M.D., Growth Factor Division, National Cancer Center Research Institute, 5-1-1 Tsukiji, Chuo-ku, Tokyo 104-0045, Japan. E-mail: rsakai@gan2.res.ncc.go.jp.

tion of ALK, it is still unclear whether these molecules are the physiological ligands of ALK.

Neuroblastoma is one of the most common pediatric tumors derived from the sympathoadrenal linage of the neural crest. Tumors found in patients under the age of 1 year are usually favorable and often show spontaneous differentiation and regression.[19] Amplification of the N-*myc* gene occurs in approximately 25% of neuroblastomas and correlates with the aggressiveness of the disease. In addition to N-*myc* gene amplification, the expression of various genes has significant correlation with the stage of and prognosis for neuroblastoma. A high level of TrkA expression is predictive of a favorable outcome,[20] whereas TrkB is highly expressed in immature neuroblastomas with N-*myc* amplification.[21] High expression of caspase-1, -3, and -8 is correlated with favorable neuroblastomas.[22,23] On the other hand, survivin, which suppresses caspase and promotes the cell survival signal, is significantly expressed,[24] and telomerase is activated[25] in unfavorable tumors. There may be a critical difference in the expression of other molecules, including RTKs, in neuroblastoma. A recent paper showed that full-length ALK is detected in almost one-half of the cell lines derived from neuroblastomas and neuroectodermal tumors.[26] We have recently shown using mass-spectrometry analysis that ALK is a major phosphoprotein associated with hyperphosphorylated ShcC in several neuroblastoma cell lines.[27] In these cells, ALK was markedly activated, and it induced the constitutive phosphorylation of ShcC and mitogen-activated protein kinase (MAPK), regardless of stimulation by epidermal growth factor (EGF) or nerve growth factor.[27] These findings strongly suggest that constitutively activated ALK kinase plays a physiological role in the development of neuroblastoma.

In this study, we investigated the biological function of the constitutively activated ALK kinase in neuroblastoma. The RNA interference (RNAi) technique using specific sets of small interfering RNA (siRNA) was induced to inhibit the *ALK* gene expression in human neuroblastoma cells with or without gene amplification of *ALK*. The effects of disrupted ALK expression on cell survival or downstream signaling, such as MAPKs or Akt pathways, are examined to understand the biological meaning of ALK amplification in neuroblastoma cells. We also performed Southern blot analysis of primary neuroblastoma tumors from 85 patients to check whether the *ALK* gene amplification was actually present in neuroblastoma tissues. Furthermore, we sought the *ALK* gene expression in human neuroblastoma tissues using immunohistochemical analysis.

Materials and Methods

Cell Culture

Cell lines of human neuroblastoma were maintained in RPMI 1640 supplemented with 10% fetal calf serum (Sigma, St. Louis. MO), penicillin, and streptomycin at 37°C in a humidified 5% CO_2 incubator.

Reverse Transcription-Polymerase Chain Reaction (RT-PCR) Analysis

Total RNA was extracted with ISOGEN (Nippongene Japan, Toyama, Japan) from NB-39-nu and SK-N-MC cells. The PCR primer pair 5′-AGGTTCTGGCTGCAGATGGT-3′ and 5′-ACATTGTTCTCTCGAGTGCAGAC-3′ corresponding to the cytoplasmic portion of human ALK was prepared. As much as 0.25 μg of total RNA was reverse transcribed and amplified with the SuperScript One-step RT-PCR with the Platinum *Taq* kit (Invitrogen Life Technologies, Carlsbad, CA) in a total volume of 50l including 2× reaction mix, 0.2 μmol/L of each primer, and 1 μl of RT/Platinum *Taq* Mix. Amplification conditions consisted of cDNA synthesis and predenaturation at 50°C for 30 minutes and 94°C for 2 minutes followed by 25 cycles at 94°C for 15 seconds, 58°C for 30 seconds, and 72°C for 45 seconds. A final amplification for 7 minutes at 72°C finished the PCR. The product was separated with 1.2% agarose gel electrophoresis and analyzed using the Quality One System (Bio-Rad, Hercules, CA).

Immunochemical Analysis of Proteins

Immunoprecipitation and immunoblotting were performed as described previously.[27] The polyclonal antibodies against the CH1 domains of ShcC (amino acids 306–371) and the anti-ALK antibody (αALK) that was against the cytoplasmic portion (amino acid 1379–1524) of human ALK were prepared as described previously.[27,28] An anti-phosphotyrosine antibody (4G10) was obtained from UBI. Anti-p44/42 MAPKs, anti-phospho-p44/42 MAPKs, anti-Akt, and anti-phospho-Akt antibodies were purchased from Cell Signaling (Beverly, MA). Anti-EGF receptor (EGFR), anti-Ret, and anti-TrkA antibodies were purchased from Santa Cruz Biotechnology (Santa Cruz, CA). *In vitro* kinase assay for ALK was performed as previously described.[27] Anti-ALK immunoprecipitates were incubated with or without Poly-Glu/Tyr as an exogenous substrate.

Immunocytostaining

For ALK/TOTO-3, immunostaining using anti-ALK antibody was performed at first, and then nuclei were stained using TOTO-3. The cells seeded on the 24-well plates were washed with phosphate-buffered saline (PBS) three times and fixed with 4% paraformaldehyde (methanol free) for 5 minutes at room temperature. The cells were rinsed with PBS twice and then permeabilized with 0.2% Triton X-100 solution in PBS for 10 minutes at room temperature. The cells were blocked with 5% goat serum and 3% bovine serum albumin–Tris-buffered saline for 30 minutes at room temperature. The blocking solution was drained off, and the cells were incubated with a 1:1000 dilution of αALK for 1 hour at room temperature. The cells were rinsed with PBS three times and incubated with a 1:2000 dilution of Alexa fluor (Molecular Probes, Eugene, OR) and 1: 100 dilution of TOTO-3 (Molecular Probes) for 30 minutes at room temperature. The cells were washed three times with PBS and mounted in glycerol-based 2.5% 1,4-diazabicyclo[2,2,2] octan. Confocal laser scanning analysis was carried out. For ALK/TUNEL, we first carried out TUNEL and then proceeded to standard immunocytochemistry using anti-ALK antibody. TUNEL was performed using the DeadEnd Fluorometric TUNEL System (Promega, Madison, WI) with the following modifications. The NB-39-nu cells seeded on the 24-well plates that were treated with siRNAs were washed with PBS twice and fixed with 4% paraformaldehyde (methanol free) for 25 minutes at 4°C. The cells were rinsed with PBS twice and then permeabilized with 0.2% Triton X-100 solution in PBS for 5 minutes at room temperature. The cells were washed with PBS twice and covered with an equilibration buffer (from the kit) for 10 minutes at room temperature. The equilibration buffer was drained off, and a reaction buffer containing the equilibration buffer, nucleotide mix, and terminal deoxynucleotidyl transferase enzyme was added to the cells and incubated at 37°C for 1 hour, avoiding exposure to light. The cells were incubated for 15 minutes at room temperature with 2× standard saline citrate to stop the reaction. The cells were washed with PBS three times and then stained for ALK using immunofluorescence as follows. The cells were blocked with 2% bovine serum albumin (Boehringer Mannheim, Germany) for 30 minutes at room temperature. The blocking solution was drained off, and the cells were incubated with a 1:1000 dilution of αALK for 1 hour at room temperature. The cells were rinsed with PBS three times and incubated with a 1:40 dilution of rhodamine-conjugated goat anti-rabbit secondary antibody (Santa Cruz Biotechnology) for 30 minutes at room temperature. The cells were washed three times with PBS and then mounted and observed in the same manner as that for ALK/TOTO-3.

Table 1. Patient Characteristics of Neuroblastoma Tissues with *ALK* Gene Gain or Amplification

Case	Age*	Primary tumor		Copy nos. of *ALK*‡	Amplification of N-*myc* (*n*)
		Location	Clinical stage†		
1	3y5m	Adrenal gland	IV	2.0 ± 0.2	+ (35)
2	5y0m	Peritoneum	IV	1.8 ± 0.1	+ (>150)
3	2y7m	Abdomen	IV	2.1 ± 0.8	+ (150)
4	8m	Adrenal gland	I	3.0 ± 1.0	−
5	4y9m	Abdomen	IV	2.0 ± 0.2	−
6	3y9m	Adrenal gland	III	2.7 ± 0.2	+ (>150)
7	1y4m	Adrenal gland	IV	2.8 ± 1.0	+ (150)
8	1y7m	Adrenal gland	IV	9.5 ± 2.2	+ (>100)

*Age of onset: year (y), month (m).
†The staging criterion was based on the International Neuroblastoma Staging System.
‡The averages of the calculated copy numbers from three independent blottings are shown.

DNA Extraction and Southern Blotting

Genomic DNAs derived from neuroblastoma cell lines were obtained from cultured cells as described using the procedure of Perucho et al.[29] Samples of 85 neuroblastoma tissues were collected at the Chiba Cancer Center and stored as forms of genomic DNA. The characteristics of some of these patients are shown in Table 1. The stage criterion was based on the International Neuroblastoma Staging System.[30] Samples of 5 μg of DNA digested by *Eco*RI were electrophoresed in 0.8% agarose gel and blotted onto nitrocellulose filters (Hybond-N+; Amersham, Piscataway, NJ). The probes for detecting the *ALK* gene, N-*myc* gene, and *ShcC* gene were used in our previous study.[27] The intensities of these signals were measured using a Molecular Imager FxPro (Bio-Rad). This study was approved by the ethical judging committee of the National Cancer Center and the Chiba Cancer Center of Japan.

RNA Interference Technique

Twenty-one-nucleotide double-stranded RNAs were synthesized and purified using Dharmacon Research (Lafayette, CO). To suppress the expression of ALK protein, two different pairs of ALK siRNAs, ALK-siRNA1 and ALK-siRNA2, were obtained. The sequences were 5′-GAGUCUGGCAGUUGACUUCdTdT-3′ for ALK-siRNA1 and 5′-GCUCCGGCGUGCCAAGCAGdTdT-3′ for ALK-siRNA2, corresponding to coding region 153 to 171 and 399 to 417 relative to the first nucleotide of the start codon, respectively. Entire sequences were derived from the sequence of human *ALK* mRNA (accession no. HSU62540). An siRNA, targeting a sequence in the firefly (*Photinus pyralis*) luciferase mRNA, was used as a negative control (Dharmacon) (luc-siRNA). We also used a scramble siRNA, Scramble Duplex II (Dharmacon) (s-siRNA) as a mismatch siRNA control in addition to luc-siRNA.

NB-39-nu cells were trypsinized, diluted with growth medium containing 10% fetal calf serum, and transferred to 12-well plates at 6 × 10^4 cells per well for 24 hours before transfection. The transfection of siRNA was carried out using jetSI (Poly plus transfection). A total of 100 μl of serum-free growth medium and 4 μl of jetSI per well were preincubated for 5 to 10 minutes at room temperature. While the incubation was being performed, 100 μl of serum-free growth medium was mixed with 5 μl of 20 μmol/L siRNA duplex (100 pmol). Total siRNA amounts of 50, 100, and 200 pmol were checked in preliminary experiments to find out 100 pmol is the minimal and optimal amount in this scale of RNAi. The 100 μl of jetSI serum-free medium solution was added to the 100 μl of siRNA

duplex solution, gently mixed, and incubated for 30 minutes at room temperature. The growth medium on the cells was removed, and 800 μl of serum-free medium was added to each well. A total of 200 μl of the entire mixture was overlaid onto the cells, and cells were incubated for 4 hours at 37°C in a 5% CO_2 incubator. After incubation, 1 ml of medium containing 4% fetal calf serum was added without removing the transfection mixture (final concentration 2%). The cells were assayed 84 hours after transfection. SK-N-MC cells were seeded in 12-well plates at a concentration of 1.3×10^5 cells per well. These were treated with siRNAs in the same way as NB-39-nu and assayed 48 hours after transfection. In the 24-well plate, the cells were seeded at the same concentration as the 12-well plate, and siRNAs and all other reagents were used at half volume. After transfection, the cells were examined under a light microscope every day.

Double Staining for ALK and TUNEL

For double staining, we first carried out TUNEL and then proceeded to standard immunocytochemistry using anti-ALK antibody. TUNEL was performed using the DeadEnd Fluorometric TUNEL System (Promega) with the following modifications. The NB-39-nu cells seeded on the 24-well plates that were treated with siRNAs were washed with PBS twice and fixed with 4% paraformaldehyde (methanol free) for 25 minutes at 4°C. The cells were rinsed with PBS twice and then permeabilized with 0.2% Triton X-100 solution in PBS for 5 minutes at room temperature. The cells were washed with PBS twice and covered with an equilibration buffer (from the kit) for 10 minutes at room temperature. The equilibration buffer was drained off, and a reaction buffer containing the equilibration buffer, nucleotide mix, and terminal deoxynucleotidyl transferase enzyme was added to the cells and incubated at 37°C for 1 hour, avoiding exposure to light. The cells were incubated for 15 minutes at room temperature with 2× standard saline citrate to stop the reaction. The cells were washed with PBS three times and then stained for ALK using immunofluorescence as follows. The cells were blocked with 2% bovine serum albumin (Boehringer Mannheim) for 30 minutes at room temperature. The blocking solution was drained off, and the cells were incubated with a 1:1000 dilution of αALK for 1 hour at room temperature. The cells were rinsed with PBS three times and incubated with a 1:40 dilution of rhodamine-conjugated goat anti-rabbit secondary antibody (Santa Cruz Biotechnology) for 30 minutes at room temperature. The cells were washed three times with PBS and mounted in glycerol-based 2.5% 1,4-diazabicyclo[2,2,2] octan. Confocal laser scanning analysis was carried out.

DNA Fragmentation Assay

To detect apoptotic DNA cleavage, DNA fragmentation assay was performed using an Apoptotic DNA Ladder kit (Chemicon International, Inc., Temecula, CA). The cells seeded on the 12-well plates that were treated with siRNAs as previously mentioned were collected in 1.5-ml microcentrifuge tubes. The cells were washed with PBS, centrifuged, and lysed with 20 μl of TE lysis buffer. The lysates were incubated with 5 μl of enzyme A (RNase A) at 37°C for 10 minutes and then at 55°C for 30 minutes after the addition of 5 μl of Enzyme B (Proteinase K). Afterward, 5 μl of ammonium acetate solution and 100 μl of absolute ethanol were added, and the samples were kept at −20°C for 10 minutes. The samples were centrifuged, and the pellets were washed with 70% ethanol. Then the DNA pellets were dissolved in 30 μl of DNA suspension buffer. DNA fragmentations were visualized by electrophoresis on 2% agarose gel containing ethidium bromide.

Immunohistochemistry

As for positive control, tumor xenograft was made by injection of NB-39-nu cells subcutaneously in 5-week-old SCID mice. Immunohistochemical staining with ALK antibody (αALK) (1:1000), was performed on 16 human neuroblastoma tumors selected from the surgical pathology file at the Department of Pathology, Aichi Medical University based on the results of histopathology evaluation[31] and N-*myc* status. All of those tumor samples were obtained before chemotherapy and irradiation therapy and included nine favorable histology cases with nonamplified N-*myc* (FH&NA), two unfavorable histology cases with amplified N-*myc* (UH&A), and five unfavorable histology cases with nonamplified N-*myc* (UH&NA).

Four-micrometer-thick sections from the formalin-fixed and paraffin-embedded tissue samples were deparaffinized and microwaved for three times for 5 minutes in Na-citrate buffer (pH 6.0) for antigen retrieval. The slides were first immersed in 0.3% hydrogen peroxide in methanol for 20 minutes and then in 10% normal goat serum for 30 minutes. The primary antibody (αALK) was then applied at 4°C overnight, followed by a standard staining procedure using the Vectastain ABC kit (Vector Laboratories, Burlingame, CA). Sections were counterstained with hematoxylin for light microscopic review and evaluation. ALK was always positively detected in the cytoplasm of NB-39-nu tumor xenograft and in the cytoplasm and neuritic processes of normal ganglion cells in the separate positive control sections as well as in the test sections as built-in control, whenever available. As for the negative controls, normal rabbit immunoglobulins (1:500 dilution; Vector Laboratories) or preimmune serum for α ALK (1:1000 dilution) was applied as the primary antibody.

Results

Significant Amplification of the ALK Gene and Constitutive Activation of ALK Kinase in Three Neuroblastoma Cell Lines

As shown in Figure 1A, NB-39-nu, Nagai, and NB-1 cells have significant levels of amplification of the *ALK* gene (30–40 copies per cell) among 25 neuroblastoma and neuroepithelioma cell lines examined. Other cell lines such as SK-N-MC have only one copy of the *ALK* gene just like the other types of solid tumor cell lines used as controls. *In vitro* kinase assay revealed outstanding ALK kinase activity in these three cell lines compared with other cells (Figure 1B), which is consistent with our previous study.[27] To examine whether overexpressed and activated ALK affects the expression of other RTKs in these cells, protein expression levels of RTKs, including EGFR, Ret, and TrkA, are compared with other cell lines. Significantly high levels of expression of EGFR and TrkA were observed in two of three cell lines overexpressing ALK (Figure 1C, top and bottom). Ret expression was commonly elevated in all three cell lines with activated ALK, especially in Nagai and NB-39-nu (Figure 1C, middle), consistent with previous study by Northern blotting.[32] Although it is unknown whether overexpression of these RTKs is related to overexpression of ALK, no obvious down-regulation of other RTKs was found in these *ALK*-amplified cell lines.

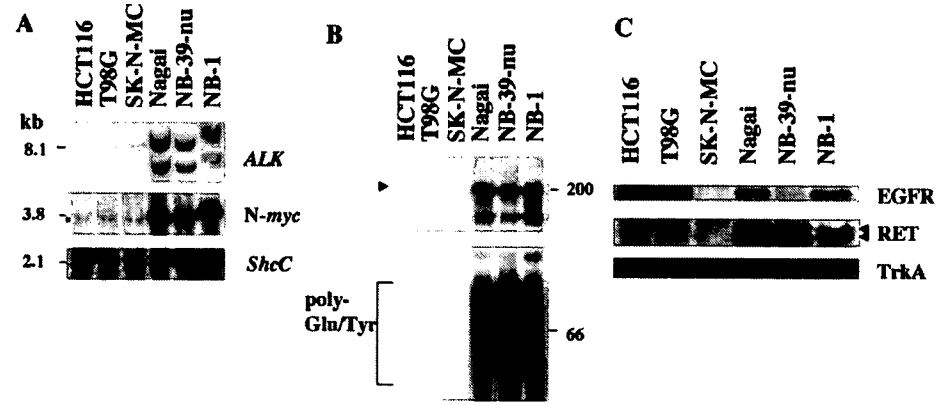

Figure 1. Marked gene amplification of the *ALK* locus and significant elevation of kinase activity of ALK in NB-39-nu, Nagai, and NB-1 cells. **A:** To detect ALK gene amplification, samples of 10 μg of DNA were digested with *Eco*RI. Fragments of about 2.5, 3.1, 6.1, and 8.1 kb were detected using the ^{32}P-labeled probe prepared as previously described.[27] Amplification of the N-*myc* gene was detected using the same filter re-hybridized with the probe for N-*myc*. As a control for the amounts of DNA, the same filter was re-hybridized with the probe for *ShcC*. **B:** *In vitro* kinase assay of ALK in neuroblastoma cells immunoprecipitated with αALK was performed as previously described.[27] Kinase reaction was performed without (**top panel**) or with (**bottom panel**) poly-Glu/Tyr (4:1) as exogenous substrates. Autophosphorylated ALK protein is marked by an **arrow**. Phosphorylated poly-Glu/Tyr is detected as smear indicated by the bracket. **C:** The expression patterns of other receptor tyrosine kinases in neuroblastoma cell lines. Each cell line was harvested, and about 30 μg of whole-cell lysates was subjected to Western blot analysis using the antibodies as indicated on the right. RET proteins are marked by **arrows**.

Inhibition of Activated ShcC, MAPKs, and Akt by Suppressing Activated ALK

To investigate the effect of suppressing the ALK expression level in *ALK*-amplified neuroblastoma cells using the RNAi technique, we synthesized two different RNA duplexes directed against nucleotide positions 153 to 171 and 399 to 417 within coding region *ALK* cDNA (ALK-siRNA1 and ALK-siRNA2, respectively). Because co-transfection of ALK-siRNA1 and ALK-siRNA2 was very effective in suppressing ALK expression, we performed all experiments presented here using a combination of two siRNAs, although similar results were obtained using only ALK-siRNA2. A sequence against the firefly luciferase gene (luc-siRNA) was used as a negative control. The expression of ALK protein is remarkably elevated in NB-39-nu and Nagai compared with other neuroblastoma cell lines, such as SK-M-MC (Figure 2A), caused by gene amplification.[27] The RNA duplexes were transfected into NB-39-nu cells with *ALK* gene amplification and SK-N-MC cells containing only a single copy of the *ALK* gene. We also tried to introduce ALK-siRNAs in several different neuroblastoma cell lines with or without *ALK* amplification in addition to NB-39-nu and SK-N-MC cells, resulting in partial or no reduction of ALK expression presumably due to the unsuccessful introduction in those cells. Therefore, we decided to use these two cell lines to perform further analysis of the effect of ALK knockdown by RNAi technique. RT-PCR analysis revealed that ALK mRNA level was reduced in both NB-39-nu cells and SK-N-MC cells treated with ALK-siRNAs, not in the cells treated with luc-siRNA and s-siRNA (Figure 2B). Both expression and phosphorylation of ALK kinase were significantly suppressed in the NB-39-nu cells treated with ALK-siRNAs compared with a mock-transfection control or cells treated with luc-siRNA (Figure 2C). In these cells, phosphorylation of ShcC was also suppressed despite the unchanged total amount of ShcC (Figure 2C), demonstrating that ShcC is a potent substrate of activated ALK kinase and that activation of ALK is actually responsible for the hyperphosphorylation of ShcC in these cancer cells. While the expression of downstream molecules, such as p44/42 MAPKs and Akt, was not affected by ALK-siRNAs, phosphorylation of these molecules was markedly reduced (Figure 2C). These results suggest that the Ras-MAPK pathway and the phosphatidylinositol 3-kinase/Akt pathway are dominantly regulated by activated ALK kinase in these cells. Interestingly, in SK-N-MC cells treated with ALK-siRNAs, phosphorylation levels of ShcC, p44/42 MAPKs, and Akt were not affected by

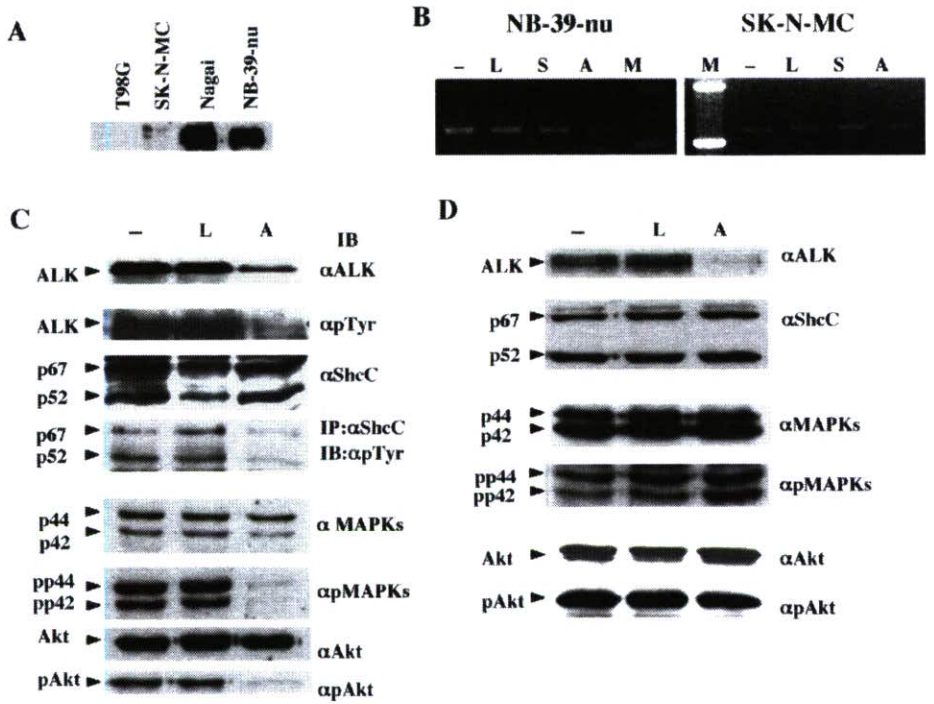

Figure 2. Suppression of ALK expression by siRNAs and changes in downstream molecules NB-39-nu cells and SK-N-MC cells. **A:** Expression levels of ALK protein in neuroblastoma cell lines including NB-39-nu and SK-N-MC. Each cell line was harvested, and about 30 μg of whole-cell lysates was subjected to Western blot analysis using αALK. **B:** mRNA levels of *Alk* in NB-39-nu cells. The cells were lysed at 84 hours after transfection and analyzed by RT-PCR. –, mock transfection; L, cells treated with luc-siRNA; S, cells treated with s-siRNA; A, cells treated with ALK-siRNAs; M, marker. **C:** NB-39-nu cells were harvested 84 hours after transfection. About 10 μg of whole-cell lysates or 250 μg of lysates immunoprecipitated with αShcC was subjected to Western blot analysis using the antibodies as indicated on the right. –, mock transfection; L, cells treated with luc-siRNA; A, cells treated with ALK-siRNAs. **D:** SK-N-MC cells were harvested 48 hours after transfection. About 10 μg of whole-cell lysates was subjected to Western blot analysis using the antibodies as indicated on the right. Bands of ShcC are marked by **arrows**. –, mock transfection; L, cells treated with luc-siRNA; A, cells treated with ALK-siRNAs.

ALK-siRNAs despite further suppression of the basal ALK expression level (Figure 2D), indicating that these pathways are not under the control of ALK in SK-N-MC cells.

Induction of Apoptosis by Suppression of Activated ALK

At 84 hours after transfection, apoptotic morphological changes, such as cell rounding, cytoplasmic blebbing, and irregularities of shape, were observed in NB-39-nu cells treated with ALK-siRNAs, whereas no significant changes were seen in the mock-transfected cells or in the luc-siRNA and the s-siRNA treated cells (Figure 3A). These morphological changes were not observed in SK-N-MC cells treated with ALK-siRNAs (data not shown). At 90 hours after transfection, NB-39-nu cells treated with ALK-siRNAs started to detach from the dish due to cell death.

To examine the localization of expression of ALK kinase, we performed double staining by anti-ALK antibody and TOTO-3, which stains the nucleus, in several neuroblastic cell lines. As shown in Figure 1D, unexpectedly, ALK protein overexpressed in NB-39-nu cells is localized in both membrane and cytoplasm. ALK staining was very weak in cell lines such as YT-nu and SK-N-MC with one copy of the *ALK* gene, however, its localization appeared to be the same as in NB-39-nu (data not shown). It was observed that the expression of ALK was completely lost after the RNAi-induced suppression of ALK (Figure 3C, top). To confirm whether the cell death resulted from apoptosis, cells were also analyzed by immunofluorescent TUNEL staining in NB-39-nu cells. TUNEL staining was clearly positive in these cells at 84 hours after transfection (Figure 3C, middle), indicating that apoptosis was induced in NB-39-nu cells treated with ALK-siRNAs. No significant TUNEL staining was observed in the mock-transfected cells or the luc-siRNA treated cells. Finally, DNA fragmentation assay was performed to measure the endonuclease activity accompanied by apoptosis. The formation of significant DNA fragmentation was observed in the NB-39-nu cells but not in SK-N-MC cells treated with ALK-siRNAs (Figure 3D), indicating that cell apoptosis was induced through the suppression of ALK only in the NB-39-nu cells. This suggests that signaling pathways downstream of activated ALK dominantly regulate the survival of neuroblastoma cells with amplified ALK; therefore, the loss of ALK protein results in apoptotic changes to these cells.

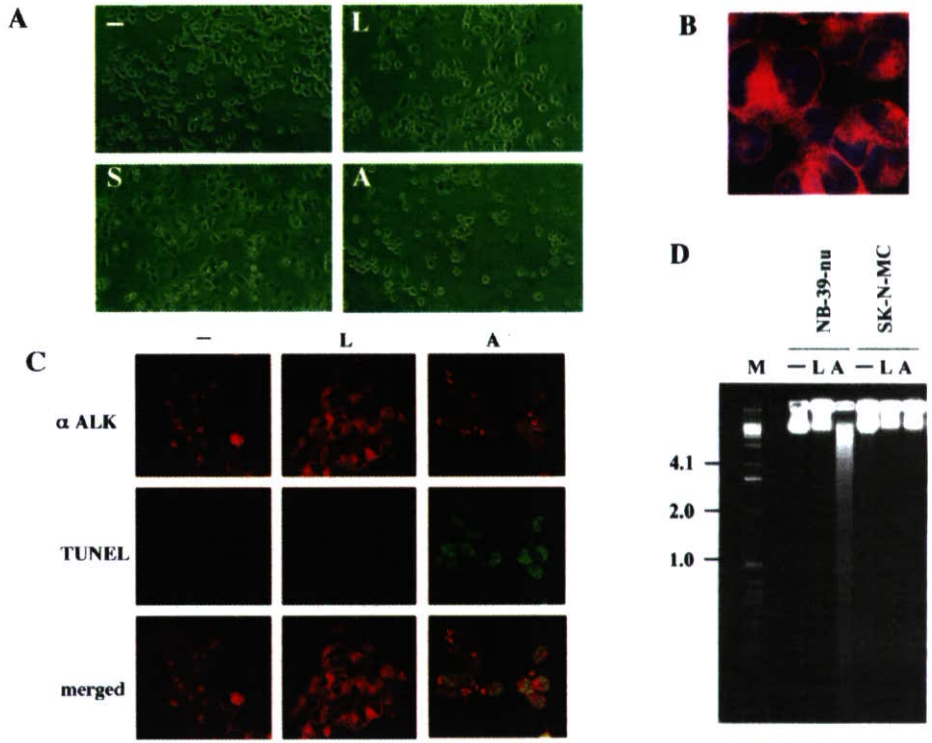

Figure 3. Induction of apoptosis in NB-39-nu cells treated with ALK-siRNAs. **A:** NB-39-nu cells on the dish were observed 84 hours after transfection under a light microscope. –, mock transfection; L, cells treated with luc-siRNA; S, cells treated with s-siRNA; A, cells treated with ALK-siRNAs. **B:** Cytoplasmic expression of ALK by immunocytostaining. The cells were stained for the expression of ALK (red) and apoptotic cells by TOTO-3 (blue). **C:** Cells on 24-well plates were fixed, and TUNEL assay was followed by staining with αALK (GST). The cells were stained for the expression of ALK (red) and apoptotic cells by TUNEL (green). –, mock transfection; L, cells treated with luc-siRNA; A, cells treated with ALK-siRNAs. **D:** DNA fragmentation assay in NB-39-nu cells and SK-N-MC cells treated with siRNAs. Genomic DNA was extracted 84 hours and 48 hours after transfection in NB-39-nu and in SK-N-MC, respectively. They were analyzed using electrophoresis. –, mock transfection; L, cells treated with luc-siRNA; A, cells treated with ALK-siRNAs; M, marker.

Expression of ALK in Primary Neuroblastoma Tissues

Immunohistochemically, ALK was positively detected both in the cytoplasm of the neuroblastic cells and in the fine meshwork of neuropil of seven of nine tumors with favorable histology cases with nonamplified *N-myc* (FH&NA) (Figure 4, B and C). All seven unfavorable histology tumors (two UH&A tumors and five UH&NA tumors) were positive in the cytoplasm and/or in the fine meshwork of neuropil for ALK (Figure 4A). There was no correlation between the frequency or intensity of ALK-staining and histology of neuroblastoma tissues, showing majority of neuroblastoma samples showed a detectable amount of ALK. There was no significant staining using preimmune serum from the same rabbit as that for anti-ALK antibody (data not shown). Essentially the same results were obtained using a mouse monoclonal antibody against human ALK (ALK1: DAKO) (data not shown).

Amplification of the ALK Gene in Primary Neuroblastoma Tissues

It is essential to show whether ALK overexpression or gene amplification occurs in actual human neuroblastoma tissues in addition to neuroblastoma cell lines.

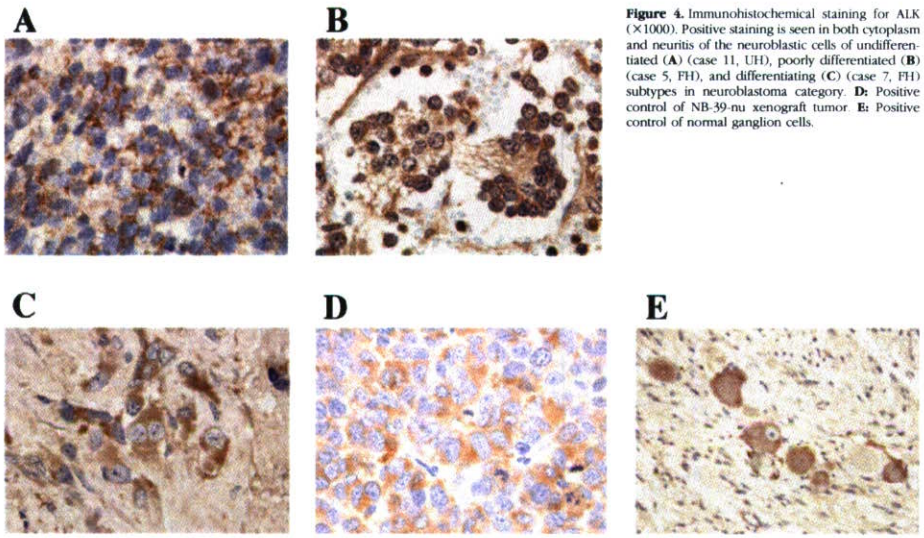

Figure 4. Immunohistochemical staining for ALK (×1000). Positive staining is seen in both cytoplasm and neuritis of the neuroblastic cells of undifferentiated (**A**) (case 11, UH), poorly differentiated (**B**) (case 5, FH), and differentiating (**C**) (case 7, FH) subtypes in neuroblastoma category. **D:** Positive control of NB-39-nu xenograft tumor. **E:** Positive control of normal ganglion cells.

Therefore, the mRNA amount of ALK kinase was first examined by RT-PCR on 32 primary neuroblastoma tissues (16 tissues with N-*myc* amplification and 16 tissues without N-*myc* amplification). Two of 32 cases showed slight elevation of *ALK* mRNA expression using several primer sets beyond the average expression level (data not shown).

To obtain more precise information about the copy numbers of *ALK*, we next analyzed the genomic DNAs of primary neuroblastoma tissues using Southern blot analysis. Whole purified DNA samples of tumors from 85 patients were examined. About the same number of N-*myc*-positive and N-*myc*-negative samples were collected to examine the relation between *Alk* and N-*myc* amplification. The intensities of signals on Southern blot membranes corresponding to the *ALK* gene and control *ShcC* gene, which is located on 9q22, were measured using a Molecular Imager FxPro (Bio-Rad), and the ratio of *ALK* signals to *ShcC* signals was calculated for each sample. Because more than 80% (70 samples) showed consistent ratios with each other in each experiment, these samples are treated as putative "single copy" controls. As several other samples showed apparently elevated intensity ratios, suggesting *ALK* amplification, relative copy numbers of *ALK* were calculated in comparison with average intensity ratios of putative single copy controls in each experiment. The results showed that there was significant *ALK* gene amplification in 8 of 85 patients (9.4%) (Figure 5). Seven of these eight cases, however, had only 1.8 to 3.0 copies of the *ALK* gene, suggesting a moderate gain of chromosomal focus rather than severe amplification. There was only one case that had outstanding amplification of ALK with approximately 10 copies. N-*myc* gene amplification was also detected in this case. The characteristics of the eight patients with *ALK* gain or amplification are shown in Table 1. Whereas seven of eight patients were classified as Stage III or IV (one as Stage III and six as Stage IV), the rest was classified as Stage I. The case with *ALK* amplification had N-*myc* amplification and was classified as Stage IV. Seven of eight patients were more than 1 year of age.

Discussion

Studies on ALK kinase demonstrate that activated ALK is involved in malignant tumor formation as forms of fusion proteins that force oligomerization of this kinase. We recently showed that the intact form of ALK protein is constitutively activated by *ALK* gene amplification in three neuroblastoma cell lines, indicating a novel mechanism of activation of ALK kinase in malignancies.[27] In this study, amplification of the *ALK* gene was detected in primary neuroblastoma tissues for the first time. This suggests that activated ALK kinase plays a real role in the pathophysiology of neuroblastoma, such as giving a more malignant phenotype to the tumors by perturbing signal transduction. Recently, Motegi et al[33] showed that ALK transmits both mitogenic and differentiation signals, and that the MAPK pathway plays an important role in these effects in SK-N-SH cells without *ALK* gene amplification. Together with the fact that activated ALK surpasses regulation by other RTKs in cell lines with *ALK* gene amplification,[27] our new results showing apoptotic changes caused by the suppression of activated ALK protein clearly demonstrate the dominant role of ALK kinase in the survival of the *ALK*-amplified type of neuroblastoma.

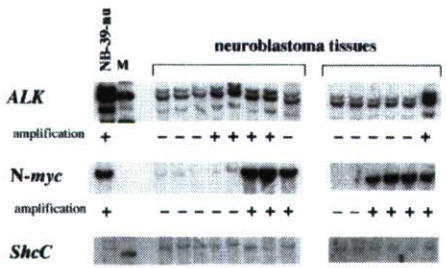

Figure 5. Detection of gene amplification of *ALK* and N-*myc* in primary neuroblastoma tissues. *ALK* was amplified in eight cases, and five of these eight cases are shown. The probe for *ALK* was removed from the filters, and the filters were re-hybridized in turn with other probes. Of eight cases with *ALK* amplification, N-*myc* amplification was detected in six cases and not detected in two cases. The probe for *ShcC* was used as a control for the amounts of DNA. M, marker.

The frequency and copy numbers of gene amplification of ALK were significantly lower in neuroblastic tumors compared with neuroblastic cell lines. Remarkable amplification of the *ALK* gene was detected in 1 tumor tissue of 85 tumor samples examined. Three neuroblastoma cell lines with *ALK* amplification had more than 30 copies of *ALK*, whereas primary neuroblastoma containing *ALK* gene amplification had within a range of 2 to 10 copies. This may be due to underestimation of the copy number in the tumor cells because of contamination of stromal cells and lymphocytes into the tumor tissues.[34,35] There may also be a mechanism in which cells with a higher copy number of *ALK* become the major population during the establishment of cell lines because of their growth advantage. Immunohistochemical analysis demonstrated, however, universal cytoplasmic expression of ALK in a wide range of neuroblastoma tumor samples, suggesting some transcriptional or posttranslational regulation of the ALK amount might exist in neuroblastoma cells. Although, due to the condition of the samples, we were unable to obtain information on the copy numbers of the *ALK* gene as for the samples used in the immunohistochemical analysis, further immunohistochemical screening may reveal neuroblastoma tissues with an outstanding amount of ALK protein because of gene amplification.

The N-*myc* gene was also amplified in this tumor and in all three cell lines with *ALK* amplification (NB-39-nu, Nagai, and NB-1). N-*myc* is located on 2p24.3 and *ALK* is on 2p23.2, suggesting that there is a tendency to synchronic amplification between N-*myc* and *ALK*. We were unable to conclude that there was an association between ALK amplification and prognosis mainly due to the limited number of positive samples and the short-term follow-up. Moreover, the *ALK* gene locus appears too far from the N-*myc* gene locus to be within a single amplicon. Further analysis in a greater number of samples with longer follow-up is necessary.

The activation of ALK results in hyperphosphorylation of ShcC in neuroblastoma cells, and NB-39-nu cells treated with ALK-siRNAs show suppressed tyrosine phosphorylation of ShcC, followed by apoptotic changes to these cells, suggesting that ShcC is a physiological substrate of the activated ALK kinase and that the ALK-ShcC pathway dominantly controls the survival of NB-39-nu cells even with the existence of other RTKs, such as EGFR, TrkA, and Ret. In neuronal cells, both ShcB (Sli/SCK) and ShcC (Rai/N-Shc) can bind activated RTKs, including the EGFR and Trk receptor.[36-39] Mice lacking both ShcB and ShcC exhibit a significant loss of sympathetic neurons, suggesting that ShcB and ShcC act in supporting sympathetic development and survival.[28] A recent study also showed that ShcC is a physiological substrate of Ret kinase and that it exerts a prosurvival function in neuronal cells.[40] Although high levels of TrkA expression correlate with a favorable outcome of neuroblastoma patients,[20] TrkA expression was significantly high in NB-39-nu and Nagai, which derive from tumors with a poor prognosis. This discrepancy may also be explained by the overwhelming control of cell survival by ALK kinase in these cell lines. Neuronal apoptosis is regulated through the action of critical protein kinase cascades, such as the phosphatidylinositol 3-kinase/Akt pathway and the Ras-MAPK pathway.[41,42] Apparently, neither pathway is properly controlled by EGF or nerve growth factor in NB-39-nu cells or Nagai cells.[27] Here, we also demonstrated that the suppression of activated ALK blocks MAPKs and Akt in these cells, resulting in apoptosis. On the other hand, the activity of MAPKs and Akt was not reduced by the suppression of a single copy of *ALK* in SK-N-MC cells. These results suggest that activation of ALK kinase completely remodeled the cellular signaling transduction pathways through ShcC so that cell survival entirely depended on signals originating from ALK kinase.

In conclusion, phosphorylation of several signaling molecules and cancer survival might be under the control of activated ALK kinase when gene amplification of ALK is as significant as in NB-39-nu cells, although the frequency of gene amplification in neuroblastoma tissues is not high. Cytoplasmic expression of ALK in neuroblastoma cells may suggest distinct function of this kinase in cell proliferation and survival. These findings further suggest that activated ALK kinase will be indispensable information for prognosis and treatment of neuroblastoma although the frequency is low.

References

1. Ullrich A, Schlessinger J: Signal transduction by receptors with tyrosine kinase activity. Cell 1990, 61:203–212
2. Heldin CH: Dimerization of cell surface receptors in signal transduction. Cell 1995, 80:213–223
3. Blume-Jensen P, Hunter T: Oncogenic kinase signalling. Nature 2001, 411:355–365
4. Pawson T: Protein modules and signalling networks. Nature 1995, 373:573–580
5. Kozlowski M, Larose L, Lee F, Le DM, Rottapel R, Siminovitch KA: SHP-1 binds and negatively modulates the c-Kit receptor by interaction with tyrosine 569 in the c-Kit juxtamembrane domain. Mol Cell Biol 1998, 18:2089–2099
6. Morris SW, Kirstein MN, Valentine MB, Dittmer KG, Shapiro DN, Saltman DL, Look AT: Fusion of a kinase gene ALK, to a nucleolar protein gene NPM, in non-Hodgkin's lymphoma. Science 1994, 263:1281–1284

7. Shiota M, Fujimoto J, Semba T, Satoh H, Yamamoto T, Mori S: Hyperphosphorylation of a novel 80 kDa protein-tyrosine kinase similar to Ltk in a human Ki-1 lymphoma cell line, AMS3. Oncogene 1994, 9:1567–1574
8. Bridge JA, Kanamori M, Ma Z, Pickering D, Hill DA, Lydiatt W, Lui MY, Colleoni GW, Antonescu CR, Ladanyi M, Morris SW: Fusion of the ALK gene to the clathrin heavy chain gene, CLTC, in inflammatory myofibroblastic tumor. Am J Pathol 2001, 159:411–415
9. Iwahara T, Fujimoto J, Wen D, Cupples R, Bucay N, Arakawa T, Mori S, Ratzkin B, Yamamoto T: Molecular characterization of ALK, a receptor tyrosine kinase expressed specifically in the nervous system. Oncogene 1997, 14:439–449
10. Morris SW, Naeve C, Mathew P, James PL, Kirstein MN, Cui X, Witte DP: ALK, the chromosome 2 gene locus altered by the t(2;5) in non-Hodgkin's lymphoma, encodes a novel neural receptor tyrosine kinase that is highly related to leukocyte tyrosine kinase (LTK). Oncogene 1997, 14:2175–2188
11. Ben-Neriah Y, Bauskin AR: Leukocytes express a novel gene encoding a putative transmembrane protein-kinase devoid of an extracellular domain. Nature 1988, 333:672–676
12. Maru Y, Hirai H, Takaku F: Human ltk: gene structure and preferential expression in human leukemic cells. Oncogene Res 1990, 5:199–204
13. Bernards A, de la Monte SM: The ltk receptor tyrosine kinase is expressed in pre-B lymphocytes and cerebral neurons and uses a non-AUG translational initiator. EMBO J 1990, 9:2279–2287
14. Pulford K, Lamant L, Morris SW, Butler LH, Wood KM, Stroud D, Delsol G, Mason DY: Detection of anaplastic lymphoma kinase (ALK) and nucleolar protein nucleophosmin (NPM)-ALK proteins in normal and neoplastic cells with the monoclonal antibody ALK1. Blood 1997, 89:1394–1404
15. Shiota M, Fujimoto J, Takenaga M, Satoh H, Ichinohasama R, Abe M, Nakano M, Yamamoto T, Mori S: Diagnosis of t(2;5)(p23;q35)-associated Ki-1 lymphoma with immunohistochemistry. Blood 1994, 84:3648–3652
16. Duyster J, Bai RY, Morris SW: Translocations involving anaplastic lymphoma kinase (ALK). Oncogene 2001, 20:5623–5637
17. Stoica GE, Kuo A, Aigner A, Sunitha I, Souttou B, Malerczyk C, Caughey DJ, Wen D, Karavanov A, Riegel AT, Wellstein A: Identification of anaplastic lymphoma kinase as a receptor for the growth factor pleiotrophin. J Biol Chem 2001, 276:16772–16779
18. Stoica GE, Kuo A, Powers C, Bowden ET, Sale EB, Riegel AT, Wellstein A: Midkine binds to anaplastic lymphoma kinase (ALK) and acts as a growth factor for different cell types. J Biol Chem 2002, 277:35990–35998
19. Evans AE, D'Angio GJ, Randolph J: A proposed staging for children with neuroblastoma: children's cancer study group A. Cancer 1971, 27:374–378
20. Nakagawara A, Arima-Nakagawara M, Scavarda NJ, Azar CG, Cantor AB, Brodeur GM: Association between high levels of expression of the TRK gene and favorable outcome in human neuroblastoma. N Engl J Med 1993, 328:847–854
21. Nakagawara A, Azar CG, Scavarda NJ, Brodeur GM: Expression and function of TRK-B and BDNF in human neuroblastomas. Mol Cell Biol 1994, 14:759–767
22. Nakagawara A, Nakamura Y, Ikeda H, Hiwasa T, Kulda K, Su MS, Zhao H, Cnaan A, Sakiyama S: High levels of expression and nuclear localization of interleukin-1 beta converting enzyme (ICE) and CPP32 in favorable human neuroblastomas. Cancer Res 1997, 57:4578–4584
23. Posmantur R, McGinnis K, Nadimpalli R, Gilbertsen RB, Wang K: Characterization of CPP32-like protease activity following apoptotic challenge in SH-SY5Y neuroblastoma cells. J Neurochem 1997, 68:2328–2337
24. Adida C, Berrebi D, Peuchmaur M, Reyes-Mugica M, Altieri DC: Anti-apoptosis gene, survivin, and prognosis of neuroblastoma. Lancet 1998, 351:882–883
25. Hiyama E, Hiyama K, Yokoyama T, Matsuura Y, Piatyszek MA, Shay JW: Correlating telomerase activity levels with human neuroblastoma outcomes. Nat Med 1995, 1:249–255
26. Lamant L, Pulford K, Bischof D, Morris SW, Mason DY, Delsol G, Mariame B: Expression of the ALK tyrosine kinase gene in neuroblastoma. Am J Pathol 2000, 156:1711–1721
27. Miyake I, Hakomori Y, Shinohara A, Gamou T, Saito M, Iwamatsu A, Sakai R: Activation of anaplastic lymphoma kinase is responsible for hyperphosphorylation of ShcC in neuroblastoma cell lines. Oncogene 2002, 21:5823–5834
28. Sakai R, Henderson JT, O'Bryan JP, Elia AJ, Saxton TM, Pawson T: The mammalian ShcB and ShcC phosphotyrosine docking proteins function in the maturation of sensory and sympathetic neurons. Neuron 2000, 28:819–833
29. Perucho M, Goldfarb M, Shimizu K, Lama C, Fogh J, Wigler M: Human-tumor-derived cell lines contain common and different transforming genes. Cell 1981, 27:467–476
30. Brodeur GM, Pritchard J, Berthold F, Carlsen NL, Castel V, Castelberry RP, De Bernardi B, Evans AE, Favrot M, Hedborg F, Kaneko M, Kemshead J, Lampert F, Lee RE, Look AT, Pearson AD, Philip T, Roald B, Sawada T, Seeger RC, Tsuchida Y, Voute PA: Revisions of the international criteria for neuroblastoma diagnosis, staging, and response to treatment. J Clin Oncol 1993, 11:1466–1477
31. Shimada H, Ambros IM, Dehner LP, Hata J, Joshi VV, Roald B, Stram DO, Gerbing RB, Lukens JN, Matthay KK, Castleberry RP: The International Neuroblastoma Pathology Classification (the Shimada system). Cancer 1999, 86:364–372
32. Ikeda I, Ishizaka Y, Tahira T, Suzuki T, Onda M, Sugimura T, Nagao M: Specific expression of the ret proto-oncogene in human neuroblastoma cell lines. Oncogene 1990, 5:1291–1296
33. Motegi A, Fujimoto J, Kotani M, Sakuraba H, Yamamoto T: ALK receptor tyrosine kinase promotes cell growth and neurite outgrowth. J Cell Sci 2004, 117:3319–3329
34. Slamon DJ, Clark GM, Wong SG, Levin WJ, Ullrich A, McGuire WL: Human breast cancer: correlation of relapse and survival with amplification of the HER-2/neu oncogene. Science 1987, 235:177–182
35. Tsuda H, Hirohashi S, Shimosato Y, Hirota T, Tsugane S, Yamamoto H, Miyajima N, Toyoshima K, Yamamoto T, Yokota J, Yoshida T, Sakamoto H, Terada M, Sugimura T: Correlation between long-term survival in breast cancer patients and amplification of two putative oncogene-coamplification units: hst-1/int-2 and c-erbB-2/ear-1. Cancer Res 1989, 49:3104–3108
36. Ganju P, O'Bryan JP, Der C, Winter J, James IF: Differential regulation of SHC proteins by nerve growth factor in sensory neurons and PC12 cells. Eur J Neurosci 1998, 10:1995–2008
37. Nakamura T, Komiya M, Gotoh N, Koizumi S, Shibuya M, Mori N: Discrimination between phosphotyrosine-mediated signaling properties of conventional and neuronal Shc adapter molecules. Oncogene 2002, 21:22–31
38. Nakamura T, Muraoka S, Sanokawa R, Mori N: N-Shc and Sck, two neuronally expressed Shc adapter homologs: their differential regional expression in the brain and roles in neurotrophin and Src signaling. J Biol Chem 1998, 273:6960–6967
39. O'Bryan JP, Songyang Z, Cantley L, Der CJ, Pawson T: A mammalian adaptor protein with conserved Src homology 2 and phosphotyrosine-binding domains is related to Shc and is specifically expressed in the brain. Proc Natl Acad Sci USA 1996, 93:2729–2734
40. Pelicci G, Troglio F, Bodini A, Melillo RM, Pettirossi V, Coda L, De Giuseppe A, Santoro M, Pelicci PG: The neuron-specific Rai (ShcC) adaptor protein inhibits apoptosis by coupling Ret to the phosphatidylinositol 3-kinase/Akt signaling pathway. Mol Cell Biol 2002, 22:7351–7363
41. Yuan J, Yankner BA: Apoptosis in the nervous system. Nature 2000, 407:802–809
42. De Vita G, Melillo RM, Carlomagno F, Visconti R, Castellone MD, Bellacosa A, Billaud M, Fusco A, Tsichlis PN, Santoro M: Tyrosine 1062 of RET-MEN2A mediates activation of Akt (protein kinase B) and mitogen-activated protein kinase pathways leading to PC12 cell survival. Cancer Res 2000, 60:3727–3731

Behavioral/Systems/Cognitive

Hippocampal Synaptic Modulation by the Phosphotyrosine Adapter Protein ShcC/N-Shc via Interaction with the NMDA Receptor

Yoshiaki Miyamoto,[1] Ling Chen,[2] Masahiro Sato,[1] Masahiro Sokabe,[2,3] Toshitaka Nabeshima,[4] Tony Pawson,[5] Ryuichi Sakai,[6] and Nozomu Mori[1,7]

[1]Department of Molecular Genetics, National Institute for Longevity Sciences, Oobu 474-8522, Japan, [2]Cell Mechanosensing Project, International Cooperative Research Project–Japan Science and Technology Agency, and Departments of [3]Physiology and [4]Neuropsychopharmacology and Hospital Pharmacy, Nagoya University Graduate School of Medicine, Nagoya 466-8560, Japan, [5]Department of Molecular and Medical Genetics, University of Toronto, Toronto, Ontario M5S 1A8, Canada, [6]Growth Factor Division, National Cancer Center Research Institute, Tokyo 104-0045, Japan, and [7]Department of Anatomy and Neurobiology, Nagasaki University School of Medicine, Nagasaki 852-8523, Japan

N-Shc (neural Shc) (also ShcC), an adapter protein possessing two phosphotyrosine binding motifs [PTB (phosphotyrosine binding) and SH2 (Src homology 2) domains], is predominantly expressed in mature neurons of the CNS and transmits neurotrophin signals from the TrkB receptor to the Ras/mitogen-activated protein kinase (MAPK) pathway, leading to cellular growth, differentiation, or survival. Here, we demonstrate a novel role of ShcC, the modulation of NMDA receptor function in the hippocampus, using *ShcC* gene-deficient mice. In behavioral analyses such as the Morris water maze, contextual fear conditioning, and novel object recognition tasks, ShcC mutant mice exhibited superior ability in hippocampus-dependent spatial and nonspatial learning and memory. Consistent with this finding, electrophysiological analyses revealed that hippocampal long-term potentiation in ShcC mutant mice was significantly enhanced, with no alteration of presynaptic function, and the effect of an NMDA receptor antagonist on its expression in the mutant mice was notably attenuated. The tyrosine phosphorylation of NMDA receptor subunits NR2A and NR2B was also increased, suggesting that ShcC mutant mice have enhanced NMDA receptor function in the hippocampus. These results indicate that ShcC not only mediates TrkB-Ras/MAPK signaling but also is involved in the regulation of NMDA receptor function in the hippocampus via interaction with phosphotyrosine residues on the receptor subunits and serves as a modulator of hippocampal synaptic plasticity underlying learning and memory.

Key words: **ShcC/N-Shc; phosphotyrosine adapter protein; learning and memory; long-term potentiation; hippocampus; NMDA receptor**

Introduction

Long-term potentiation (LTP) in the hippocampus, a well characterized form of activity-dependent synaptic plasticity, serves as a major cellular mechanism of learning and memory (Bliss and Collingridge, 1993; Malenka and Nicoll, 1999). The NMDA and AMPA types of glutamate receptors (GluRs) play critical roles in the induction of hippocampal LTP (Tsien et al., 1996; Zamanillo et al., 1999). In addition to the primary importance of the glutamate receptors, it has been reported that neurotrophins, particularly brain-derived neurotrophic factor (BDNF), modulate the maintenance of hippocampal LTP through the activation of TrkB receptor tyrosine kinases (Poo, 2001; Lu, 2003). Also, a variety of intracellular signaling cascades, including the Ras/mitogen-activated protein kinase (MAPK) pathway, are reported to influence LTP formation (Ohno et al., 2001; Silva, 2003).

The BDNF-activated TrkB receptors recruit various adapter proteins such as Shc, Frs-2, and phospholipase-Cγ (PLCγ). The adapter proteins are tyrosine phosphorylated by the activated TrkB receptors and determine the flow of downstream intracellular signaling cascades to cellular growth, differentiation, or survival. Binding of Shc or Frs-2 leads to the activation of Ras/MAPK and PI3K (phosphoinositide-3 kinase)/Akt pathways, whereas binding of PLCγ stimulates the release of intracellular Ca^{2+} via inositol 1,4,5-trisphosphate (IP3) and thereby activates the Ca^{2+}–calmodulin-dependent kinase IV (CaMKIV) pathway (Kaplan and Miller, 2000; Patapoutian and Reichardt, 2001). Therefore, it is hypothesized that TrkB-Ras/MAPK signaling plays a role in the hippocampal LTP underlying learning and memory (Adams and Sweatt, 2002; Ying et al., 2002).

The Shc family consists of ShcA/Shc (p66, p52, and p46 isoforms), ShcB/Sck (p68), and ShcC/neural Shc (N-Shc) (p69 and p55), and possesses two modular regions that bind to phosphorylated tyrosine-containing peptide motifs: a PTB (phosphoty-

Received March 3, 2004; revised Dec. 30, 2004; accepted Jan. 3, 2005.

The initial part of this work was supported by the program "Protecting the Brain" of the Core Research for Evolutional Science and Technology–Japan Science and Technology Agency, and later, in part, by a Virtual Research Institute of Aging fund of Nippon Boehringer Ingelheim, the Uehara Memorial Research Fund, Funds for Comprehensive Research on Aging and Health from Ministry of Health, Labor, and Welfare, and grants-in-aid from the Ministry of Education, Culture, Sports, Science, and Technology of Japan. We thank Dr. T. Nakamura for valuable advice and I. Nakano and Y. Kadokawa for technical assistance and laboratory maintenance.

Correspondence should be addressed to Dr. Nozomu Mori, Department of Anatomy and Neurobiology, Nagasaki University School of Medicine, 1-12-4 Sakamoto, Nagasaki 852-8523, Japan. E-mail: morinosm@net.nagasaki-u.ac.jp.

DOI:10.1523/JNEUROSCI.3030-04.2005

 0270-6474/05/251826-10$15.00/0

rosine binding) domain and an SH2 (Src homology 2) domain. All of the Shc family members serve to link a number of receptor tyrosine kinases with multiple intracellular signaling cascades. ShcA is widely expressed in most tissues, whereas both ShcB and ShcC are predominantly expressed in the nervous system (Cattaneo and Pelicci, 1998; Ravichandran, 2001). The brain-enriched ShcC would be in a good position to modulate the hippocampal LTP via regulation of TrkB-Ras/MAPK signaling, because it has been implicated in the BDNF-TrkB signaling toward the Ras/MAPK pathway in cultured cells (Nakamura et al., 1998; Liu and Meakin, 2002).

Recent studies revealed that the so-called "Shc site" of the TrkB receptor (Tyr^{515}) was not relevant to the hippocampal LTP, because mice with a targeted point mutation of the TrkB–Shc site showed apparently no significant change in LTP formation (Korte et al., 2000; Minichiello et al., 2002). These findings are in contrast to the aforementioned hypothesis pointing to a role for TrkB-Ras/MAPK signaling in the hippocampal LTP. Accordingly, in the present study, we attempted to clarify whether the phosphotyrosine adapter protein *ShcC*, which binds the TrkB–Shc site leading to the Ras/MAPK pathway, is involved in hippocampal functions, using *ShcC* gene-deficient mice. Based on the results presented herein, we propose a novel role for ShcC in hippocampal synaptic plasticity, as evidenced by the enhancement of hippocampal LTP and hippocampus-dependent learning and memory in ShcC mutant mice.

Materials and Methods

Animals. Mice lacking ShcC were generated by Sakai et al. (2000). The homozygous mutant mice (−/−; 3 months of age) and the littermate 2 wild-type mice (+/+; 3 months of age) were obtained by crossing F2 heterozygous mutant mice (+/−). The genotypes of mice were determined by Southern blot analyses of tail DNA. C57BL/6 mice (Nihon SLC, Hamamatsu, Japan) were used for biochemical analyses of the Shc family members. The mice were housed in plastic cages and were kept in a regulated environment (24 ± 1°C; 50 ± 5% humidity), with a 12 h light/dark cycle (lights on at 9:00 A.M.). Food and tap water were available *ad libitum*. All of the experiments were performed in accordance with the Guidelines for Animal Experiments of the Nagoya University School of Medicine. The procedures involving animals and their care were conducted in conformity with the international guidelines *Principles of Laboratory Animal Care* (National Institutes of Health publication 85-23, revised 1985).

Plasmids and antibodies. Plasmids encoding cDNAs of mouse p52-ShcA, p68-ShcB, and p55-ShcC were as described previously (Kojima et al., 2001) and were epitope-tagged with T7 at the N terminus. Antibodies against ShcA (catalog #S68020) and ShcC (S55720) were obtained from Transduction Laboratories (San Diego, CA). Antibody against ShcB was prepared as described previously (Sakai et al., 2000). Anti-phosphotyrosine antibody (catalog #05-321) was purchased from Upstate Biotechnology (Charlottesville, VA). Antibodies against NR1 (catalog #sc-9058), NR2A (catalog #sc-9056), NR2B (catalog #sc-9057), postsynaptic density 95 (PSD95) (catalog #sc-6926), Src (catalog #sc-5266), Fyn (catalog #sc-434), and the Src family (catalog #sc-18) were from Santa Cruz Biotechnology (Santa Cruz, CA). Anti-phospho-Src family (Tyr^{418}) antibody (catalog #44-660) was purchased from Biosource (Camarillo, CA).

Northern blot analysis. Total RNAs were isolated using TRIzol reagents (Invitrogen, Carlsbad, CA). Isolated total RNAs (20 μg) were electrophoresed on a formalin/agarose gel and blotted onto a positively charged nylon membrane. Specific cDNA probes for the Shc family members were made by Megaprime DNA labeling systems and [α-^{32}P]dCTP (Amersham Biosciences, Piscataway, NJ) and purified with NucTrap Probe Purification Columns (Stratagene, La Jolla, CA). Membranes were hybridized with the ^{32}P-labeled cDNA probes as described previously (Nakamura et al., 1998).

In situ *hybridization analysis.* Mouse brain sections (15 μm) were cut on a cryostat, thaw-mounted on poly-L-lysine-coated slides, and stored at −80°C until use. The frozen brain sections were brought to room temperature and air-dried. The sections were postfixed with 4% paraformaldehyde in 0.1 M phosphate buffer, acetylated with 0.25% acetic anhydride in 0.1 M triethanolamine, and dehydrated through an ascending series of ethanol concentrations. To prepare antisense and sense cRNA probes, the plasmids encoding cDNA of ShcA, ShcB, or ShcC were linearized by cutting at a single site (antisense, *Eco*RI; sense, *Hin*dIII). *In vitro* transcription was performed using RNA polymerase (antisense, T7 RNA polymerase; sense, SP6 RNA polymerase) and [α-^{35}S]UTP (ICN Biomedicals, Costa Mesa, CA). *In situ* hybridization with the ^{35}S-labeled cRNA probes was performed as described previously (Nakamura et al., 1998). The sections were counterstained with thionine and dehydrated. The images were captured by the HC-2000 video camera system (Fuji Photo Film, Tokyo, Japan) and reconstructed using computer software.

Western blot analysis and immunoprecipitation assay. Mouse brains were homogenized in a lysis buffer [50 mM Tris-HCl, pH 7.5, 150 mM NaCl, 5 mM EDTA, 10 mM NaF, 1 mM sodium orthovanadate, 1% Triton X-100, 0.5% sodium deoxycholate, 1 mM phenylmethylsulfonyl fluoride, and protease inhibitor mixture (Complete; Roche, Mannheim, Germany)] or a modified lysis buffer containing 0.1% SDS for immunoprecipitation assays. For Western blot analysis, total proteins (10 μg) were separated by SDS-PAGE and blotted onto a polyvinylidene difluoride (PVDF) membrane. For immunoprecipitation assays, total proteins (500 μg) were incubated with an appropriate antibody and then protein G-Sepharose was added and further incubated. The immunoprecipitates were recovered by centrifugation and resuspended in a sample buffer. The samples (10 μl) were separated by electrophoresis and blotted onto a PVDF membrane. The membranes were incubated with primary antibodies, and proteins were detected by HRP-conjugated secondary antibodies using the ECL detection kit (Amersham Biosciences).

Histological analysis. Mouse brains were perfused with 4% paraformaldehyde in PBS and removed. Sections (15 μm) were cut, mounted on slides, and stored at −80°C until use. Nissl staining was done according to standard procedures. The images were captured with an HC-2000 video camera system. For immunochemical staining, the sections were permeabilized with 0.2% Triton X-100, blocked with 3% BSA, and incubated with antibody against microtubule-associated protein 2 (MAP2) (catalog #M1406; Sigma, St. Louis, MO). To detect specific signals for MAP2, the sections were incubated with Alexa Fluor 488-conjugated secondary antibody (catalog #A-11029; Molecular Probes, Eugene, OR). Fluorescence images were obtained with the confocal imaging system Micro Radiance (Bio-Rad Laboratories, Hercules, CA).

Behavioral analysis. To measure locomotor activity, a mouse was placed in a transparent acrylic cage with a black Plexiglas floor (45 × 26 × 40 cm), and locomotion and rearing were measured for 60 min using infrared counters (Scanet SV-10; Toyo Sangyo, Toyama, Japan).

To measure nociceptive responses to electric footshock, a mouse was placed in a transparent Plexiglas cage with a grid floor for footshock (25 × 30 × 11 cm) and an ascending footshock series (0.01, 0.02, 0.03, 0.04, 0.05, 0.06, 0.08, 0.10, 0.13, 0.16, 0.20, 0.25, 0.30, 0.40, 0.50, and 0.60 mA for 0.5 s; 30 s interval) was delivered through an electric shock generator (NS-SG01; Neuroscience, Tokyo, Japan). The electric current needed to elicit first flinching, vocalizing, or jumping behavior was recorded as the footshock threshold.

For the Morris water maze task, a pool (120 cm in diameter) was prepared with white plastic, and the water temperature was maintained at 20°C. Swimming paths were analyzed by a computer system with a video camera (AXIS-90 Target/2; Neuroscience). In the hidden-platform test, the platform (7 cm in diameter) was submerged 1 cm below the water surface. Mice did not swim in the pool before training. Three starting positions were used pseudorandomly, and each mouse was trained with three trials per day for 6 d. After reaching the platform, the mouse was allowed to remain on it for 30 s. If the mouse did not find the platform within 60 s, the trial was terminated and the animal was put on the platform for 30 s. In the platform transfer test, the mouse swam for 60 s in the pool without the platform. In the visible-platform test, the black platform was located 1 cm above the water surface.

For the fear conditioning task, a mouse was placed in a training cage (25 × 30 × 11 cm), which consisted of transparent Plexiglas with a grid floor for footshock, and the freezing response as the immobility time was measured for 2 min in the absence of sound and footshock (preconditioning) using Scanet SV-10AQ (Toyo Sangyo), which can measure automatically the immobility time by digital counters with infrared sensors. In the conditioning, the mouse was again placed in the cage, and the pretrial time of 2 min was followed by a 15 s tone stimulus (80 dB). During the last 5 s of the tone stimulus, a footshock of 0.8 mA was delivered through a shock generator (NS-SG01; Neuroscience). This procedure was repeated four times with 15 s intervals. In the pseudoconditioning, the mouse was exposed to the conditioning without footshock. For the contextual test 24 h after the conditioning, the mouse was placed back in the same cage in the absence of sound and footshock. For the cued test 24 h after the conditioning, the mouse was placed in a novel cage (45 × 26 × 40 cm), which was made of a transparent acrylic cage with a black Plexiglas floor, in the presence of a continuous tone stimulus.

For the novel object recognition task, a mouse was habituated to a black plastic cage (30 × 30 × 50 cm) for 3 d. In the training, two novel objects were placed in the cage, and the mouse was allowed to explore freely for 5 min. Time spent exploring each object was recorded manually. In retentions 2 or 24 h after the training, the mouse was placed back in the same cage, in which one of the familiar objects used in the training was replaced by a novel object, and allowed to explore for 5 min. Exploratory preference, a ratio of time spent exploring any one of the two objects (training) or the novel one (retention) over the total time spent exploring both objects, was used to measure recognition memory.

Electrophysiological analysis. Mouse brains were removed and kept in artificial CSF (ACSF) (in mM: 128 NaCl, 1.7 KCl, 26 $NaHCO_3$, 1.2 KH_2PO_4, 2.4 $CaCl_2$, 1.3 $MgSO_4$, and 10 glucose). ACSF was saturated with a mixture of 95% O_2/5% CO_2. Slices of the hippocampus (350 μm) were prepared using a microslicer (DTK-1500; Dosaka EM, Kyoto, Japan) and placed for 1 h in an incubation chamber filled with ACSF. The slices were stained with a voltage-sensitive dye, RH 482 (0.1 mg/ml; Nippon Kanko-Shikiso Kenkyusho, Okayama, Japan). The stained slices were transferred to a recording chamber mounted on an inverted microscope (IMT-2; Olympus, Tokyo, Japan). The recording chamber was continuously perfused with ACSF. The optical recording system (HR Deltaron 1700; Fuji Photo Film) consists of an area sensor with 128 × 128 photodiodes and a data-processing unit. Each photodiode receives optical signals from a 25 × 25 μm sample area, thus creating a 3.3 × 3.3 mm recording field. For optical recordings, an ACSF-filled glass electrode was placed in the hippocampal CA3 area. Schaffer collateral afferents were then stimulated with 300 μA/200 μs pulses, and a test stimulus was delivered at 0.06 Hz by a stimulator (SEN-3301; Nihon Kohden, Tokyo, Japan). In each trial, background signals were recorded for 10 ms before the electrical stimulus and stored as a reference image. Images after the stimulus were recorded at 0.6 ms/frame, and the difference signals from the reference image were digitized into 8 bit signals. The digitized signals were then amplified 400 times. To improve the signal-to-noise ratio, 16 trial images were averaged into a single image. A total of 150 sequential images, corresponding to a ~90 ms recording time, were collected from one experiment. The level of neuronal activities was indicated with pseudocolor (256 colors). To analyze the time course of activities in a given sample area, data from each pixel were stored, retrieved, and plotted as a function of time using Origin 5.0 (OriginLab, Northampton, MA).

In vitro *kinase assay.* Immunoprecipitates from the hippocampus were suspended in Src kinase reaction buffer (in mM: 100 Tris-HCl, pH 7.5, 125 $MgCl_2$, 25 $MnCl_2$, 2 EGTA, 0.2 sodium orthovanadate, and 2 dithiothreitol). The kinase assay was performed using a Src kinase kit (catalog #17-131; Upstate Biotechnology).

Pharmacological treatment of tissue slices. The hippocampi were quickly dissected and sliced in two directions at a thickness of 350 μm using a McIlwain tissue chopper (Mickle Laboratory Engineering, Gomshall, UK). The hippocampal slices were incubated at 37°C for 1 h in the netwell chamber (Corning, Corning, NY) filled with ACSF, which was continuously saturated with a mixture of 95% O_2/5% CO_2, and then exposed to ACSF in the presence of glutamate (100 μM), glycine (10 μM), and spermidine (1 mM) for 5 min. After a wash in ice-cold ACSF, the slices were homogenized in the modified lysis buffer.

Statistical analysis. All of the data were expressed as mean ± SEM. Statistical differences between the mutant mice and the wild-type mice were determined with Student's *t* comparison test. In the analysis of the visible or hidden test in the Morris water maze test, statistical differences were determined by an ANOVA with repeated measures. In the analysis of the transfer test in the Morris water maze, fear conditioning, and novel object recognition tasks, statistical differences among values for individual groups were determined by ANOVA, followed by the Student–Newman–Keuls multiple comparisons test when *F* ratios were significant ($p < 0.05$).

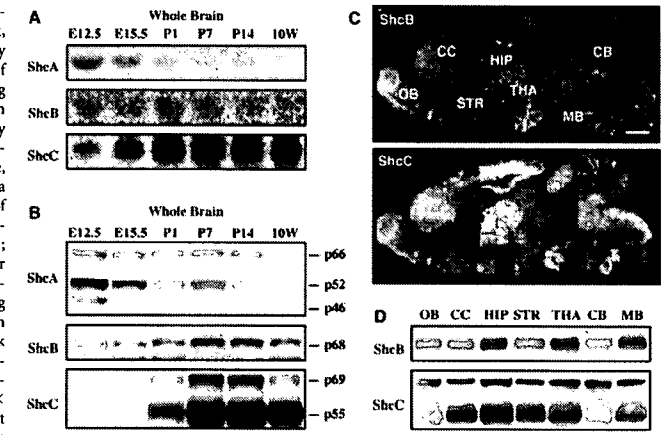

Figure 1. Expression profiles of Shc family members in the brain. *A*, mRNA expression of Shc family members during brain development. Total RNAs from whole brain in various developmental stages were examined by Northern blot analysis. *B*, Protein expression of Shc family members during brain development. Protein extracts from whole brain in various developmental stages were examined by Western blot analysis. *C*, mRNA expression of ShcB and ShcC in the mature brain [10 weeks of age (10W)]. mRNAs were examined by *in situ* hybridization analysis. Scale bar, 1 mm. *D*, Protein expression of ShcB and ShcC in various regions of the mature brain (10W). Protein extracts from various regions of the brain were examined by Western blot analysis. E12.5 and E15.5, Embryonic days 12.5 and 15.5; OB, olfactory bulb; CC, cerebral cortex; HIP, hippocampus; STR, striatum; THA, thalamus; CB, cerebellum; MB, midbrain.

Results

ShcC/N-Shc, a major phosphotyrosine adapter protein in the mature hippocampus

The gene expression of Shc-related phosphotyrosine adapter proteins was under dynamic regulation during the mammalian brain development (Fig. 1*A*,*B*). The expression level of ShcA, both the mRNA and protein, decreased during perinatal development and almost disappeared by 10 weeks of age. In contrast, that of ShcC increased gradually during postnatal development, with a peak at approximately postnatal day 7 (P7) to P14. However, ShcB mRNA levels remained low and invariable at all of the developmental stages, whereas its protein levels existed relatively high at P7 and P14. *In situ* hybridization analysis of young adults at 10

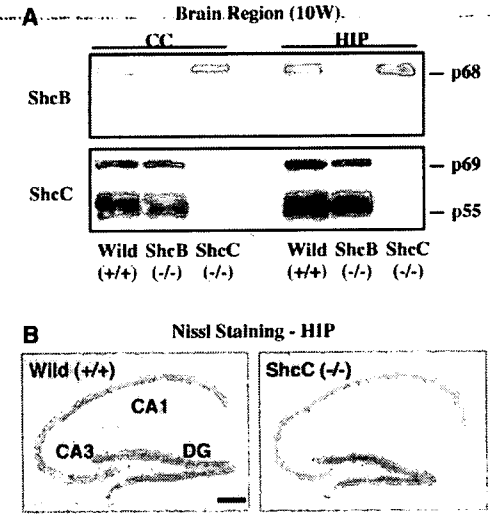

Figure 2. Hippocampal morphology in ShcC mutant mice. *A*, Protein expression of ShcB and ShcC in ShcC mutant mice [10 weeks of age (10W)]. Protein extracts from the cerebral cortex (CC) and hippocampus (HIP) of ShcB and ShcC mutant mice were examined by Western blot analysis. *B*, Nissl staining in the hippocampus of ShcC mutant mice (10W). DG, Dentate gyrus. Scale bar, 200 μm.

weeks of age revealed that ShcC mRNA was highly expressed in the cerebral cortex, hippocampus, and thalamus (Fig. 1*C*). In contrast, the expression of ShcB mRNA was rather ubiquitous (Fig. 1*C*). The regional expression of ShcC protein correlated with the mRNA data, whereas that of ShcB protein was different from mRNA and showed some deviations (i.e., a few high expressions in the hippocampus, thalamus, and midbrain) (Fig. 1*D*). The expression of ShcA was negligible in the various regions of the brain at 10 weeks of age (data not shown). These findings indicate that ShcC is the primary phosphotyrosine adapter protein among the Shc family members in the hippocampus of adult animals.

Histological appearance of hippocampal neurons in ShcC mutant mice

ShcC mutant mice exhibited a complete loss of ShcC protein, but the expression of ShcB was unaffected in most regions of the brain at 10 weeks of age (Fig. 2*A*, cerebral cortex and hippocampus). Neuroanatomically, the hippocampus of ShcC mutant mice revealed no gross structural abnormalities on Nissl staining compared with that of wild-type mice (Fig. 2*B*). MAP2 immunostaining for the dendrites of neurons in the hippocampal CA1 area of the mutant mice gave a pattern indistinguishable from that in wild-type mice (data not shown). Thus, the deficiency of ShcC did not significantly alter the hippocampal morphology in the mature brain.

Enhancement of hippocampus-dependent learning and memory in ShcC mutant mice

To investigate whether a deficiency of ShcC affects neuronal functions of the mature brain, we examined the performance of ShcC mutant mice in several behavioral paradigms. We first tested motor coordination and nociceptive response. The motility in a novel environment was measured for both horizontal (locomotion) and vertical (rearing) activities. Neither locomotion nor rearing during a 60 min observation period differed significantly between the wild-type mice (locomotion, 13,122.2 ± 1197.8 counts; rearing, 70.7 ± 13.8 counts) and ShcC mutant mice (locomotion, 13,355.0 ± 1405.0 counts; rearing, 81.8 ± 14.1 counts). Furthermore, no aberrant nociceptive responses to electric footshocks were observed in the ShcC mutant mice: the footshock threshold in the mutant mice (flinching, 0.045 ± 0.002 mA; vocalizing, 0.233 ± 0.027 mA; jumping, 0.425 ± 0.031 mA) was the same as that in wild-type mice (flinching, 0.045 ± 0.004 mA; vocalizing, 0.228 ± 0.015 mA; jumping, 0.400 ± 0.046 mA). These results indicate no apparent abnormalities in either motor or sensory neuronal systems in the ShcC mutant mice, consistent with previous observations (Sakai et al., 2000).

We next tested spatial and nonspatial learning and memory in ShcC mutant mice using the paradigms of the Morris water maze, fear conditioning, and novel object recognition tasks. In the Morris water maze task, both the wild-type and ShcC mutant mice managed to learn the visible-platform test, but the escape latency to the platform was shorter for the mutant mice (ANOVA with repeated measures; $F_{(1,22)} = 4.446$; $p = 0.0010$) (Fig. 3*Aa*). In the hidden-platform test, which requires the activation of the NMDA receptors in the hippocampus (Morris et al., 1982; Tsien et al., 1996), ShcC mutant mice required less time to reach the platform than wild-type mice (ANOVA with repeated measures; $F_{(1,34)} = 3.689$; $p = 0.0034$) (Fig. 3*Ab*). Swimming speeds of the wild-type and ShcC mutant mice in the visible- and hidden-platform tests were essentially the same (swimming speed on the first day of the hidden-platform test; wild-type mice, 17.9 ± 1.2 cm/s; ShcC mutant mice, 18.6 ± 1.1 cm/s). Moreover, in the platform transfer test conducted after the hidden-platform test, the ShcC mutant mice exhibited greater preference for the trained quadrant than the wild-type mice (Fig. 3*Ac*).

We tested for associative memory in the contextual and cued fear conditioning tasks. The former is hippocampus dependent, whereas the latter is hippocampus independent (Phillips and LeDoux, 1992). Both types of fear conditioning task also require the activation of the NMDA receptors (Davis et al., 1987; Kim et al., 1992). The contextual and cued fear conditioning tasks were measured 24 h after an aversive event (footshock) using two separate sets of genotype groups. The freezing response before the footshock (preconditioning) did not differ between the wild-type and ShcC mutant mice (Fig. 3*B*). In the contextual fear conditioning test, the freezing response 24 h after the footshock in both the wild-type and ShcC mutant mice significantly increased compared with the preconditioning and pseudoconditioning groups, respectively, with the mutant mice exhibiting a much stronger response than wild-type mice (Fig. 3*B*). In contrast, in the cued fear conditioning test, there was no significant difference in the freezing response 24 h after the footshock between the wild-type mice (62.6 ± 5.1%) and ShcC mutant mice (64.6 ± 3.3%).

To examine visual recognition memory in ShcC mutant mice, we used a novel object recognition task, in which the activation of the NMDA receptors in the hippocampus is essential for the formation of recognition memory (Rampon et al., 2000). We used a 5 min training protocol to assess the enhancement of learning and memory. There was no difference in exploratory preference during the training between the wild-type and ShcC mutant mice (Fig. 3*C*), indicating that the two groups essentially had the same levels of curiosity and/or motivation to explore the two objects.

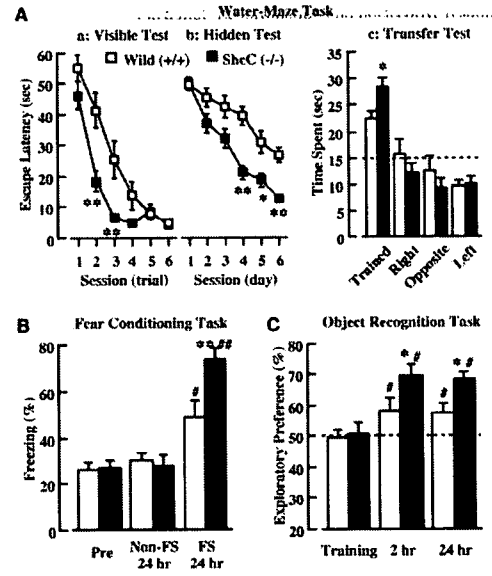

Figure 3. Hippocampus-dependent learning and memory in ShcC mutant mice. *A*, Morris water maze task. Escape latency in the visible (*a*)- and hidden (*b*)-platform tests. *c*, The time spent in each quadrant in the transfer test 24 h after the hidden-platform test. The time spent in the trained quadrant was significantly longer than that in any other quadrants in both the wild-type and ShcC mutant mice ($p < 0.05$; Student–Newman–Keuls multiple comparisons test). The dotted line represents performance by chance (15 s). *B*, Contextual fear conditioning test. The freezing response was measured for 2 min 24 h after the conditioning [FS (footshock)] or pseudoconditioning (Non-FS). *C*, Novel object recognition test. The time spent exploring two objects was measured for 5 min during training and retention 2 or 24 h after the training. The dotted line represents performance by chance (50%). Data represent mean ± SEM (n = 8–18). $^{*}p < 0.05$ and $^{**}p < 0.01$ versus corresponding wild type (+/+). $^{\#}p < 0.05$ and $^{\#\#}p < 0.01$ versus corresponding non-FS or training value in wild type (+/+).

In 2 and 24 h retention, however, ShcC mutant mice exhibited greater preference toward the novel object than wild-type mice (Fig. 3*C*).

Overall, these findings in the three different paradigms suggest that hippocampus-dependent spatial and nonspatial learning and memory is enhanced in the ShcC mutant mice, and this enhancement reflects neither increased motor activity nor altered nociceptive sensitivity.

Enhancement of hippocampal LTP in ShcC mutant mice

To investigate the synaptic properties in the hippocampus of ShcC mutant mice, we performed electrophysiological analyses using hippocampal slices. We used a high-speed optical recording technique in the hippocampal CA1 area by stimulating Schaffer collateral afferents from the CA3 area. With this technique, the optical signals evoked in the stratum radiatum of the CA1 area were broken down into two distinct elements, an initial spike-like component and an immediately following slow component, which could be separated by a notch in the control (Fig. 4*Aa*, arrow). These components represent the presynaptic fiber volley (PSFV) and EPSP, respectively, because the spike-like component left in Ca^{2+}-free medium (Fig. 4*Ab*) is eliminated by tetrodotoxin (TTX; 1 μM) (Fig. 4*Ad*) and the slow component is

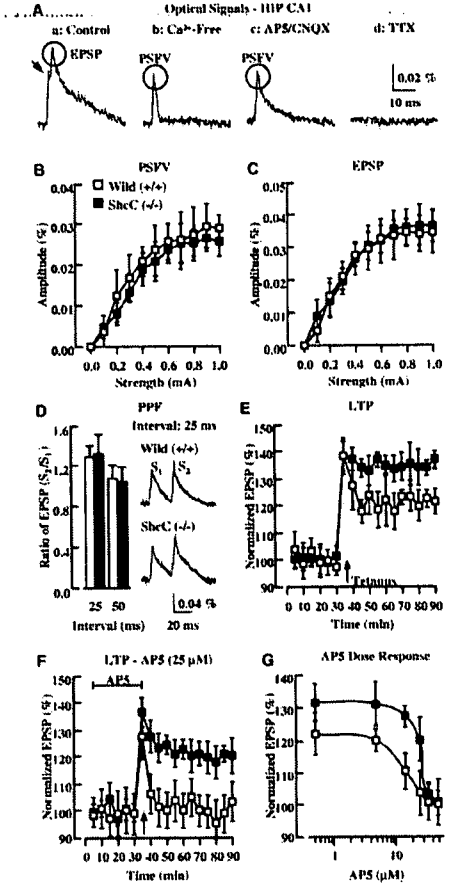

Figure 4. Hippocampal synaptic transmission and LTP in ShcC mutant mice. *A*, Optical signals in the stratum radiatum of the hippocampal (HIP) CA1 area. Representative traces of optical signal in response to an electrical stimulus of the Schaffer collateral fibers are shown. The control signal (*a*) is composed of PSFV (arrow) and EPSP; the former could be separated by treatment with Ca^{2+}-free medium (*b*) or AP-5 (50 μM)/CNQX (10 μM) (*c*) and eliminated by treatment with TTX (1 μM) (*d*). *B*, Amplitude of PSFV versus stimulus intensity. *C*, Amplitude of EPSP versus stimulus intensity. The input–output relationship of PSFV or EPSP is plotted against stimulus intensity at the Schaffer collateral-CA1 synapses (5 slices from 4 wild-type mice; 5 slices from 5 ShcC mutant mice). *D*, Paired-pulse facilitation (PPF). The data represent the facilitation of the second EPSP (S_2) relative to the first EPSP (S_1). Traces are the synaptic responses evoked by paired-pulse stimulation (interval, 25 ms) (4 slices from 3 wild-type mice; 4 slices from 3 ShcC mutant mice). *E*, Hippocampal LTP. Each point represents the mean ± SEM EPSP normalized to the baseline EPSP, which was the mean of EPSP for 20–30 min (7 slices from 4 wild-type mice; 7 slices from 4 ShcC mutant mice). Tetanic stimulation induced LTP at 90 min in the wild-type mice (121.2 ± 5.0%) and ShcC mutant mice (136.8 ± 3.4%; $p < 0.05$). *F*, Treatment with NMDA receptor antagonist AP-5. Each point represents the normalized mean of EPSP ± SEM in the presence of AP-5 (25 μM) for 5–35 min (4 slices from 4 wild-type mice; 6 slices from 4 ShcC mutant mice). Tetanic stimulation with AP-5 treatment failed to induce LTP in the wild-type mice (103.5 ± 7.0% at 90 min), and induced LTP in ShcC mutant mice (120.1 ± 6.7% at 90 min; $p < 0.05$). *G*, Dose–effect of AP-5 on LTP expression. Each point represents the normalized mean ± SEM EPSP at 60 min after the tetanic stimulation in the presence of different concentrations of AP-5 (4 slices from 4 wild-type mice; 6 slices from 4 ShcC mutant mice) (EC_{50}: wild-type mice, 15.2 μM; ShcC mutant mice, 26.6 μM).

blocked by D-2-amino-5-phosphonovaleric acid (AP-5; 50 μM)/6-cyano-7-nitroquinoxaline-2,3-dione (CNQX; 10 μM), competitive NMDA and AMPA receptor antagonists (Fig. 4*Ac*).

Initial experiments were designed to examine the input–output relationship of synaptic transmission by measuring two distinct components for a range of stimulus intensities. The amplitude of PSFV in the wild-type and ShcC mutant mice was almost the same (Fig. 4*B*), indicating that presynaptic properties were not altered in the mutant mice. There was no difference in the amplitude of EPSP between the wild-type and ShcC mutant mice (Fig. 4*C*), indicating that basal synaptic transmission remains normal in the mutant mice. Similarly, paired-pulse facilitation, which is a short-term enhancement of synaptic efficacy in response to a closely spaced second stimulus and reflects the probability of neurotransmitter release from afferent neurons, differed little between the wild-type and ShcC mutant mice (Fig. 4*D*). These results suggest that synaptic transmission does not deteriorate at the hippocampal Schaffer collateral-CA1 synapses in the ShcC mutant mice.

The LTP in the hippocampal CA1 area, a typical form of synaptic plasticity, is known to involve the activation of the NMDA receptors in its induction. We next examined the synaptic plasticity at hippocampal CA1 synapses using a high-frequency conditioning, tetanic stimulation (100 Hz; 1 s) to induce LTP. There was a marked difference in the expression of hippocampal LTP between the wild-type and ShcC mutant mice (Fig. 4*E*). The early phase of LTP in ShcC mutant mice was consistently enhanced during observation up to 60 min after the tetanic stimulation (wild-type mice, 121.2 ± 5.0%; ShcC mutant mice, 136.8 ± 3.4%; $p < 0.05$) (Fig. 4*E*, EPSP at 90 min). The treatment with AP-5 (25 μM) before the tetanic stimulation in wild-type mice completely blocked the expression of LTP, whereas that in ShcC mutant mice induced LTP (EPSP at 90 min) (wild-type mice, 103.5 ± 7.0%; ShcC mutant mice, 120.1 ± 6.7%; $p < 0.05$) (Fig. 4*F*). As shown in Figure 4*G*, AP-5 dose-dependently inhibited the expression of LTP in both the wild-type and ShcC mutant mice, but with different EC_{50} values of AP-5 between the two groups (wild-type mice, 15.2 μM; ShcC mutant mice, 26.6 μM). These results suggest that the enhancement of hippocampal LTP in ShcC mutant mice would arise from the functional alteration of postsynaptic NMDA receptors in the hippocampal CA1 area, because presynaptic function is normal in this area.

Increased phosphorylation of the NMDA receptors in the hippocampus of ShcC mutant mice

The NMDA receptors are formed by NR1 (GluRζ1) and NR2A to NR2D (GluRε1 to GluRε4) subunits (Hollmann and Heinemann, 1994; Nakanishi and Masu, 1994), and their activity is modulated by either the subunit composition of the receptor (Kutsuwada et al., 1992; Monyer et al., 1994) or phosphorylation of the subunits (Wang and Salter, 1994; Yu et al., 1997). To investigate NMDA receptor activity in the hippocampus of ShcC mutant mice, we examined the expression and phosphorylation levels of the receptor subunits. There was no difference in the expression level of the NR2A, NR2B, or NR1 subunit in the hippocampus between the wild-type and ShcC mutant mice (Fig. 5*A*). The expression level of PSD95, which regulates the signaling by the NMDA receptors, was the same in ShcC mutant mice as in wild-type mice (Fig. 5*A*). However, the tyrosine phosphorylation level of NR2A or NR2B in ShcC mutant mice showed a significant increase compared with that in wild-type mice (Fig. 5*A*). These findings suggest that the basal function of the NMDA receptors in the hippocampus of ShcC mutant mice is enhanced by the hyperphosphorylation at tyrosine residues of the receptor subunits.

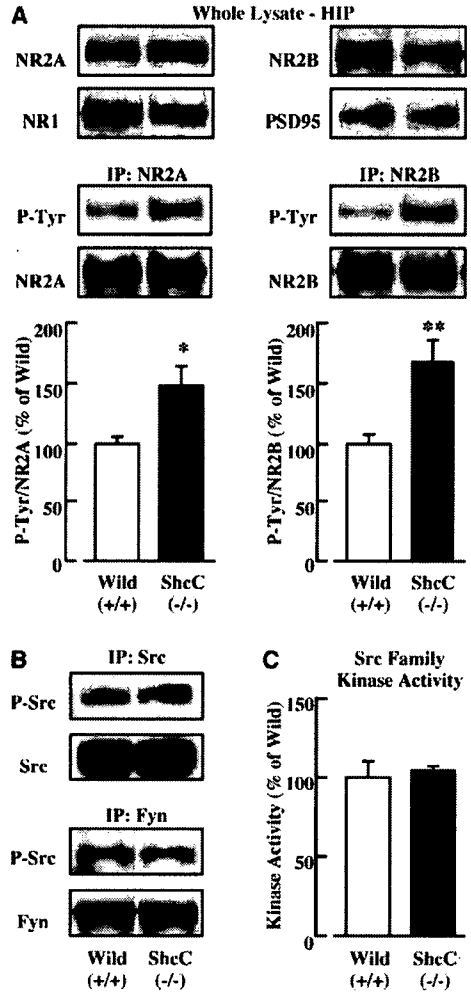

Figure 5. Phosphorylation of the NMDA receptors and kinase activity of the Src family in the hippocampus of ShcC mutant mice. *A*, Expression and tyrosine phosphorylation of the NR2A and NR2B subunits. The whole lysates of the hippocampus (HIP) were immunoblotted with anti-NR2A, -NR2B, -NR1, or -PSD95 antibody. To dissociate the NMDA receptor complex, hippocampal lysates with a modified lysis buffer were boiled for 5 min. The immunoprecipitates (IP) obtained with anti-NR2A or -NR2B antibody were immunoblotted with anti-phosphotyrosine (P-Tyr) antibody. *B*, Tyrosine phosphorylation at the activation site of Src and Fyn. The immunoprecipitates prepared with anti-Src or -Fyn antibody were immunoblotted with anti-phospho-Src (P-Src) family antibody. *C*, Kinase activity of the Src family *in vitro*. The immunoprecipitates obtained with anti-Src family antibody were subjected to an *in vitro* Src kinase assay. Data represent mean ± SEM ($n = 4$). *$p < 0.05$ and **$p < 0.01$ versus corresponding wild type (+/+).

Because the tyrosine phosphorylation of subunits NR2A and NR2B of the NMDA receptors is known to be modulated by the

Src family of cytoplasmic tyrosine kinases, including Src and Fyn (Hisatsune et al., 1999; Nakazawa et al., 2001), we tested the kinase activity of this family in the hippocampus of ShcC mutant mice. However, there was no notable difference in the tyrosine phosphorylation level at the activation site of Src or Fyn between the wild-type and ShcC mutant mice (Fig. 5*B*). Moreover, the kinase activity of the Src family in the mutant mice was similar to that in wild-type mice (Fig. 5*C*). These results indicate that increased tyrosine phosphorylation of the NMDA receptors in the ShcC mutant mice is not attributable to the activation of Src and Fyn.

Interaction of ShcC/N-Shc with the NMDA receptors and the Src family in the hippocampus

To clarify the regulatory mechanism of ShcC in NMDA receptor function involved in hippocampal synaptic plasticity, we investigated whether ShcC interacts with the NMDA receptors and the Src family. In an immunoprecipitation assay using lysates prepared from the hippocampus of wild-type mice, the NR1 or NR2B subunit of the NMDA receptors coprecipitated greatly with ShcC compared with other Shc family members (Fig. 6*A*). Similarly, Src (or Fyn) also interacted with ShcC (Fig. 6*A*). To further test whether these interactions would be affected by the activation of excitatory synaptic transmission, we examined the interaction between ShcC and the NR2B subunit or the Src family under conditions of glutamate stimulation in hippocampal slices from wild-type mice. After a 5 min stimulation with glutamate (100 μM) in the presence of glycine (10 μM) and spermidine (1 mM), both endogenous coactivators for the NMDA receptors, the amount of NR2B subunit coimmunoprecipitated with ShcC increased significantly (Fig. 6*B*). In the same conditions, the interaction of Src (or Fyn) with ShcC also increased significantly (Fig. 6*B*). These findings indicate that ShcC binds to the NMDA receptors and also associates with Src and/or Fyn in the mature hippocampus, and the formation of this ternary complex is stimulated by the activation of the excitatory glutamatergic neuronal system.

Discussion

In the present study, we demonstrated that the phosphotyrosine adapter protein ShcC/N-Shc is implicated in the modulation of hippocampal synaptic plasticity. However, as described in Introduction, hippocampal LTP may not rely on the Shc-mediated TrkB-Ras/MAPK signaling (Korte et al., 2000; Minichiello et al., 2002). Rather than the Shc/Ras/MAPK pathway, the PLCγ/IP3/CaMKIV pathway may be more relevant to the modulation of hippocampal LTP immediately downstream of the TrkB receptor (Minichiello et al., 2002). Thus, our results were unexpected, and we were interested in the novel role of ShcC to modulate the hippocampal LTP underlying learning and memory. We therefore estimate that the role of ShcC in hippocampal synaptic plasticity is independent of the Ras/MAPK pathway from the TrkB receptor and is critical to the modulation of NMDA receptor function, based on the attenuated effect of an NMDA receptor antagonist on LTP expression and the increased tyrosine phosphorylation of the NMDA receptors in the hippocampus of ShcC mutant mice.

Role of ShcC/N-Shc in hippocampal synaptic plasticity via interaction with the NMDA receptor

We have shown here that ShcC specifically interacted with the NR2B subunit of the NMDA receptors and Src (or Fyn) of tyrosine kinases in the hippocampus, and these interactions were

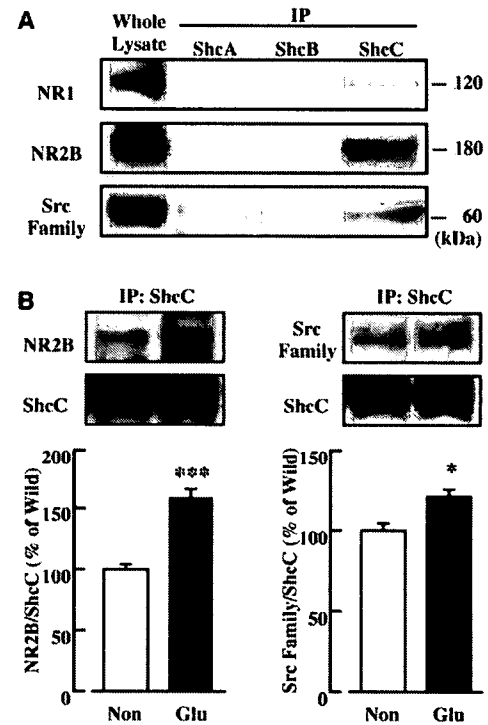

Figure 6. Interaction of ShcC with the NMDA receptors and the Src family in the hippocampus. *A*, Coimmunoprecipitation with Shc family members in the hippocampus. The immunoprecipitates (IP) obtained with antibodies for ShcA, ShcB, or ShcC were immunoblotted with anti-NR1, -NR2B, or -Src family antibody. *B*, Coimmunoprecipitation with ShcC in the hippocampus after glutamate (Glu) stimulation. Hippocampal slices were treated with glutamate (100 μM)/glycine (10 μM)/spermidine (1 mM) for 5 min. The immunoprecipitates (IP) prepared with anti-ShcC antibody were immunoblotted with anti-NR2B or -Src family antibody. Data represent mean ± SEM ($n = 4$). *$p < 0.05$ and ***$p < 0.001$ versus corresponding wild type (+/+).

enhanced by glutamate stimulation. The NR2B subunit is phosphorylated at several tyrosine residues by Src and Fyn (Hisatsune et al., 1999; Nakazawa et al., 2001), and the phosphorylation levels are upregulated by tetanic stimulation to induce hippocampal LTP (Rosenblum et al., 1996; Rostas et al., 1996). Thus, it is plausible that ShcC affects NMDA receptor function by binding to the receptor subunit via its phosphotyrosine binding property in an activity-dependent manner. Therefore, ShcC would regulate the receptor activation in the hippocampal LTP through Src family kinase-mediated tyrosine phosphorylation.

The elevated tyrosine phosphorylation levels of NMDA receptor subunits and normal kinase activity levels of the Src family in the hippocampus of ShcC mutant mice suggest that ShcC is implicated in the dephosphorylation of the receptor subunits. If the phosphorylation of the NMDA receptors is downregulated in the presence of ShcC, a potential role of ShcC could be to recruit a certain protein tyrosine phosphatase to the receptor multicomplex or to activate directly or indirectly a phosphatase for phosphotyrosine residues on the receptor subunits. Thus, ShcC binds

the phosphorylated NMDA receptor subunits and also may modulate the dephosphorylation status of the receptor subunits. Alternatively, if the NMDA receptor phosphorylation is upregulated in the presence of ShcC, the interaction of ShcC with a phosphorylated tyrosine of the receptor subunits may mask other tyrosine residues on the subunits from additional phosphorylation by the Src family. Otherwise, ShcC may inhibit activation of an unknown tyrosine kinase for the receptor subunits. Therefore, ShcC would contribute to the interaction between Src-like tyrosine kinase and a tyrosine phosphatase around the NMDA receptor multicomplex, to modulate the hippocampal synaptic plasticity via the receptor activation.

In general, synaptic plasticity is considered a leading candidate for a cellular mechanism of learning and memory (Bliss and Collingridge, 1993; Malenka and Nicoll, 1999), and a good correlation between NMDA receptor-dependent LTP and spatial learning and memory has been demonstrated (Tsien et al., 1996; Tang et al., 1999). Therefore, the superior hippocampus-dependent learning and memory in ShcC mutant mice would be primarily caused by the enhanced NMDA receptor-dependent hippocampal LTP. As evidence to support the above estimation, the difference in the performance of ShcC mutant mice between the contextual and cued fear conditioning tasks should be mentioned. The contextual associative memory is hippocampus dependent, whereas the cued associative memory is hippocampus independent (Phillips and LeDoux, 1992). Both associative memories also depend on the amygdala (Lavond et al., 1993) and NMDA receptor activation (Davis et al., 1987; Kim et al., 1992). Thus, the enhancement of only the former in ShcC mutant mice suggests the specific activation of the NMDA receptors in the hippocampus of the mutant mice.

However, the enhancement of behavioral performance in ShcC mutant mice was observed not only in the hidden-platform test of the Morris water maze task that depends on the hippocampus but also in the visible-platform test that is not necessarily hippocampus dependent. Thus, the performance of ShcC mutant mice in the present behavioral tasks may not be affected by only a specific improvement of hippocampus-dependent learning and memory. There are several explanations for the better performance of ShcC mutant mice in the latter test (e.g., the alteration of motility, emotionality, and visual acuity). Although there was at least no difference in the motility, especially swimming ability, of ShcC mutant mice, emotionality such as motivation to escape from water may be affected by alterations of NMDA receptor function in the hippocampus, because the alterations are known to influence emotion-associated neuronal circuits in other regions of the brain (e.g., the dopaminergic and serotonergic neuronal systems in the cerebral cortex and striatum) (Mohn et al., 1999; Miyamoto et al., 2001). Currently, there is no evidence that ShcC is involved in emotionality and those neuronal systems. However, because ShcC is expressed in the retinal ganglion cell during perinatal development (Nakazawa et al., 2002), a loss of ShcC may have some influence on the performance of visual acuity. Therefore, there is a need to investigate the emotional and visual performance in ShcC mutant mice.

Upstream and downstream signaling of the ShcC/N-Shc associated with hippocampal synaptic plasticity

We discussed above that ShcC plays a role in the modulation of hippocampal synaptic plasticity via interaction with the postsynaptic NMDA receptors but not with the BDNF-stimulated TrkB receptors. This idea is consistent with the findings that ShcC accumulates in the PSD (Suzuki et al., 1999) and BDNF is required for presynaptic but not postsynaptic modulation of LTP in the hippocampal CA3–CA1 synapses (Xu et al., 2000; Zakharenko et al., 2003). However, it remains possible that ShcC is involved in TrkB-mediated hippocampal synaptic plasticity at the postsynapses, because BDNF was taken up by postsynaptic neurons in an activity-dependent manner (Kohara et al., 2001). Thus, the enhanced hippocampal LTP in ShcC mutant mice may be caused in part by alterations of postsynaptic TrkB receptor signaling, for example, through activation of the PLCγ-mediated TrkB–IP3/CaMKIV pathway that is proposed to be relevant to hippocampal LTP (Minichiello et al., 2002). More studies are needed to clarify the signaling capabilities of the BDNF-stimulated TrkB receptors in the absence of ShcC and the signaling ability of ShcC as a go-between adapter protein for the TrkB and NMDA receptors, because NMDA receptor activation is frequently associated with TrkB-mediated hippocampal LTP (Suen et al., 1997; Levine et al., 1998). In addition, it is essential to investigate directly the NMDA receptor synaptic responses in ShcC mutant mice, because our findings showed only differences in the contribution of NMDA receptor to hippocampal LTP in the mutant mice.

Similarly to ShcC mutant mice, mice lacking H-Ras showed enhanced hippocampal LTP and tyrosine phosphorylation of the NMDA receptors (Manabe et al., 2000). These enhancements explained why the deficiency of H-Ras increased Src kinase activity and subsequently potentiated the receptor function associated with hippocampal LTP (Thornton et al., 2003). These findings might suggest that ShcC modulates NMDA receptor function for hippocampal LTP via inhibition of Src kinase activity through the Ras family, including H-Ras, because ShcC transmits BDNF-stimulated TrkB receptor signaling to the Ras/MAPK pathway (Nakamura et al., 1998; Liu and Meakin, 2002). In this study, however, Src and Fyn kinase activity were unaffected in the hippocampus of ShcC mutant mice, which was distinct from the case of H-Ras mutant mice.

Hippocampal synaptic modulation by ShcC may also involve other molecules. A novel 250 kDa Rho-GTPase activating protein (GAP) Grit (Nakamura et al., 2002), also termed RICS (Rho GAP involved in the β-catenin–N-cadherin and NMDA receptor signaling) (Okabe et al., 2003) or p250GAP (Nakazawa et al., 2003), is suggested to be involved in modulation of NMDA receptor signaling. Grit was identified originally as a binding partner of ShcC and is involved in neurotrophin-dependent neurite outgrowth via the specific modulation of cytoskeletal actin dynamics (Nakamura et al., 2002). Actin dynamics in dendritic spines have been implicated in hippocampal LTP (Engert and Bonhoeffer, 1999; Matus, 2000). Grit interacted with the NR2B subunit of the NMDA receptors, and this interaction was modulated by the receptor activation (Nakazawa et al., 2003). These findings suggest that Grit regulates the NMDA receptor-dependent actin reorganization in dendritic spines. Thus, the absence of ShcC may also influence the localization of Grit and further affect the postsynaptic remodeling of the cytoskeleton underneath the NMDA receptors, which is associated with hippocampal LTP underlying learning and memory (Milner et al., 1998). It could be that multiple molecules are needed to regulate synaptic function for hippocampal LTP (Sanes and Lichtman, 1999; Inoue and Okabe, 2003); however, ShcC would be a modulatory component of these molecules at the hippocampal synapses.

In summary, our observations revealed that the enhancement of hippocampal LTP in ShcC mutant mice is primarily attributable to an alteration of NMDA receptor function rather than an effect on the TrkB–Shc site. The current study established that the neural-specific phosphotyrosine adapter protein ShcC/N-Shc is a modulator of hippocampal synaptic plasticity underlying learning and memory.

References

Adams JP, Sweatt JD (2002) Molecular psychology: roles for the ERK MAP kinase cascade in memory. Annu Rev Pharmacol Toxicol 42:135–163.

Bliss TV, Collingridge GL (1993) A synaptic model of memory: long-term potentiation in the hippocampus. Nature 361:31–39.

Cattaneo E, Pelicci PG (1998) Emerging roles for SH2/PTB-containing Shc adaptor proteins in the developing mammalian brain. Trends Neurosci 21:476–481.

Davis M, Hitchcock J, Rosen JB (1987) Anxiety and the amygdala: pharmacological and anatomical analysis of the fear-potentiated startle paradigm. In: The psychology of learning and motivation (Bower GH, ed), pp 263–305. New York: Academic.

Engert F, Bonhoeffer T (1999) Dendritic spine changes associated with hippocampal long-term synaptic plasticity. Nature 399:66–70.

Hisatsune C, Umemori H, Mishina M, Yamamoto T (1999) Phosphorylation-dependent interaction of the *N*-methyl-D-aspartate receptor ε2 subunit with phosphatidylinositol 3-kinase. Genes Cells 4:657–666.

Hollmann M, Heinemann S (1994) Cloned glutamate receptors. Annu Rev Neurosci 17:31–108.

Inoue A, Okabe S (2003) The dynamic organization of postsynaptic proteins: translocating molecules regulate synaptic function. Curr Opin Neurobiol 13:332–340.

Kaplan DR, Miller FD (2000) Neurotrophin signal transduction in the nervous system. Curr Opin Neurobiol 10:381–391.

Kim JJ, Fanselow MS, DeCola JP, Landeira-Fernandez J (1992) Selective impairment of long-term but not short-term conditional fear by the *N*-methyl-D-aspartate antagonist APV. Behav Neurosci 106:591–596.

Kohara K, Kitamura A, Morishima M, Tsumoto T (2001) Activity-dependent transfer of brain-derived neurotrophic factor to postsynaptic neurons. Science 291:2419–2423.

Kojima T, Yoshikawa Y, Takada S, Sato M, Nakamura T, Takahashi N, Copeland NG, Gilbert DJ, Jenkins NA, Mori N (2001) Genomic organization of the Shc-related phosphotyrosine adapters and characterization of the full-length Sck/ShcB: specific association of p68-Sck/ShcB with pp135. Biochem Biophys Res Commun 284:1039–1047.

Korte M, Minichiello L, Klein R, Bonhoeffer T (2000) Shc-binding site in the TrkB receptor is not required for hippocampal long-term potentiation. Neuropharmacology 39:717–724.

Kutsuwada T, Kashiwabuchi N, Mori H, Sakimura K, Kushiya E, Araki K, Meguro H, Masaki H, Kumanishi T, Arakawa M, Mishina M (1992) Molecular diversity of the NMDA receptor channel. Nature 358:36–41.

Lavond DG, Kim JJ, Thompson RF (1993) Mammalian brain substrates of aversive classical conditioning. Annu Rev Psychol 44:317–342.

Levine ES, Crozier RA, Black IB, Plummer MR (1998) Brain-derived neurotrophic factor modulates hippocampal synaptic transmission by increasing *N*-methyl-D-aspartic acid receptor activity. Proc Natl Acad Sci USA 95:10235–10239.

Liu HY, Meakin SO (2002) ShcB and ShcC activation by the Trk family of receptor tyrosine kinases. J Biol Chem 277:26046–26056.

Lu B (2003) BDNF and activity-dependent synaptic modulation. Learn Mem 10:86–98.

Malenka RC, Nicoll RA (1999) Long-term potentiation—a decade of progress? Science 285:1870–1874.

Manabe T, Aiba A, Yamada A, Ichise T, Sakagami H, Kondo H, Katsuki M (2000) Regulation of long-term potentiation by H-Ras through NMDA receptor phosphorylation. J Neurosci 20:2504–2511.

Matus A (2000) Actin-based plasticity in dendritic spines. Science 290:754–758.

Milner B, Squire LR, Kandel ER (1998) Cognitive neuroscience and the study of memory. Neuron 20:445–468.

Minichiello L, Calella AM, Medina DL, Bonhoeffer T, Klein R, Korte M (2002) Mechanism of TrkB-mediated hippocampal long-term potentiation. Neuron 36:121–137.

Miyamoto Y, Yamada K, Noda Y, Mori H, Mishina M, Nabeshima T (2001) Hyperfunction of dopaminergic and serotonergic neuronal systems in mice lacking the NMDA receptor epsilon1 subunit. J Neurosci 21:750–757.

Mohn AR, Gainetdinov RR, Caron MG, Koller BH (1999) Mice with reduced NMDA receptor expression display behaviors related to schizophrenia. Cell 98:427–436.

Monyer H, Burnashev N, Laurie DJ, Sakmann B, Seeburg PH (1994) Developmental and regional expression in the rat brain and functional properties of four NMDA receptors. Neuron 12:529–540.

Morris RG, Garrud P, Rawlins JN, O'Keefe J (1982) Place navigation impaired in rats with hippocampal lesions. Nature 24:681–683.

Nakamura T, Muraoka S, Sanokawa R, Mori N (1998) N-Shc and Sck, two neuronally expressed Shc adapter homologs. Their differential regional expression in the brain and roles in neurotrophin and Src signaling. J Biol Chem 273:6960–6967.

Nakamura T, Komiya M, Sone K, Hirose E, Gotoh N, Morii H, Ohta Y, Mori N (2002) Grit, a GTPase-activating protein for the Rho family, regulates neurite extension through association with the TrkA receptor and N-Shc and CrkL/Crk adapter molecules. Mol Cell Biol 22:8721–8734.

Nakanishi S, Masu M (1994) Molecular diversity and functions of glutamate receptors. Annu Rev Biophys Biomol Struct 23:319–348.

Nakazawa T, Komai S, Tezuka T, Hisatsune C, Umemori H, Semba K, Mishina M, Manabe T, Yamamoto T (2001) Characterization of Fyn-mediated tyrosine phosphorylation sites on GluR ε2 (NR2B) subunit of the *N*-methyl-D-aspartate receptor. J Biol Chem 276:693–699.

Nakazawa T, Nakano I, Sato M, Nakamura T, Tamai M, Mori N (2002) Comparative expression profiles of Trk receptors and Shc-related phosphotyrosine adapters during retinal development: potential roles of N-Shc/ShcC in brain-derived neurotrophic factor signal transduction and modulation. J Neurosci Res 68:668–680.

Nakazawa T, Watabe AM, Tezuka T, Yoshida Y, Yokoyama K, Umemori H, Inoue A, Okabe S, Manabe T, Yamamoto T (2003) p250GAP, a novel brain-enriched GTPase-activating protein for Rho family GTPases, is involved in the *N*-methyl-D-aspartate receptor signaling. Mol Biol Cell 14:2921–2934.

Ohno M, Frankland PW, Chen AP, Costa RM, Silva AJ (2001) Inducible, pharmacogenetic approaches to the study of learning and memory. Nat Neurosci 4:1238–1243.

Okabe T, Nakamura T, Nishimura YN, Kohu K, Ohwada S, Morishita Y, Akiyama T (2003) RICS, a novel GTPase-activating protein for Cdc42 and Rac1, is involved in the β-catenin-N-cadherin and *N*-methyl-D-aspartate receptor signaling. J Biol Chem 278:9920–9927.

Patapoutian A, Reichardt LF (2001) Trk receptors: mediators of neurotrophin action. Curr Opin Neurobiol 11:272–280.

Phillips RG, LeDoux JE (1992) Differential contribution of amygdala and hippocampus to cued and contextual fear conditioning. Behav Neurosci 106:274–285.

Poo MM (2001) Neurotrophins as synaptic modulators. Nat Rev Neurosci 2:24–32.

Rampon C, Tang YP, Goodhouse J, Shimizu E, Kyin M, Tsien JZ (2000) Enrichment induces structural changes and recovery from nonspatial memory deficits in CA1 NMDAR1-knockout mice. Nat Neurosci 3:238–244.

Ravichandran KS (2001) Signaling via Shc family adapter proteins. Oncogene 20:6322–6330.

Rosenblum K, Dudai Y, Richter-Levin G (1996) Long-term potentiation increases tyrosine phosphorylation of the *N*-methyl-D-aspartate receptor subunit 2B in rat dentate gyrus *in vivo*. Proc Natl Acad Sci USA 93:10457–10460.

Rostas JA, Brent VA, Voss K, Errington ML, Bliss TV, Gurd JW (1996) Enhanced tyrosine phosphorylation of the 2B subunit of the *N*-methyl-D-aspartate receptor in long-term potentiation. Proc Natl Acad Sci USA 93:10452–10456.

Sakai R, Henderson JT, O'Bryan JP, Elia AJ, Saxton TM, Pawson T (2000) The mammalian ShcB and ShcC phosphotyrosine docking proteins function in the maturation of sensory and sympathetic neurons. Neuron 28:819–833.

Sanes JR, Lichtman JW (1999) Can molecules explain long-term potentiation? Nat Neurosci 2:597–604.

Silva AJ (2003) Molecular and cellular cognitive studies of the role of synaptic plasticity in memory. J Neurobiol 54:224–237.

Suen PC, Wu K, Levine ES, Mount HT, Xu JL, Lin SY, Black IB (1997) Brain-derived neurotrophic factor rapidly enhances phosphorylation of the postsynaptic *N*-methyl-D-aspartate receptor subunit 1. Proc Natl Acad Sci USA 94:8191–8195.

Suzuki T, Mitake S, Murata S (1999) Presence of up-stream and down-

stream components of a mitogen-activated protein kinase pathway in the PSD of the rat forebrain. Brain Res 840:36–44.
Tang YP, Shimizu E, Dube GR, Rampon C, Kerchner GA, Zhuo M, Liu G, Tsien JZ (1999) Genetic enhancement of learning and memory in mice. Nature 401:63–69.
Thornton C, Yaka R, Dinh S, Ron D (2003) H-Ras modulates NMDA receptor function via inhibition of Src tyrosine kinase activity. J Biol Chem 278:23823–23829.
Tsien JZ, Huerta PT, Tonegawa S (1996) The essential role of hippocampal CA1 NMDA receptor-dependent synaptic plasticity in spatial memory. Cell 87:1327–1338.
Wang YT, Salter MW (1994) Regulation of NMDA receptors by tyrosine kinases and phosphatases. Nature 369:233–235.
Xu B, Gottschalk W, Chow A, Wilson RI, Schnell E, Zang K, Wang D, Nicoll RA, Lu B, Reichardt LF (2000) The role of brain-derived neurotrophic factor receptors in the mature hippocampus: modulation of long-term potentiation through a presynaptic mechanism involving TrkB. J Neurosci 20:6888–6897.
Ying SW, Futter M, Rosenblum K, Webber MJ, Hunt SP, Bliss TV, Bramham CR (2002) Brain-derived neurotrophic factor induces long-term potentiation in intact adult hippocampus: requirement for ERK activation coupled to CREB and upregulation of Arc synthesis. J Neurosci 22:1532–1540.
Yu XM, Askalan R, Keil II GJ, Salter MW (1997) NMDA channel regulation by channel-associated protein tyrosine kinase Src. Science 275:674–678.
Zakharenko SS, Patterson SL, Dragatsis I, Zeitlin SO, Siegelbaum SA, Kandel ER, Morozov A (2003) Presynaptic BDNF required for a presynaptic but not postsynaptic component of LTP at hippocampal CA1–CA3 synapses. Neuron 39:975–990.
Zamanillo D, Sprengel R, Hvalby O, Jensen V, Burnashev N, Rozov A, Kaiser KM, Koster HJ, Borchardt T, Worley P, Lubke J, Frotscher M, Kelly PH, Sommer B, Andersen P, Seeburg PH, Sakmann B (1999) Importance of AMPA receptors for hippocampal synaptic plasticity but not for spatial learning. Science 284:1805–1811.

Crk-Associated Substrate Lymphocyte Type Is Required for Lymphocyte Trafficking and Marginal Zone B Cell Maintenance[1]

Sachiko Seo,* Takashi Asai,* Toshiki Saito,* Takahiro Suzuki,* Yasuyuki Morishita,† Tetsuya Nakamoto,* Motoshi Ichikawa,* Go Yamamoto,* Masahito Kawazu,* Tetsuya Yamagata,* Ryuichi Sakai,‡ Kinuko Mitani,§ Seishi Ogawa,* Mineo Kurokawa,[2]* Shigeru Chiba,* and Hisamaru Hirai*

The lymphocyte-specific Cas family protein Cas-L (Crk-associated substrate lymphocyte type) has been implicated to function in lymphocyte movement, mediated mainly by integrin signaling. However, its physiological role is poorly understood. In this study we analyzed the function of Cas-L in lymphocytes using gene-targeted mice. The mutant mice showed a deficit of marginal zone B (MZB) cells and a decrease of cell number in secondary lymphoid organs. An insufficient chemotactic response and perturbed cell adhesion were observed in Cas-L-deficient lymphocytes, suggesting that the aberrant localization was responsible for the deficit of MZB cells. Moreover, we found that lymphocyte trafficking was altered in Cas-L-deficient mice, which gave a potential reason for contraction of secondary lymphoid tissues. Thus, Cas-L affects homeostasis of MZB cells and peripheral lymphoid organs, which is considered to be relevant to impaired lymphocyte migration and adhesion. *The Journal of Immunology*, 2005, 175: 3492–3501.

The Crk-associated substrate (Cas)[3] lymphocyte-specific protein Cas-L, also known as human enhancer of filamentation 1 (1), was originally identified as a 105-kDa protein that is tyrosine-phosphorylated by the ligation of β_1 integrin in peripheral T cells (2). Cas-L is a docking protein in focal adhesion and consists of an N-terminal Src homology (SH)3 domain, a substrate domain containing multiple tyrosine motifs for SH2-binding sites, a serine-rich region, and a C-terminal dimerization motif (2). Owing to its homology with p130Cas (3), Cas-L is recognized as a member of the Cas family. Cas is expressed ubiquitously and plays a crucial role in integrin-mediated signaling. Our group demonstrated that the lack of Cas protein resulted in fetal death because of perturbed organogenesis (4). In contrast, Cas-L is predominantly expressed in lymphocytes and epithelial cells (1, 2), which implies that it has distinct functions from Cas.

Integrins are a family of adhesion receptors composed of α and β subunits. They are involved in cell-cell and cell-matrix interactions and induce various biological signals for cell adhesion, migration, apoptosis, proliferation, and differentiation (5–8). Among the integrin family, β_1 integrin constitutes the largest group that mediate cell attachment via fibronectin or VCAM-1. Previous reports showed that Cas-L is tyrosine-phosphorylated by binding to focal adhesion kinase or Pyk-2 in the SH3 domain upon engagement of β_1 integrin (9, 10). Subsequently, the phosphorylated Cas-L regulates several signals involved in cell motility (11–13) and cell adhesion (14) as a downstream effecter of focal adhesion kinase. In addition, Cas-L functions as a signal transducer of TCR (12, 15, 16), BCR (17), and G protein-coupled calcitonin receptor (18). The biological functions of Cas-L in lymphocytes, however, remain to be determined.

Early B cell development arises in bone marrow as immature B cells expressing surface IgM emigrate to the spleen (19). In the spleen, immature B cells can differentiate into follicular B (FOB) cells and marginal zone B (MZB) cells characterized by $IgM^{low}IgD^{high}CD21^{int}CD23^{high}$ and $IgM^{high}IgD^{low}CD21^{high}CD23^{low}$, respectively (20). A number of studies using gene-targeted mice have demonstrated loss of MZB cells in the mutant mice, and this defect of MZB cells was explained by two major mechanisms: failure of MZB cell development and impaired localization. MZB cell development is presumably related to BCR or Notch signal, as suggested from studies of mice lacking Aiolos, Lyn, Notch2, or RBP-J (21–24). The hypothesis of perturbed localization was derived from observations of altered lymphocyte motility in mice lacking Pyk-2, DOCK2, or Lsc (25–27). Despite several investigations, however, the precise mechanism of MZB cell development and localization remains unclear. In particular, no relevant mouse model that recapitulates a defect of integrin-mediated MZB cell retention has been obtained so far.

Lymphocyte trafficking is a multistep process mediated by chemokines and adhesion molecules (28). Lymphocytes express several kinds of chemokine receptors and integrin receptors. The chemokine CXCL12, previously called stromal cell-derived factor

*Department of Hematology and Oncology, Graduate School of Medicine, and †Department of Pathology, Faculty of Medicine, University of Tokyo, Tokyo, Japan; ‡Growth Factor Division, National Cancer Center Research Institute, Tokyo, Japan; and §Department of Hematology, Dokkyo University School of Medicine, Tochigi, Japan

Received for publication January 25, 2005. Accepted for publication July 1, 2005.

The costs of publication of this article were defrayed in part by the payment of page charges. This article must therefore be hereby marked *advertisement* in accordance with 18 U.S.C. Section 1734 solely to indicate this fact.

[1] This work was supported by grants-in-aid from the Ministry of Education, Culture, Sports, Science and Technology of Japan, and the Ministry of Health, Labor and Welfare of Japan.

[2] Address correspondence and reprint requests to Dr. Mineo Kurokawa, Department of Hematology and Oncology, Graduate School of Medicine, University of Tokyo, 7-3-1 Hongo, Bunkyo-ku, Tokyo 113-8655, Japan. E-mail address: kurokawa-tky@umin.ac.jp

[3] Abbreviations used in this paper: Cas, Crk-associated substrate; Cas-L, Cas lymphocyte-type; MZB, marginal zone B; FOB, follicular B; ES, embryonic stem; EGFP, enhanced GFP; TNP, 2,4,6-trinitrophenyl; KLH, keyhole limpet hemocyanin; SH, Src homology.

0022-1767/05/$02.00

1, is integral for mature B cell movement and is expressed in secondary lymphoid tissues, the red pulp in spleen, and the medullary cord in lymph nodes (29, 30). CXCL13, known as B lymphocyte chemoattractant, plays a crucial role in proper localization of B cells in peripheral lymphoid organs (31). With regard to adhesion molecules, previous studies have indicated that the integrin receptors LFA–1 ($\alpha_L\beta_2$) and VLA–4 ($\alpha_4\beta_1$) are involved in lymphocyte homing to peripheral lymph nodes or the splenic white pulp (32–34).

To elucidate the physiological function of Cas-L, we generated Cas-L-deficient mice using gene-targeting strategy. The mutant mice showed reduced numbers of lymphocytes in secondary lymphoid organs and an almost complete loss of MZB cells in the spleen. We demonstrated that Cas-L regulates responses to chemokines and adhesion molecules, and that its deficiency may be related to aberrant peripheral lymphoid organization including MZB cell maintenance.

Materials and Methods

Generation of Cas-L$^{-/-}$ *mice*

A genomic mouse C57BL/6 library was screened with a 300-bp *Cas-L* probe that included the SH3 region of *Cas-L*. A 15-kb clone identified with this probe was subcloned in pBlueScript and all of the genomic sequence was defined. A targeting vector was constructed using the following procedure. The enhanced GFP (pEGFP; Clontech) was directly combined with the *Cas-L* genome at the site of *Hin*dIII within exon 2, and a neomycin resistance cassette was infused to the vector. Electroporation was performed to insert the targeting vector into TT2 embryonic stem (ES) cells. Clones that underwent homologous recombination were selected in the presence of G418 and confirmed by PCR with a primer set containing the left arm. Correctly targeted ES clones were aggregated with eight cell-stage mouse embryos, and male chimeras were crossed with C57BL/6 females to generate mutant mice. To reveal a deficiency of the *Cas-L* gene in mutant mice, Southern blot analysis using the probe indicated was performed (see Fig. 1*A*). Mice were backcrossed with C57BL/6 mice eight times and bred under pathogen-free conditions. Analyses were performed using mainly 8- to 12-wk-old sex-matched littermates.

Western blot analysis

To confirm the deletion of Cas-L protein, thymi from wild-type and *Cas-L*$^{-/-}$ mice were homogenized in cold RIPA buffer (150 mM NaCl, 1% Nonidet P-40, 50 mM Tris (pH 8.0) and 5 mM EDTA-3Na). Cell lysates were incubated with anti-Cas Ab (BD Transduction Laboratories), which cross-reacts to Cas-L, and protein G-Sepharose (Amersham Biosciences) overnight at 4°C. The products of immunoprecipitation were segregated by 7.5% SDS-PAGE. The blotting was conducted with anti-goat human enhancer of filamentation 1 mAb, which developed against a peptide mapping at the N terminus (Santa Cruz Biotechnology).

Cell counts and flow cytometric analysis

Cells from each tissue were washed twice with PBS after hemolysis and enumerated. Peripheral blood was obtained by puncturing the retro-orbital venous plexus and cells were counted using an automatic cell counter (ERMA). Prepared cells were stained with relevant mAbs. Analyses were performed using FACSCalibur (BD Biosciences) and CellQuest software.

Immunohistochemistry

Spleens were frozen in Tissue-Tek OCT compound (Sakura Finetechnical) and cut at 5 μm. Sections were stained with FITC anti-mouse IgD and biotin anti-mouse IgM (BD Pharmingen) diluted to 1/100. IgM expression was detected using Alexa Fluor 594-conjugated streptavidin (Molecular Probes) diluted to 1/250. Confocal laser scanning microscope (Bio-Rad) was used.

Reconstitution of MZB cells

Bone marrow cells (Ly5.2$^+$) were derived from both sides of the femurs, and mononuclear cells were collected using Histopaque (Sigma-Aldrich). Mononuclear cells (1×10^6) in PBS with 10% FCS were i.v. injected into sublethally irradiated (950 rad) 8- to 10-wk-old female wild-type mice with Ly5.1 (C57BL/6). The recipients were sacrificed after 12 wk. The cells of donor origin, separated based on their cell surface expression of Ly5.1 or Ly5.2, were investigated for the presence of MZB cells using FACSCalibur. Fc block was performed by using anti-CD16/32 Abs (BD Pharmingen) to avoid any nonspecific binding of Ly5.

Measurement of intracellular Ca^{2+} concentration

Splenic B cells were purified as described and loaded with 3 μM Indo-1 (Molecular Probes) in RPMI 1640 medium with 1% FCS at 37°C for 45 min. After a rinse of Indo-1, the cells were stained with PerCP anti-mouse B220 (BD Pharmingen) to confirm the B cell fraction. Prepared cells were adjusted to 1×10^7 cells/ml and warmed to 37°C for 5 min. The basal Ca^{2+} concentration was recorded for 30 s. The increase in intracellular free Ca^{2+} after stimulation by 10 μg/ml anti-IgM F(ab')$_2$ (Jackson ImmunoResearch Laboratories) was subsequently measured for a further 5 min on LSR II (BD Biosciences).

Proliferation assay

Fresh splenocytes were purified by negative selection with MACS microBeads (Miltenyi Biotec). The purified splenic B cells were cultured in 96-well plates (10^5 cells/well) with several concentrations of anti-IgM F(ab')$_2$ (Jackson ImmunoResearch Laboratories) or with the combination of 3 μg/ml anti-IgM F(ab')$_2$, 5 μg/ml anti-CD40 (BD Pharmingen), 10 ng/ml recombinant mouse IL-4 (Genzyme/Techne), and 20 μg/ml LPS (Sigma-Aldrich) for 52 h. [^{3}H]Thymidine was added at 1 μCi/well and incubation was done for an additional 8 h.

Immunization and measurement of serum Ig titers

Seven- to 8-wk-old mice were immunized i.p. with 10 μg of 2,4,6-trinitrophenyl keyhole limpet hemocyanin (TNP-KLH; Biosearch Technologies) mixed with alum, given as a booster injection on day 21. Peripheral blood was obtained on day 28. TNP-specific Abs were determined by ELISA with the use of TNP-BSA (LSL). Ten- to 12-wk-old mice were immunized i.p. with 4×10^8 CFU of *Streptococcus pneumoniae* strain R36A, a kind gift of H. Ito, University of Kagoshima (Kagoshima, Japan). Serum was collected on day 7 and the anti-phosphorylcholine-specific Ig levels were measured by ELISA using phosphorylcholine-BSA (Biosearch Technologies). Nonparametric tests were performed on each Ig level.

Migration and adhesion assays

For chemotaxis assays, 5-μm pore-sized transwells (Costar) were used. Splenocytes were stained with CD21, CD23, B220, and Thy1.2. The prepared cells (1.5×10^6) in 100 μl of RPMI 1640 medium were added to the insert, and the bottom chamber was supplied with 450 μl of RPMI 1640 with CXCL12, CXCL13, or CCL21 (Genzyme/Techne) at various concentrations. Migration of the cells to the lower chamber was allowed for 3 h at 37°C. The cells prepared from wild-type or *Cas-L*$^{-/-}$ mice were counted and the number of FOB or T cells was calculated as a control by FACSCalibur. Subsequently, migrated cells were counted and the ratio of FOB or T cells to control cells was calculated. For adhesion assays, erythrocyte-depleted splenocytes on tissue culture plates were incubated at 37°C for 30 min to remove adherent macrophages and stained for CD21, CD23, B220, and Thy1.2. Microtiter wells for adhesion assays were coated with 0.5% BSA, various concentrations of human VCAM-1 (Genzyme/Techne), or recombinant mouse ICAM-1/Fc chimera (R&D Systems) by 1 h incubation at 37°C. Prepared cells (5×10^4 cells/well) were loaded in the precoated wells. After incubation at 37°C for 30 min, control cells in BSA-coated wells were collected and nonadherent cells were discarded. To detach adherent cells, 100 μl of RPMI 1640 medium with 5 mM EDTA and 0.5% BSA was added to each well and the plate was incubated for 15 min on ice. Removed cells were collected and counted on FACSCalibur. Each subset was presented by comparison with the number of the control cells.

Lymphocyte trafficking assay

Splenocytes (Ly5.2$^+$) from 8- to 10-wk-old wild-type or *Cas-L*$^{-/-}$ mice were divided into two portions. One portion was adjusted to a concentration of 4×10^7 cells/ml and labeled with a 3 μM BCECF-AM (2',7'-bis(carboxyethyl)-4(or 5)-carboxyfluorescein diacetoxymethyl ester; Dojindo Molecular Technologies) solution by incubation at 37°C for 10 min. The other portion was left unlabeled. Labeled cells from *Cas-L*$^{-/-}$ mice and unlabeled cells from wild-type mice were mixed equivalently and injected i.v. into 10- to 12-wk-old female wild-type mice with Ly5.1 (5×10^7 cells/mouse). To eliminate the effect of labeling with BCECF-AM, a complementary experiment was performed simultaneously. After 48 h, cells isolated from spleen, lymph nodes, and peripheral blood of each mouse were stained with Ly5.1, Ly5.2, and CD3 (or B220), and donor cells were separated from recipient cells using Ly5.1 and Ly5.2 by FACSCalibur. To avoid any nonspecific binding of Ly5, Fc block was performed using anti-CD16/32 Abs. The ratio of *Cas-L*$^{-/-}$ cells to control cells was evaluated by detecting BCECF-AM-positive cells among donor lymphocytes that colonized the spleen, lymph nodes, and peripheral blood.

Statistical analyses

Values of p for differences between groups were determined by Student's t test using Microsoft Excel software. Statistical analyses of measured serum Ig level were performed by Mann-Whitney U test.

Results

Generation of Cas-L-deficient mice

To generate Cas-L-deficient mice, the 1.2-kb *Cas-L* genomic region that contains exon 2 encoding the N-terminal SH3 domain in the Cas-L protein was replaced with EGFP and a neomycin resistance cassette by homologous recombination in ES cells. EGFP was introduced into the exon to generate a fusion protein (Fig. 1*A*). Correct integration of the targeting vector into the *Cas-L* genomic locus was identified by PCR and Southern blot analysis. Two ES cell lines with successful homologous recombination were used to generate chimeric mice and mutant mouse lines were established through germ-line transmission. The mutant loci were confirmed by Southern blot analysis of DNA isolated from the tale (Fig. 1*B*). Western blot analysis of cell lysates from the thymus showed a loss of Cas-L protein in mutant mice, although the possibility remains that truncated Cas-L proteins lacking the exon 2-dependent sequence were not detected (Fig. 1*C*). *Cas-L* mutant (*Cas-L*$^{-/-}$) mice were born with the expected Mendelian frequency and were apparently indistinguishable from wild-type littermates.

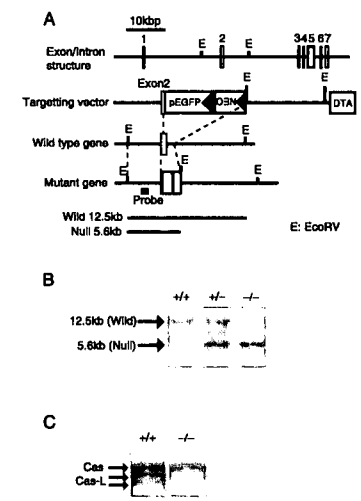

FIGURE 1. Generation of *Cas-L* mutant mice. *A*, Gene-targeting strategy. The exon coding the SH3 domain of *Cas-L* was replaced by EGFP and the neomycin resistance gene (Neo). The length of each diagnostic fragment and the probe position for Southern blotting are indicated. Restriction enzyme *Eco*RV was used for diagnosis. *B*, Southern blot analysis. Genomic DNA from the tails of wild-type (+/+), heterozygous (+/−), and homozygous (−/−) mice were digested with *Eco*RV. Hybridizations were performed with the probe shown in *A*. *C*, Western blot analysis. Proteins from thymi of wild-type and *Cas-L*$^{-/-}$ mice were examined by Western blot analysis using human enhancer of filamentation 1 mAb. The most slowly migrating band indicates Cas protein, whereas two faster migrating bands represent Cas-L proteins.

Reduced lymphocytes in peripheral lymphoid organs from Cas-L$^{-/-}$ *mice*

Because Cas-L is preferentially expressed in lymphocytes (2), we first examined peripheral lymphocyte populations in *Cas-L*$^{-/-}$ mice. *Cas-L*$^{-/-}$ mice had normal numbers of peripheral blood cells, which showed no morphological abnormality (Fig. 2*A*). No obvious alteration in the B or T cell populations was observed. Subsequent analyses of splenocytes showed a significant reduction of the total lymphocyte number, to ~50% of that in wild-type mice (Fig. 2*B*). Both B cell and T cell numbers in the spleen were significantly diminished in the absence of Cas-L. The ratio of T cells to B cells in the spleen was increased, which showed that B cells were more affected than T cells (data not shown). The populations of T and B cells in the lymph nodes were also investigated. The total number of lymphocytes and the numbers of T and B cells in *Cas-L*$^{-/-}$ were significantly reduced compared with those in wild-type mice (Fig. 2*C*). T cell subsets in the peripheral blood and secondary lymphoid tissues were assessed by measuring the cell surface expression of CD4 and CD8. The results showed a normal ratio of CD4 to CD8 in the mutant mice (data not shown). To examine whether these reductions result from abnormal hemopoiesis in the bone marrow, we analyzed the total cell number and

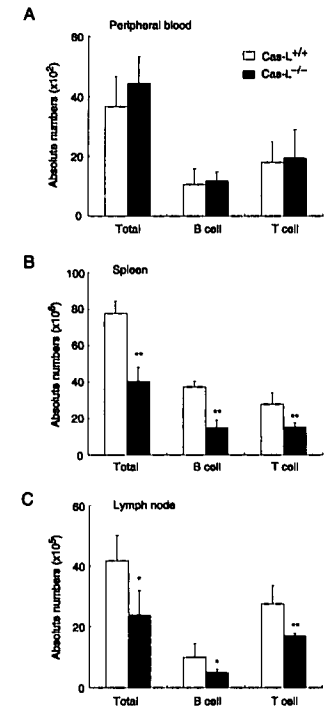

FIGURE 2. Peripheral lymphocyte population in Cas-L-deficient mice. Cells from peripheral blood (*A*), spleen (*B*), and lymph nodes (*C*) were collected from 8- to 10-wk-old mice and counted. B and T cell subsets were stained for CD19 and TCR-β, respectively, and analyzed by FACS. Data are mean ± SD from the experiments using seven mice. *, $p < 0.05$ and **, $p < 0.01$ analyzed with Student's t test.

B cell population in the bone marrow based on the criteria of Hardy et al. (35). The findings revealed no difference in the number of B cell subsets, suggesting that early B cell development was intact in the mutant mice (Table I). As for the thymus, no abnormality was detected in CD4 or CD8 single positive cell populations (data not shown). Taken together, these results indicate that Cas-L affects normal homeostasis in peripheral lymphoid compartments.

MZB cell defect in Cas-L-deficient mice

Because initial analyses showed a striking reduction in the number of B cells in the spleen of *Cas-L*$^{-/-}$ mice, late B cell development in the spleen was investigated. We examined the cell surface expression of CD21 and CD23 to discriminate among newly formed B cells (B220^{+}CD21^{low}CD23^{low}), FOB cells (B220^{+}CD21^{int}CD23^{high}), and MZB cells (B220^{+}CD21^{high}CD23^{low}). *Cas-L*$^{-/-}$ mice showed a marked decrease in the MZB cell population and a complementary increase in the percentage of FOB cells (Fig. 3*A*). The absolute numbers of both MZB cells and FOB cells were decreased (Table I). We next analyzed the splenic B cell compartment in *Cas-L*$^{-/-}$ mice by measuring other B cell markers, including IgM and IgD. The B220^{+}IgM^{high}IgD^{low} population, which includes MZB cells (21), was also reduced in *Cas-L*$^{-/-}$ mice compared with wild-type mice (Fig. 3*B*, Fraction III type cells, and Table I). To confirm the defect of MZB cells in *Cas-L*$^{-/-}$ mice, the expression of CD1d, which is a distinctive marker of MZB cells (36), was analyzed in B220^{+}IgM^{high}IgD^{low} cells. Decreased CD1d^{high} cell population was found in *Cas-L*$^{-/-}$ mice compared with wild-type mice (Fig. 3*C*). Consistent with the results from flow cytometric analyses, histological examination of the spleen showed that the IgM^{high}IgD^{low} MZB cell number was reduced in the absence of Cas-L (Fig. 3*D*).

MZ is composed of several kinds of cells in addition to MZB cells such as stromal cells and macrophages. The MZB cell defect could result from either cell autonomous impairment or an incomplete microenvironment that supports B cell differentiation. To determine which possibility is more likely in *Cas-L*$^{-/-}$ mice, we examined the reconstitution of MZB cells after reciprocal cell transfer between wild-type mice and *Cas-L*$^{-/-}$ mice. The transfer of Cas-L-deficient bone marrow into sublethally irradiated congenic wild-type hosts did not result in the reconstitution of MZB cells (Fig. 4, *middle panel*). In contrast, the transfer of bone marrow cells from wild-type mice into sublethally irradiated *Cas-L*$^{-/-}$ recipients resulted in the generation of normal MZB cell population (Fig. 4, *right panel*). Thus, these results demonstrated that Cas-L is integral for the maintenance of MZB cells and that the defect of MZB cells in these mice is intrinsic to *Cas-L*$^{-/-}$ B cells.

BCR-mediated signaling and immune responses in the absence of Cas-L

Among a number of reports that analyzed the mechanism of the MZB cell deficit, some reports have indicated that the absence of MZB cells arises from enhanced BCR signaling (21, 23). Cas-L is also suggested to be involved in BCR-mediated signal transduction (17). Therefore the defect of MZB cells in *Cas-L*$^{-/-}$ mice might result from aberrant BCR signaling. To test this issue, Ca^{2+} mobilization assays were performed. The results showed that the extent of Ca^{2+} flux in *Cas-L*$^{-/-}$ B cells was slightly decreased compared with that in wild-type B cells (Fig. 5*A*). We next investigated the mitogenic responses of *Cas-L*$^{-/-}$ splenic B cells. The proliferations of *Cas-L*$^{-/-}$ B cells in response to graded concentrations of anti-IgM were comparable to those of the control cells (Fig. 5*B*). Moreover, no significant differences were observed in the proliferation resulting from the combination of anti-IgM, anti-CD40, or IL-4 (Fig. 5*C*).

In addition, we analyzed the involvement of Cas-L in the humoral immune response. The measurements of Ig isotype levels in the serum from nonimmunized *Cas-L*$^{-/-}$ mice showed a decrease in IgG2a compared with the serum from wild-type mice (Fig. 5*D*). Subsequently, we immunized mice against TNP-conjugated KLH, which is a T cell-dependent Ag. The concentrations of TNP-specific Abs in *Cas-L*$^{-/-}$ mice revealed a normal response to the T cell-dependent Ag (Fig. 5*E*). Because MZB cells are indicated to be involved in the T cell-independent Ab response against phosphorylcholine (37), we next examined the levels of anti-phosphorylcholine Abs after immunization with *S. pneumoniae* strain R36A. The slightly reduced level of phosphorylcholine-specific IgM was detected in *Cas-L*$^{-/-}$ mice (Fig. 5*F*), which is compatible with the decreased number of MZB cell, although other Ig isotype levels in *Cas-L*$^{-/-}$ mice were comparable to those in wild-type mice (data not shown). Taking these findings together, the defect of MZB cells in *Cas-L*$^{-/-}$ mice is unlikely to be caused mainly by enhanced BCR signaling.

Table I. *B cell populations in Cas-L-deficient mice*[a]

Tissue	Cell Type	Cas-L$^{+/+}$	Cas-L$^{-/-}$
Spleen	Total B cells	37.4 ± 3.0 (×10^6/ml)	15.0 ± 4.1** (×10^6/ml)
	NFB cells	3.0 ± 0.8	1.2 ± 0.5**
	FOB cells	25.6 ± 7.5	11.9 ± 4.9*
	MZB cells	1.63 ± 0.2	0.2 ± 0.05**
	Fraction I	14.1 ± 4.5	6.3 ± 1.9**
	Fraction II	7.1 ± 1.8	3.6 ± 1.6**
	Fraction III	6.8 ± 1.7	2.1 ± 0.9**
Bone marrow	Total B cells	22.3 ± 6.2 (×10^5/ml)	25.1 ± 8.2 (×10^5/ml)
	Fraction A–C	2.6 ± 0.7	3.5 ± 1.0
	Fraction D	9.1 ± 3.7	9.7 ± 4.1
	Fraction E	3.2 ± 1.6	2.7 ± 1.2
	Fraction F	3.5 ± 1.8	4.5 ± 2.1
Lymph nodes	Total B cells	9.9 ± 4.5 (×10^5/ml)	5.0 ± 1.1* (×10^5/ml)
Peripheral blood	Total B cells	10.5 ± 5.4 (×10^2/ml)	11.8 ± 2.9 (×10^2/ml)

[a] Cells from the spleen, bone marrow, lymph nodes, and peripheral blood were stained with appropriate B cell markers, and each cell population was analyzed by FACS. FOB, NFB, and MZB represent follicular B, newly formed B, and marginal zone B cells, respectively. Fraction I, II, and III were defined by IgM^{low}IgD^{high}, IgM^{high}IgD^{high}, and IgM^{high}IgD^{low}, respectively. Fractions A–D were determined using the criteria of Hardy. Data are mean ± SD derived from seven mice except for the subset analysis for the spleen, where data are derived from six mice. *, $p < 0.05$ and **, $p < 0.01$ by Student's t test.

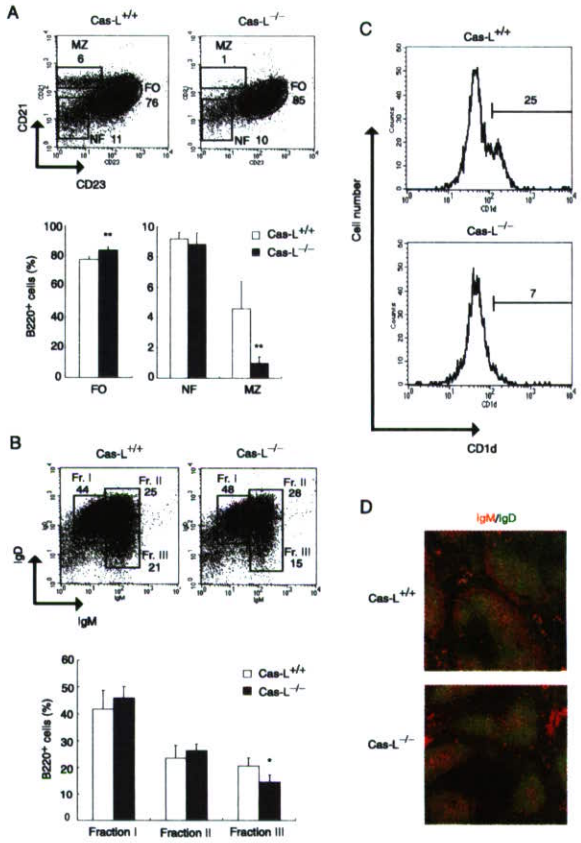

FIGURE 3. MZB cell deficit in the absence of Cas-L. *A* and *B*, FACS analysis of B cell population in spleen. Splenocytes from 8- to 10-wk-old wild-type and *Cas-L*$^{-/-}$ mice were stained for B220, CD21, and CD23 (*A*) and for B220, IgM, and IgD (*B*). The numbers indicate the percentage of each subset in B220^{+} cells. Each subset was also presented by a histogram. MZB (MZ), FOB (FB), and newly formed (NF) B cells are shown. Fraction I, II, and III were defined by IgM^{low}IgD^{high}, IgM^{high}IgD^{high}, and IgM^{high}IgD^{low}, respectively. Data are mean ± SD from three independent experiments using two mice in each case. *, $p < 0.05$ and **, $p < 0.01$, by Student's t test. *C*, The reduced number of CD1d^{high} cells in *Cas-L*$^{-/-}$ mice. Splenocytes were also stained for CD1d to confirm the reduction of MZB cells. Values denote the percentages of CD1d^{high} cells among IgM^{high}IgD^{low} B cells. *D*, Immunofluorescent histochemistry of MZB cells. Nonimmunized splenic cryosections were stained with FITC anti-IgD and Alexa Fluor 594 anti-IgM.

Aberrant migration and adhesion in Cas-L-deficient FOB cells

Previous reports had also indicated that the loss of MZB cells can result from altered lymphocyte motility, which presumably causes mal-localization (25–27). Because in vitro assays had shown that Cas-L was involved in cell movement, the loss of MZB cells in *Cas-L*$^{-/-}$ mice might be relevant to the impairment of cell migration. To address this possibility, chemotaxis assays were performed using splenocytes derived from wild-type and *Cas-L*$^{-/-}$ mice. To preclude the effect of the decrease of MZB cells in *Cas-L*$^{-/-}$ mice, we analyzed FOB cells, which account for 80% of splenic B cells and include MZB cell precursors. We examined their migration in response to CXCL12 and CXCL13, which induce a strong chemotactic reaction in peripheral B cells (29, 38). The results showed that the chemotaxis of *Cas-L*$^{-/-}$ FOB cells was decreased in a dose-dependent fashion (Fig. 6, *A* and *B*).

Considering lymphocyte localization, integrins are indispensable molecules and Cas-L plays a crucial role in the integrin-mediated pathway. Among the integrin ligands, VCAM-1 and ICAM-1 are essential for the retention of MZB cells (39). Therefore we investigated the response of *Cas-L*$^{-/-}$ FOB cells to VCAM-1 and ICAM-1 using adhesion assays. As shown in Fig. 6, *C* and *D*, FOB cells from *Cas-L*$^{-/-}$ mice showed attenuated responses to both VCAM-1 and ICAM-1 compared with those from wild-type mice.

We then performed flow cytometric analyses to evaluate the expression level of the relevant receptor for each ligand. Measurements of surface chemokine receptors (CXCR4 and CXCR5, receptors of CXCL12 and CXCL13, respectively) and integrin receptors (integrin α_4 and β_1, subunits of the receptor for VCAM-1, and α_L and β_2, subunits of the receptor for ICAM-1) on splenic B cells or FOB cells from wild-type mice and *Cas-L*$^{-/-}$ mice showed no significant difference in their expression levels (data not shown). Taken together, *Cas-L*$^{-/-}$ FOB cells show perturbed migration and adhesion, which may be associated with the defect of MZB cells.

Cas-L affects lymphocyte trafficking in secondary lymphoid organs

In *Cas-L*$^{-/-}$ mice, another significant finding is the reduced number of lymphocytes in peripheral lymphoid organs. Our findings that migration and adhesion of splenic B cells were impaired in *Cas-L*$^{-/-}$ mice suggest that the aberrant lymphocyte movement may be responsible for this reduction. Previous studies indicated that chemokines (CXCL12, CXCL13, and CCL19/CCL21) and the

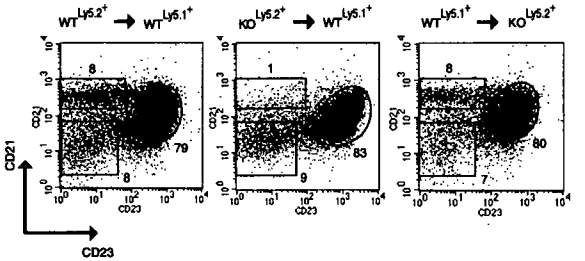

FIGURE 4. MZB cell deficit in *Cas-L*$^{-/-}$ mice is lymphocyte autonomous. Bone marrow cells from wild-type (WT Ly5.2$^+$) or *Cas-L*$^{-/-}$ 10-wk-old mice (KO Ly5.2$^+$) were transferred into lethally irradiated congenic wild-type mice (Ly5.1$^+$) (*left* and *middle panels*). Bone marrow cells from congenic wild-type mice (Ly5.1$^+$) were reciprocally injected into *Cas-L*$^{-/-}$ mice (*right panel*). Twelve weeks later, splenocytes of donor origin were stained for Ly5.1 (or Ly5.2), B220, CD21, and CD23 and analyzed by FACS. Numbers indicate the percentage of gated cells for Ly5.2$^+$ and B220$^+$ cells (*left* and *middle panels*) or for Ly5.1$^+$ and B220$^+$ cells (*right panel*). Data are representatives of three independent experiments using at least two mice in each experiment.

integrin family (VLA-4 and LFA-1, receptors of VCAM-1 and ICAM-1, respectively) have pivotal roles in lymphocyte trafficking in spleen and lymph nodes (30–34). Therefore we first examined chemotaxis and adhesiveness of splenic T cells to determine whether T cells from *Cas-L*$^{-/-}$ mice also show the same inadequate migration and adhesion as *Cas-L*$^{-/-}$ B cells. As shown in Fig. 7, *A* and *B*, the chemotaxis of *Cas-L*$^{-/-}$ T cells to CXCL12 and CCL21, both of which are known to be important chemokines for peripheral T cells (40, 41), was significantly attenuated. The adhesion assay revealed impaired adhesiveness to both VCAM-1

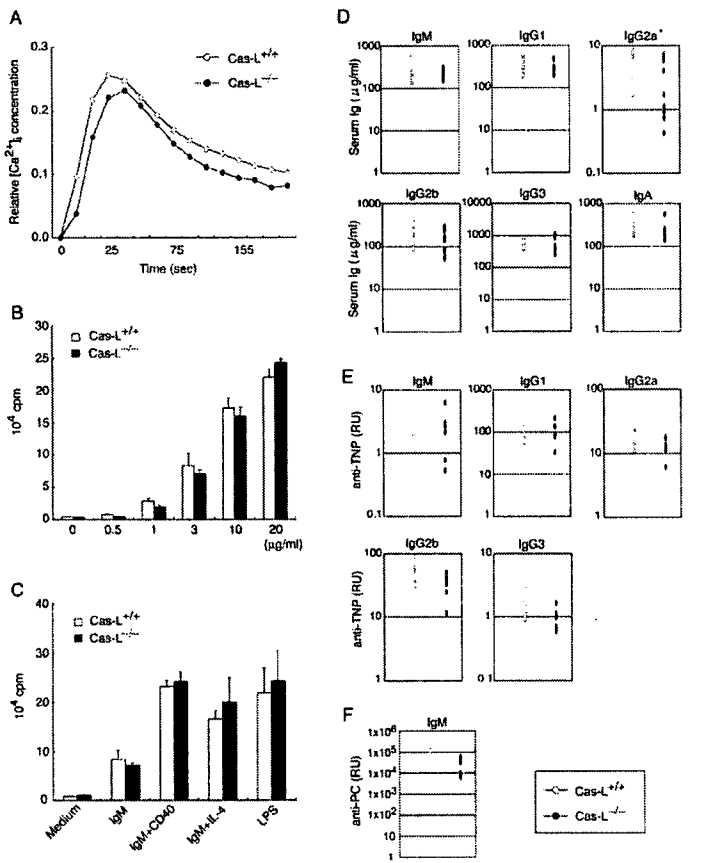

FIGURE 5. Immune responses in Cas-L-deficient mice. *A*, BCR-mediated signaling in the absence of Cas-L. Wild-type and *Cas-L*$^{-/-}$ B cells were loaded with Indo-1. The panel shows the changes of intracellular calcium concentration ($[Ca^{2+}]_i$) in B220-gated cells after stimulation with anti-IgM F(ab')$_2$ (10 μg/ml). Data are expressed as the ratio to the beginning concentration level. A representative of at least three independent experiments is shown. *B* and *C*, BCR- and LPS-mediated proliferation of splenic B cells. Proliferation of wild-type or *Cas-L*$^{-/-}$ B cells was examined by measuring [^{3}H]thymidine incorporation after stimulation with the indicated doses of anti-IgM F(ab')$_2$ (*B*). The assay was also performed with the combination of anti-IgM F(ab')$_2$ (3 μg/ml), anti-CD40 (5 μg/ml), mouse IL-4 (10 ng/ml), and LPS (20 μg/ml). The panel is representative of at least three independent experiments. *D*, Serum Ig concentrations in nonimmunized mice. Serum Ig levels in 8- to 9-wk-old wild-type and *Cas-L*$^{-/-}$ mice were measured by ELISA. Each point represents the value obtained from one mouse. *, $p < 0.05$ in Mann-Whitney *U* test. *E*, Humoral responses to T cell-dependent (TD) Ag. Seven- to 8-wk-old mice were immunized with TNP-KLH. Secondary immunization was given at day 21. TNP-specific Abs were measured in serum collected at day 28 after the initial immunization. *F*, Immune response against phosphorylcholine (PC). Ten- to 12-wk-old mice were immunized with *S. pneumoniae* strain R36A. Serum titers of anti-phosphorylcholine-specific IgM were analyzed 7 days after immunization. Data in *E* and *F* were derived from six mice per genotype. *, $p < 0.05$ by Mann-Whitney *U* test.

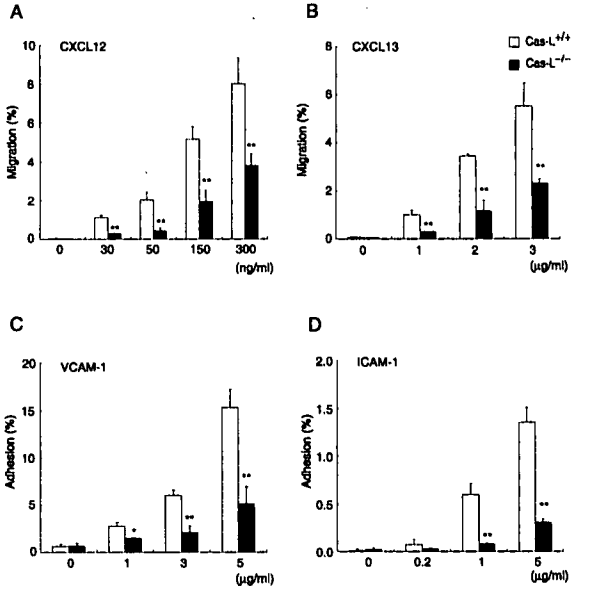

FIGURE 6. Altered B cell movement in Cas-L-deficient mice. *A* and *B*, Migration of *Cas-L*$^{-/-}$ FOB cells. Splenocytes from 8- to 10-wk-old wild-type and *Cas-L*$^{-/-}$ mice stained with CD21, CD23, and B220 were compared in a Transwell chemotaxis assay with the indicated concentrations of CXCL12 (*A*) or CXCL13 (*B*). Cell types were counted before and after migration by FACS. Results are indicated as percentages of migrated FOB cells (B220$^+$CD21^{int}CD23^{high}) for the input FOB cells. *, $p < 0.05$ by Student's *t* test. *C* and *D*, The adhesion ability in *Cas-L*$^{-/-}$ FOB cells. Splenocytes were stained for CD21, CD23, and B220. After incubation with different titers of VCAM-1 (*C*) or ICAM-1 (*D*), FOB cells among adherent cells were counted by FACS. Data shown are the ratio of adherent FOB cells to input FOB cells. Values are mean ± SD from three per group, and data are representative of at least three experiments. *, $p < 0.05$ by Student's *t* test.

and ICAM-1 in *Cas-L*$^{-/-}$ T cells compared with control cells (Fig. 7, *C* and *D*).

Given the impaired migration and adhesion of *Cas-L*$^{-/-}$ B and T cells, we performed trafficking assays in vivo to determine whether lymphocytes in *Cas-L*$^{-/-}$ mice might show altered cell movement in spleen and lymph nodes. Splenocytes isolated from wild-type and *Cas-L*$^{-/-}$ mice (Ly5.2$^+$), which were labeled with BCECF only for *Cas-L*$^{-/-}$ cells, were mixed equally and injected

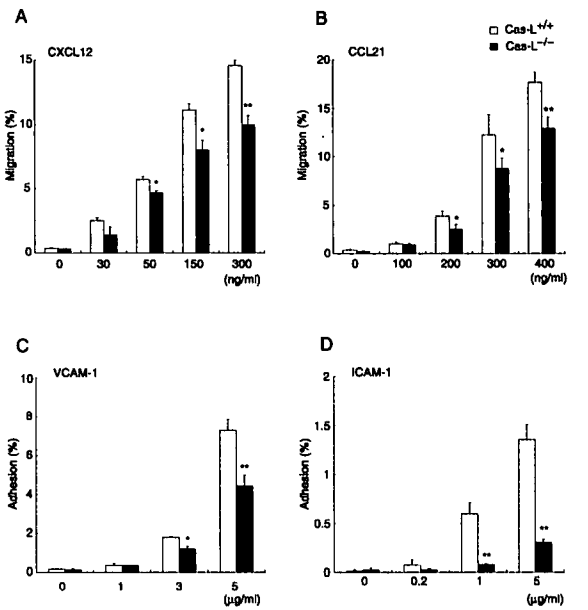

FIGURE 7. Aberrant T cell migration and adhesion in Cas-L-deficient mice. *A* and *B*, Migration of *Cas-L*$^{-/-}$ T cells. Splenocytes from wild-type and *Cas-L*$^{-/-}$ mice stained for Thy1.2 and B220 were compared in a transwell chemotaxis assay with the indicated concentrations of CXCL12 (*A*) or CCL21 (*B*). Data are presented as the ratio of migrated T cells to input T cells. *, $p < 0.05$ by Student's *t* test. *C* and *D*, The adhesion ability in *Cas-L*$^{-/-}$ T cells. Splenocytes were stained for Thy 1.2 and B220. After incubation with VCAM-1 (*C*) or ICAM-1 (*D*), the number of T cells included in the adherent cells was counted by FACS. Data show the ratio of adherent T cells to input T cells. Values are mean ± SD from three per group, and data are representative of at least three experiments. *, $p < 0.05$ by Student's *t* test.

into congenic wild-type mice (Ly5.1$^+$). Forty-eight hours after injection, splenocytes were harvested and host cells were separated from donor cells using Ly5.1. *Cas-L*$^{-/-}$ cells were discriminated from wild-type cells by the marker BCECF (Fig. 8*A*). Peripheral lymph nodes and peripheral blood were also analyzed in the same way. The number of homing *Cas-L*$^{-/-}$ cells showed a modest but significant decrease in both the spleen and lymph nodes (Fig. 8, *A* and *B*). In contrast, the ratios of total lymphocytes and B cells in peripheral blood derived from *Cas-L*$^{-/-}$ mice were elevated, although the change in the T cell ratio was not statistically significant (Fig. 8*C*). Thus, these results suggest the possibility that the reduction in the number of lymphocytes in spleen and lymph nodes of *Cas-L*$^{-/-}$ mice is due to altered lymphocyte trafficking.

Discussion

Cas-L-deficient mice have defective MZB cells, although other subsets of splenic B cells show an almost normal pattern. On the basis of previous reports, we addressed two possible reasons for this defect: distorted localization of MZB cells and impairment of MZB cell differentiation.

The first hypothesis is suggested by data indicating alteration of the migratory ability in gene-targeted mice lacking Pyk-2 or DOCK2 (25, 27). These proteins function as important mediators of G protein-coupled chemokine receptor signal transduction. A previous study showed that pertussis toxin, a Gαi inhibitor, causes the disappearance of MZB cells, suggesting that aberrant chemokine receptor signaling could give rise to defective MZB cells (27). In Cas-L-deficient mice, a decreased chemotactic response is also detected, although no obvious correlation between Cas-L and chemokine receptors has yet been reported. Taken together with our demonstration that Cas-L regulates not only integrin-mediated but also chemokine-mediated cell motility, Cas-L could have a function in the signal pathway from G protein-coupled chemokine receptor.

Gene-disrupted mice lacking DOCK2, a key molecule of chemokine-mediated Rac activation, showed complete loss of chemotactic responses, which would result in the defect of MZB cells. In Cas-L-deficient mice, however, the response to chemokines is reduced to ~50% of that seen in wild-type mice. Therefore, it would appear that abnormal chemotaxis is not enough to explain the marked reduction of MZB cells in *Cas-L*$^{-/-}$ mice. Although previous studies have stressed altered chemotactic activity to explain the absence of MZB cells, cell lodgment to the lymphoid-specific region is controlled not only by migration but also by adhesion. Significant in this regard is our observation that *Cas-L*$^{-/-}$ B cells have the impaired ability to adhere to VCAM-1 and ICAM-1, both of which are known to be indispensable molecules for the adhesion of MZB cells. In the current study, we first demonstrated that the defect of MZB cells may result from abnormalities in both migration and adhesion. These findings are also consistent with the previous reports that Cas-L functions in the pathway mediated by β_1 integrin, a receptor subset for VCAM-1. In contrast, no previous studies have clarified a correlation between Cas-L and LFA-1, which was suggested by our observation that Cas-L is required for the signaling from LFA-1.

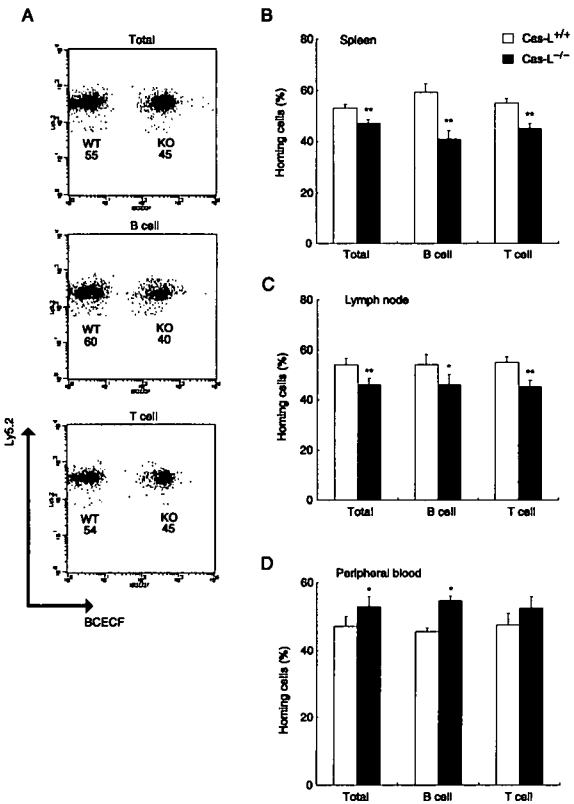

FIGURE 8. Aberrant lymphocyte trafficking in *Cas-L*$^{-/-}$ mice. BCECF-labeled splenocytes from *Cas-L*$^{-/-}$ mice (KO) were mixed with unlabeled splenocytes from wild-type (WT) mice. Both cells (Ly5.2$^+$) were injected into congenic recipient mice (Ly5.1$^+$). Forty-eight hours later, spleens, lymph nodes, and peripheral blood were harvested. Ly5.2$^+$ cells in the spleen were selected and the ratio of *Cas-L*$^{-/-}$ cells (BCECF$^+$ cells) and wild-type cells (BCECF$^-$ cells) detected in the transferred cells were presented (*A*). Data are mean ± SD from three independent experiments using two mice in each case (*B*). The assays were also performed for lymph nodes (*C*) and peripheral blood (*D*). *, $p < 0.05$ and **, $p < 0.01$ by Student's *t* test.

Although our findings suggest that Cas-L is indispensable for lymphocyte localization in MZB, they do not preclude the possibility that MZB cell development is perturbed in *Cas-L*$^{-/-}$ mice. Previous studies have indicated the involvement of signaling from BCR and Notch2 in MZB cell differentiation, both of which are membrane-bound receptors distinctly expressed on B cells. The former leads to a hypothesis that enhanced BCR signaling causes loss of MZB cells, although this remains disputable (42, 43). In this regard, Cas-L is suggested to commit to BCR signaling through association with Lyn, which negatively regulates BCR signaling by mediating inhibitory signals from CD22 and FcγRIIb (44, 45). Interestingly, previous studies reported that the absence of Lyn or CD22 resulted in loss of MZB cells with hypersensitive BCR signaling (23, 46). From these findings, we expected *Cas-L*$^{-/-}$ B cells to show enhanced BCR signal intensity. Our data, however, showed no evidence of BCR signal enhancement. Recent studies have suggested that the Notch2 signal pathway plays a pivotal role in determining MZB cell differentiation fate (22, 24). We analyzed the expression level of Notch2 in FOB cells from *Cas-L*$^{-/-}$ mice using real-time PCR, and found that it showed no obvious difference from that in wild-type B cells (data not shown). Taken as a whole, there is so far no available evidence to suggest aberrant MZB cell differentiation in *Cas-L*$^{-/-}$ mice.

Finally, another important finding in *Cas-L*$^{-/-}$ mice was the contraction of peripheral lymphoid organs. The results of our trafficking assay suggested that this contraction would have resulted from aberrant lymphocyte movement. We also examined other possibilities to explain contraction of secondary lymphoid organs: maturation arrest, insufficient proliferation, and altered cell turnover. With regard to the first possibility, flow cytometric analyses of bone marrow and thymus showed no significant abnormalities in B or T cell development that could account for this reduction (Table I and data not shown). Second, the lymphocyte proliferation assay upon BCR and LPS stimulation revealed no obvious difference between wild-type and *Cas-L*$^{-/-}$ mice (Fig. 5, *B* and *C*). Therefore the scenario of insufficient propagation of lymphocytes is unlikely. To test the third possibility, altered cell turnover, we performed an in vivo BrdU labeling assay (data not shown). The frequencies of BrdU-labeled cells in *Cas-L*$^{-/-}$ mice remained comparable to those in wild-type mice. Furthermore, no remarkable augmentation of apoptotic cells in the Cas-L-deficient spleen was detected in histological evaluation with TUNEL staining or flow cytometric analyses using annexin V assay (data not shown). Taking these findings together, it might be difficult to attribute the decreased number of peripheral lymphocytes to altered cell turnover. Therefore it would appear that lymphocyte reduction in secondary lymphoid organs is mainly due to altered lymphocyte trafficking. Because reduction of cell population is most striking in MZB cells of the spleen, we also analyzed a BCR-mediated response or cell turnover in the MZB cells. Although *Cas-L*$^{-/-}$ MZB cells showed slightly reduced Ca^{2+} flux in the Ca^{2+} mobilization assays or decreased apoptotic cells in the annexin V assay, no significant differences were obtained (data not shown). However, because the number of MZB cells in *Cas-L*$^{-/-}$ mice is very small, a subtle alteration, if any, might not have been detectable.

In summary, using gene-targeted mice, we have demonstrated that Cas-L is integral for both cell migration and adhesion, a lack of which may contribute to a defect of MZB cells in the spleen and contraction of secondary lymphoid organs.

Acknowledgments

We thank S. Aizawa for TT2 ES cells, H. Ito for *S. pneumoniae* strain R36A, S. Kumar for cDNA of Nedd9, and R. Takizawa and Y. Sato for help with the generation and breeding of *Cas-L*$^{-/-}$ mice.

Disclosures

The authors have no financial conflict of interest.

References

1. Law, S. F., J. Estojak, B. Wang, T. Mysliwiec, G. Kruh, and E. A. Golemis. 1996. Human enhancer of filamentation 1, a novel p130cas-like docking protein, associates with focal adhesion kinase and induces pseudohyphal growth in *Saccharomyces cerevisiae*. *Mol. Cell. Biol.* 16: 3327–3337.
2. Minegishi, M., K. Tachibana, T. Sato, S. Iwata, Y. Nojima, and C. Morimoto. 1996. Structure and function of Cas-L, a 105-kD Crk-associated substrate-related protein that is involved in β1 integrin-mediated signaling in lymphocytes. *J. Exp. Med.* 184: 1365–1375.
3. Sakai, R., A. Iwamatsu, N. Hirano, S. Ogawa, T. Tanaka, H. Mano, Y. Yazaki, and H. Hirai. 1994. A novel signaling molecule, p130, forms stable complexes in vivo with v-Crk and v-Src in a tyrosine phosphorylation-dependent manner. *EMBO J.* 13: 3748–3756.
4. Honda, H., H. Oda, T. Nakamoto, Z. Honda, R. Sakai, T. Suzuki, T. Saito, K. Nakamura, K. Nakao, T. Ishikawa, et al. 1998. Cardiovascular anomaly, impaired actin bundling and resistance to Src-induced transformation in mice lacking p130Cas. *Nat. Genet.* 19: 361–365.
5. Giancotti, F. G., and E. Ruoslahti. 1999. Integrin signaling. *Science* 285: 1028–1032.
6. Hynes, R. O. 1987. Integrins: a family of cell surface receptors. *Cell* 48: 549–554.
7. Ruoslahti, E., and J. C. Reed. 1994. Anchorage dependence, integrins, and apoptosis. *Cell* 77: 477–478.
8. Springer, T. A. 1990. Adhesion receptors of the immune system. *Nature* 346: 425–434.
9. Astier, A., S. N. Manié, H. Avraham, H. Hirai, S. F. Law, Y. Zhang, E. A. Golemis, Y. Fu, B. J. Druker, N. Haghayeghi, et al. 1997. The related adhesion focal tyrosine kinase differentially phosphorylates p130Cas and the Cas-like protein, p105HEF1. *J. Biol. Chem.* 272: 19719–19724.
10. Tachibana, K., T. Urano, H. Fujita, Y. Ohashi, K. Kamiguchi, S. Iwata, H. Hirai, and C. Morimoto. 1997. Tyrosine phosphorylation of Crk-associated substrates by focal adhesion kinase: a putative mechanism for the integrin-mediated tyrosine phosphorylation of Crk-associated substrates. *J. Biol. Chem.* 272: 29083–29090.
11. Miyake-Nishijima, R., S. Iwata, S. Saijo, H. Kobayashi, S. Kobayashi, A. Souta-Kuribara, O. Hosono, H. Kawasaki, H. Tanaka, E. Ikeda, et al. 2003. Role of Crk-associated substrate lymphocyte type in the pathophysiology of rheumatoid arthritis in tax transgenic mice and in humans. *Arthritis Rheum.* 48: 1890–1900.
12. Ohashi, Y., S. Iwata, K. Kamiguchi, and C. Morimoto. 1999. Tyrosine phosphorylation of Crk-associated substrate lymphocyte-type is a critical element in TCR- and β_1 integrin-induced T lymphocyte migration. *J. Immunol.* 163: 3727–3734.
13. van Seventer, G. A., H. J. Salmen, S. F. Law, G. M. O'Neill, M. M. Mullen, A. M. Franz, S. B. Kanner, E. A. Golemis, and J. M. van Seventer. 2001. Focal adhesion kinase regulates β_1 integrin-dependent T cell migration through an HEF1 effector pathway. *Eur. J. Immunol.* 31: 1417–1427.
14. Sakakibara, A., Y. Ohba, K. Kurokawa, M. Matsuda, and S. Hattori. 2002. Novel function of Chat in controlling cell adhesion via Cas-Crk-C3G-pathway-mediated Rap1 activation. *J. Cell Sci.* 115: 4915–4924.
15. Kanda, H., T. Mimura, N. Morino, K. Hamasaki, T. Nakamoto, H. Hirai, C. Morimoto, Y. Yazaki, and Y. Nojima. 1997. Ligation of the T cell antigen receptor induces tyrosine phosphorylation of p105CasL, a member of the p130Cas-related docking protein family, and its subsequent binding to the Src homology 2 domain of c-Crk. *Eur. J. Immunol.* 27: 2113–2117.
16. Kanda, H., T. Mimura, K. Hamasaki, K. Yamamoto, Y. Yazaki, H. Hirai, and Y. Nojima. 1999. Fyn and Lck tyrosine kinases regulate tyrosine phosphorylation of p105CasL, a member of the p130Cas docking protein family, in T-cell receptor-mediated signalling. *Immunology* 97: 56–61.
17. Manié, S. N., A. R. P. Beck, A. Astier, S. F. Law, T. Canty, H. Hirai, B. J. Druker, H. Avraham, N. Haghayeghi, M. Sattler, et al. 1997. Involvement of p130^{Cas} and p105(HEF1), a novel Cas-like docking protein, in a cytoskeleton-dependent signaling pathway initiated by ligation of integrin or antigen receptor on human B cells. *J. Biol. Chem.* 272: 4230–4236.
18. Zhang, Z., L. Hernandez-Lagunas, W. C. Horne, and R. Baron. 1999. Cytoskeleton-dependent tyrosine phosphorylation of the p130^{Cas} family member HEF1 downstream of the G protein-coupled calcitonin receptor.: calcitonin induces the association of HEF1, paxillin, and focal adhesion kinase. *J. Biol. Chem.* 274: 25093–25098.
19. Pillai, S. 1999. The chosen few? Positive selection and the generation of naive B lymphocytes. *Immunity* 10: 493–502.
20. Oliver, A. M., F. Martin, and J. F. Kearney. 1999. IgM^{high}CD21^{high} lymphocytes enriched in the splenic marginal zone generate effector cells more rapidly than the bulk of follicular B cells. *J. Immunol.* 162: 7198–7207.

21. Cariappa, A., M. Tang, C. Parng, E. Nebelitskiy, M. Carroll, K. Georgopoulos, and S. Pillai. 2001. The follicular versus marginal zone B lymphocyte cell fate decision is regulated by Aiolos, Btk, and CD21. *Immunity* 14: 603–615.
22. Saito, T., S. Chiba, M. Ichikawa, A. Kunisato, T. Asai, K. Shimizu, T. Yamaguchi, G. Yamamoto, S. Seo, K. Kumano, et al. 2003. Notch2 is preferentially expressed in mature B cells and indispensable for marginal zone B lineage development. *Immunity* 18: 675–685.
23. Seo, S., J. Buckler, and J. Erikson. 2001. Novel roles for Lyn in B cell migration and lipopolysaccharide responsiveness revealed using anti-double-stranded DNA Ig transgenic mice. *J. Immunol.* 166: 3710–3716.
24. Tanigaki, K., H. Han, N. Yamamoto, K. Tashiro, M. Ikegawa, K. Kuroda, A. Suzuki, T. Nakano, and T. Honjo. 2002. Notch-RBP-J signaling is involved in cell fate determination of marginal zone B cells. *Nat. Immunol.* 3: 443–450.
25. Fukui, Y., O. Hashimoto, T. Sanui, T. Oono, H. Koga, M. Abe, A. Inayoshi, M. Noda, M. Oike, T. Shirai, and T. Sasazuki. 2001. Haematopoietic cell-specific CDM family protein DOCK2 is essential for lymphocyte migration. *Nature* 412: 826–831.
26. Girkontaite, I., K. Missy, V. Sakk, A. Harenberg, K. Tedford, T. Pötzel, K. Pfeffer, and K.-D. Fischer. 2001. Lsc is required for marginal zone B cells, regulation of lymphocyte motility and immune responses. *Nat. Immunol.* 2: 855–862.
27. Guinamard, R., M. Okigaki, J. Schlessinger, and J. V. Ravetch. 2000. Absence of marginal zone B cells in Pyk-2-deficient mice defines their role in the humoral response. *Nat. Immunol.* 1: 31–36.
28. Butcher, E. C., and L. J. Picker. 1996. Lymphocyte homing and homeostasis. *Science* 272: 60–66.
29. Bleul, C. C., R. C. Fuhlbrigge, J. M. Casasnovas, A. Aiuti, and T. A. Springer. 1996. A highly efficacious lymphocyte chemoattractant, stromal cell-derived factor 1 (SDF-1). *J. Exp. Med.* 184: 1101–1109.
30. Hargreaves, D. C., P. L. Hyman, T. T. Lu, V. N. Ngo, A. Bidgol, G. Suzuki, Y. R. Zou, D. R. Littman, and J. G. Cyster. 2001. A coordinated change in chemokine responsiveness guides plasma cell movements. *J. Exp. Med.* 194: 45–56.
31. Ansel, K. M., V. N. Ngo, P. L. Hyman, S. A. Luther, R. Forster, J. D. Sedgwick, J. L. Browning, M. Lipp, and J. G. Cyster. 2000. A chemokine-driven positive feedback loop organizes lymphoid follicles. *Nature* 406: 309–314.
32. Andrew, D. P., J. P. Spellberg, H. Takimoto, R. Schmits, T. W. Mak, and M. M. Zukowski. 1998. Transendothelial migration and trafficking of leukocytes in LFA-1-deficient mice. *Eur. J. Immunol.* 28: 1959–1969.
33. Berlin-Rufenach, C., F. Otto, M. Mathies, J. Westermann, M. J. Owen, A. Hamann, and N. Hogg. 1999. Lymphocyte migration in lymphocyte function-associated antigen (LFA)-1-deficient mice. *J. Exp. Med.* 189: 1467–1478.
34. Lo, C. G., T. T. Lu, and J. G. Cyster. 2003. Integrin-dependence of lymphocyte entry into the splenic white pulp. *J. Exp. Med.* 197: 353–361.
35. Hardy, R. R., C. E. Carmack, S. A. Shinton, J. D. Kemp, and K. Hayakawa. 1991. Resolution and characterization of pro-B and pre-pro-B cell stages in normal mouse bone marrow. *J. Exp. Med.* 173: 1213–1225.
36. Roark, J. H., S. H. Park, J. Jayawardena, U. Kavita, M. Shannon, and A. Bendelac. 1998. CD1.1 expression by mouse antigen-presenting cells and marginal zone B cells. *J. Immunol.* 160: 3121–3127.
37. Martin, F., A. M. Oliver, and J. F. Kearney. 2001. Marginal zone and B1 B cells unite in the early response against T-independent blood-borne particulate antigens. *Immunity* 14: 617–629.
38. Gunn, M. D., V. N. Ngo, K. M. Ansel, E. H. Ekland, J. G. Cyster, and L. T. Williams. 1998. A B-cell-homing chemokine made in lymphoid follicles activates Burkitt's lymphoma receptor-1. *Nature* 391: 799–803.
39. Lu, T. T., and J. G. Cyster. 2002. Integrin-mediated long-term B cell retention in the splenic marginal zone. *Science* 297: 409–412.
40. Nagira, M., T. Imai, K. Hieshima, J. Kusuda, M. Ridanpää, S. Takagi, M. Nishimura, M. Kakizaki, H. Nomiyama, and O. Yoshie. 1997. Molecular cloning of a novel human CC chemokine secondary lymphoid-tissue chemokine that is a potent chemoattractant for lymphocytes and mapped to chromosome 9p13. *J. Biol. Chem.* 272: 19518–19524.
41. Nagira, M., T. Imai, R. Yoshida, S. Takagi, M. Iwasaki, M. Baba, Y. Tabira, J. Akagi, H. Nomiyama, and O. Yoshie. 1998. A lymphocyte-specific CC chemokine, secondary lymphoid tissue chemokine (SLC), is a highly efficient chemoattractant for B cells and activated T cells. *Eur. J. Immunol.* 28: 1516–1523.
42. Clayton, E., G. Bardi, S. E. Bell, D. Chantry, C. P. Downes, A. Gray, L. A. Humphries, D. Rawlings, H. Reynolds, E. Vigorito, and M. Turner. 2002. A crucial role for the p110δ subunit of phosphatidylinositol 3-kinase in B cell development and activation. *J. Exp. Med.* 196: 753–763.
43. Martin, F., and J. F. Kearney. 2000. Positive selection from newly formed to marginal zone B cells depends on the rate of clonal production, CD19, and btk. *Immunity* 12: 39–49.
44. Chan, V. W., C. A. Lowell, and A. L. DeFranco. 1998. Defective negative regulation of antigen receptor signaling in Lyn-deficient B lymphocytes. *Curr. Biol.* 8: 545–553.
45. Smith, K. G., D. M. Tarlinton, G. M. Doody, M. L. Hibbs, and D. T. Fearon. 1998. Inhibition of the B cell by CD22: a requirement for Lyn. *J. Exp. Med.* 187: 807–811.
46. Samardzic, T., D. Marinkovic, C.-P. Danzer, J. Gerlach, L. Nitschke, and T. Wirth. 2002. Reduction of marginal zone B cells in CD22-deficient mice. *Eur. J. Immunol.* 32: 561–567.

The EMBO Journal (2005) 24, 3700–3711 | © 2005 European Molecular Biology Organization | All Rights Reserved 0261-4189/05
www.embojournal.org

THE EMBO JOURNAL

Phosphorylation of ephrin-B1 via the interaction with claudin following cell–cell contact formation

Masamitsu Tanaka, Reiko Kamata and Ryuichi Sakai*

Growth Factor Division, National Cancer Center Research Institute, Tsukiji, Chuo-ku, Tokyo, Japan

The interaction of the Eph family of receptor protein tyrosine kinase and its ligand ephrin family induces bidirectional signaling via the cell–cell contacts. Although most previous studies have focused on the function of Eph–ephrin pathways in the neural system and endothelial cells, this process also occurs in epithelial and cancer cells, of which the biological involvement is poorly understood. We show that ephrin-B1 creates an *in vivo* complex with adjacent claudin1 or claudin4 via the extracellular domains of these proteins. The cytoplasmic domain of ephrin-B1 was phosphorylated on tyrosine residues upon the formation of cell–cell contacts, possibly recognizing an intercellular adhesion of claudins. Phosphorylation of ephrin-B1 induced by claudins was abolished by the treatment with 4-amino-5-(4-chlorophenyl)-7-(t-butyl)pyrazolo[3,4-d]pyrimidine, an inhibitor of the Src family kinases. Moreover, overexpression of ephrin-B1 triggered consequent change in the level of cell–cell adhesion depending on its phosphorylation. These results suggest that ephrin-B1 mediated the cell–cell adhesion of epithelial and cancer cells via a novel Eph receptor-independent mechanism.

The EMBO Journal (2005) **24**, 3700–3711. doi:10.1038/sj.emboj.7600831; Published online 6 October 2005
Subject Categories: signal transduction
Keywords: claudin; Eph; ephrin; tight junction

Introduction

The members of the Eph receptor family can be classified into two groups based on their sequence similarity and preferential binding to a subset of ligands tethered to the cell surface either by a glycosylphosphatidyl inositol anchor (ephrin-A) or a transmembrane domain (ephrin-B). The transmembrane ligand ephrin-B1 has been shown to be phosphorylated on tyrosine residues following contact with the corresponding Eph receptor ectodomain, and to have a receptor-like intrinsic signaling potential leading to transduce reverse signaling (Holland *et al*, 1996; Bruckner *et al*, 1997). At present, two major mechanisms are known to transduce signaling from ephrin-B1 (Kullander and Klein, 2002; Murai and Pasquale, 2003; Poliakov *et al*, 2004). The receptor-induced tyrosine phosphorylation of ephrin-B1 recruits Grb4 SH-adaptor protein. Since Grb4 has three SH3 domains, it could link ephrin-B1 to a vast array of signaling molecules (Cowan and Henkemeyer, 2001). Ephrin-B1 also contains PDZ-binding motif at the carboxyl-terminus, which mediates signals by association with proteins, including some phosphatase and GTPase-activating protein of heterotrimeric G proteins (Torres *et al*, 1998; Lin *et al*, 1999; Lu *et al*, 2001; Palmer *et al*, 2002). Although Eph receptors and ephrins play essential roles for proper axon pathfinding in the nervous system, some members of the Eph receptors and their ligands are expressed in epithelial cells. For example, EphB2, EphB3 and ephrin-B1 are reciprocally expressed along the crypt–villus axis in the small intestine, which controls the cell positioning along the crypt axis (Batlle *et al*, 2002). Moreover, the overexpression of Ephs and ephrins is reported in various tumors of epithelial origin (Brantley-Sieders *et al*, 2004; Surawska *et al*, 2004). However, the biological significance of Eph/ephrin in epithelial cells or carcinomas is still poorly understood.

When ephrin-B1 is overexpressed in the embryos of *Xenopus laevis* at an early developmental stage, the cell–cell adhesion of the blastomeres was significantly reduced, leading to fatal effects for the embryos (Jones *et al*, 1998). However, precise identification of the adhesion molecules involved in this phenomenon is still not clear. In order to examine whether ephrin-B1 mediates cell–cell adhesion in the mammalian epithelial cells as well, we established an MDCK cell line, showing the inducible expression of ephrin-B1 through the addition of doxycycline. The MDCK cells expressing ephrin-B1 at a high level tend to loosen the cell–cell adhesion when the cells are compared without expressing ephrin-B1. These observations led us to focus on assessing whether ephrin-B1 could be a mediator of cell–cell adhesion in epithelial cells. While analyzing the proteins involved in the complex formation with ephrin-B1, we identified claudins, which are the major constituents of the tight junctions of epithelial cells. Tight junctions locate in the most apical parts of the lateral membrane and serve as paracellular barriers to restrict the movement of ions and proteins across cell boundaries. Claudins are tetraspan transmembrane proteins comprising a multi-gene family with more than 20 members, and creating a complex with ZO-1, ZO-2 and ZO-3, which represent plaque structures underlying plasma membranes (Morita *et al*, 1999; Tsukita *et al*, 2001). Moreover, claudins are frequently overexpressed in malignant cells, in which the mature tight-junction strands are not present. However, claudin's functions in such naive-contact carcinoma cells are not clear.

In this study, we describe the physical interaction of ephrin-B1 with claudins. Although ephrin-B1 interacts with claudins on the same cell surface *in cis*, the tyrosine phosphorylation of the cytoplasmic region of ephrin-B1 was found to be markedly enhanced by the cell–cell contact formation in a manner dependent on claudin. The expression of ephrin-B1

*Corresponding author. Growth Factor Division, National Cancer Center Research Institute, 5-1-1 Tsukiji, Chuo-ku, Tokyo 104-0045, Japan.
Tel.: +81 3 3542 2511; Fax: +81 3 3542 8170;
E-mail: rsakai@gan2.res.ncc.go.jp

Received: 26 April 2005; accepted: 9 September 2005; published online: 6 October 2005

stimulates the paracellular permeability in MDCK cells, which depends on the tyrosine phosphorylation of ephrin-B1. This is the first report to show that the extracellular region of ephrin-B1 associates with a protein other than its receptor in the Eph family kinases. These observations provide further evidence for the possibility that ephrin-B1 inhibits the formation of the tight cell–cell adhesion in a wide variety of epithelial and cancer cells regardless of the existence of cognate Eph receptors.

Results

Claudin interacts with the extracellular domain (ECD) of ephrin-B1

In the attempt to identify the proteins associating with ephrin-B1, we initially screened cDNA library constructed from *Xenopus* embryos at an early stage of development by the procedure described in Figure 1A. After several rounds of screening of total 5×10^4 cDNAs, we isolated several independent cDNAs, which encode proteins coimmunoprecipitated with ephrin-B1. Among them, one clone (#12; Figure 1A) was almost identical (97% identical in amino acids) to *Xenopus* claudin4 (CLD4)L1 through the partial DNA sequencing, which is most closely related to CLD4 in mouse and human (Fujita *et al*, 2002). Therefore, we focused our study to examine the interaction of ephrin-B1 with CLD4 and also with claudin1 (CLD1), which is most widely expressed in mammalian tissues among the members of claudin family.

To confirm the physical association between claudins with ephrin-B1, coexpression and immunoprecipitation (IP) analysis was first performed in COS1 cells. It was revealed that ephrin-B1 was co-precipitated with CLD1 by the specific antibody (Figure 1B, lane 1), but not by the normal mouse IgG1 (Figure 1B, lane 2). This result was further confirmed through experiments using the antibodies in reverse order. CLD1 was co-precipitated with ephrin-B1 (Figure 1B, lanes 3 and 4, arrowhead). In addition to CLD1, the stable association of CLD4 with ephrin-B1 was demonstrated using similar experiments (Figure 1B, lanes 5–8). We also examined the association between endogenous claudins and ephrin-B1 using the HT29 colon cancer cell line, where ephrin-B1, CLD1 and CLD4 are highly expressed. CLD1 and CLD4 were co-precipitated with ephrin-B1 from the extract of HT29 cells using the specific antibody, but not by normal goat serum (NGS) (Figure 1C, lanes 1, 2, 5 and 6). Furthermore, ephrin-B1 was co-precipitated with CLD1 or CLD4 using the specific antibodies in HT29 cells, confirming a stable level of interaction among these molecules (Figure 1C, lanes 3, 4, 7, 8). In HT29 cells, claudins and ephrin-B1 were diffusely overlapped in the lateral membrane. On the other hand, in ephrin-B1-expressing MDCK cells, the localization of CLD1 was restricted to the tight junctions where ZO-1 was expressed, while ephrin-B1 showed overlapping, but a wider level of expression along the entire region in the lateral membrane (Figure 1D).

In order to determine the region within CLD1, required for the interaction with ephrin-B1, we generated deletion mutants of CLD1. Difference in the binding affinity of the mutants mainly localized at the cell membrane indicates that the cytoplasmic regions of CLD1 were not involved in the interaction with ephrin-B1 (Figure 2A, #1, 6 and 7). Within mutants localized both in the cytoplasm and cell membrane, the ones possessing the first ECD (ECD1) were tightly bound to ephrin-B1 (Figure 2A, #3 and 8), whereas mutants lacking this domain failed to associate with ephrin-B1 (Figure 2A, #2, 4 and 5), suggesting that ECD1 domain of CLD1 is responsible for binding to ephrin-B1. We also generated the same sets of CLD4 mutants with those of CLD1, and revealed that the same domain of CLD4 was necessary for the association with ephrin-B1 (data not shown). These results were further confirmed by the *in vitro* analysis using GST-tagged CLD1 mutants. The GST-fusion proteins, including each extracellular or cytoplamic domain, were incubated with the lysate of cells expressing ephrin-B1, and the association of the claudin mutant and ephrin-B1 was analyzed. The interaction between ephrin-B1 and CLD1 mutant containing ECD1 (aa 1–103) was confirmed (Figure 2B, GST-ECD1). A similar experiment for GST-tagged ephrin-B1 mutants was also performed. CLD1 interacted with the ECD of ephrin-B1 (ephrin-B1 ECD), but not the transmembrane and cytoplasmic domains (ephrin-B1 cyto) (Figure 2B).

Within the ECD of ephrin-B1, the most amino-terminal region (aa 1–166), ephrin-B1-N was required for the interaction with CLD1, because CLD1 fragment containing ECD1 ($CLD1^{1-103}$, corresponding to #8 in Figure 2A) binds to ephrin-$B1^{\Delta 167-236}$, which lacks a residual region of the ECD of ephrin-B1 (Figure 2C). Moreover, the association of ephrin-$B1^{\Delta 167-236}$ and CLD4 fragment containing ECD1 ($CLD4^{1-103}$) was also observed by similar experiments (data not shown). Therefore, we concluded that ephrin-B1-N did interact with the amino-terminal region of claudins, including the first ECD. As ephrin-B1-N also contains a region essential for interaction with EphB receptors (Himanen *et al*, 2001), we further examined whether EphB2 and claudin competitively bind to ephrin-B1 using EphB2-Fc, which is a fusion protein of the ECD of EphB2 with the Fc region of mouse immunoglobulin. Parent L cells do not express detectable claudins (Furuse *et al*, 1998); therefore, CLD4 was retrovirally transduced in L cells stably expressing ephrin-B1 (L ephrin-B1). When EphB2-Fc was added in the cell culture medium, expression of CLD4 reduced the amount of membrane-bound EphB2-Fc, which was detected by both immunoblotting (IB) analysis and immunostaining (Figure 2D). Moreover, in L cells expressing both ephrin-B1 and CLD1 (L ephrin-B1 CLD1), ephrin-B1, but not CLD1, was pulled by EphB2-Fc, while CLD1 was coimmunoprecipitated with ephrin-B1 from the same cell lysate (data not shown). Therefore, CLD1-bound ephrin-B1 does not seem to associate with EphB2-Fc. These results suggest that EphB2 and claudins may competitively associate with the ECD of ephrin-B1.

Ephrin-B1 is phosphorylated on tyrosine residues in the cytoplasmic domain by the interaction with claudin

When ephrin-B1 is stimulated using EphB2, the cytoplasmic domain of ephrin-B1 is highly phosphorylated on tyrosine residues. As the association of claudin and ephrin-B1 depends on their extracellular regions, we subsequently examined whether the phosphorylation of ephrin-B1 was triggered by the interaction with claudin. The coexpression of ephrin-B1 and CLD1 or CLD4 leads to the tyrosine phosphorylation of ephrin-B1 in COS1 cells (Figure 3A, lanes 2 and 5). However, overexpression of CLD1 mutant, which lacks the binding site with ephrin-B1 (CLD1 ΔECD1, corresponds to #2

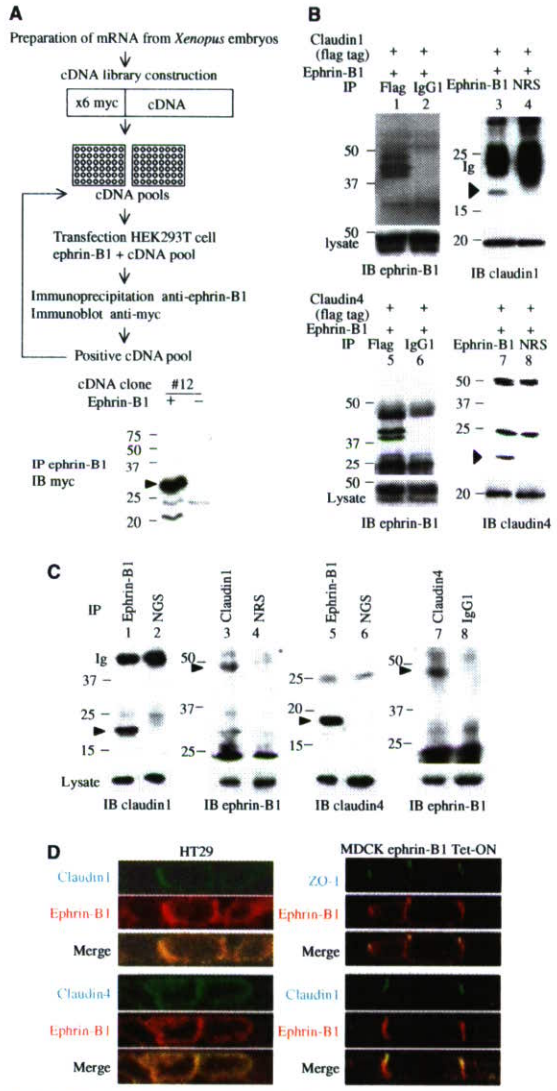

Figure 1 Ephrin-B1 forms a complex with CLD1 and CLD4: (**A**) Schematic outline of cloning procedure for the cDNAs encoding proteins associating with ephrin-B1. A detailed explanation is provided in Materials and methods. (Bottom): A plasmid encoding the cDNA (#12) was transiently transfected into COS1 cells together with or without ephrin-B1. The cell lysates were immunoprecipitated (IP) with an anti-ephrin-B1 antibody, and then subjected to IB with anti-myc antibody. It should be noted that six copies of the myc-epitope tagged with the cDNA increases the protein size around 8 kDa. (**B**) COS1 cells were transiently transfected with a plasmid encoding ephrin-B1 with that encoding flag-tagged CLD1 (lanes 1–4) or CLD4 (lanes 5–8). Cells were lysed and immunoprecipitated with an anti-flag (lanes 1, 5), mouse IgG1 (lanes 2, 6), anti-ephrin-B1 (C18 rabbit, lanes 3, 7) or normal rabbit serum (NRS) (lanes 4, 8). The precipitates were subjected to IB with anti-ephrin-B1 (C18 rabbit) or anti-claudin as indicated. The most upper band of co-precipitated ephrin-B1 at 48 kDa was partly overlapped with the band of immunoglobulin heavy chain (lane 5). The smaller-sized bands recognized with this antibody may be degradated products of ephrin-B1. (**C**) HT29 cells were lysed and immunoprecipitated (IP) with anti-ephrin-B1 (goat), anti-CLD1, anti-CLD4, NGS, and NRS or mouse IgG1, respectively, as indicated above the lanes. The precipitates were subjected to IB with anti-CLD1, anti-CLD4 or anti-ephrin-B1 (goat). Co-precipitated ephrin-B1 and claudins are indicated by arrowheads. (**D**) HT29 cells (left) or MDCK ephrin-B1 Tet-ON cells (right) were immunostained with the indicated antibodies. The corresponding computer-reconstructed vertical sections in the *X–Z* plane are shown.

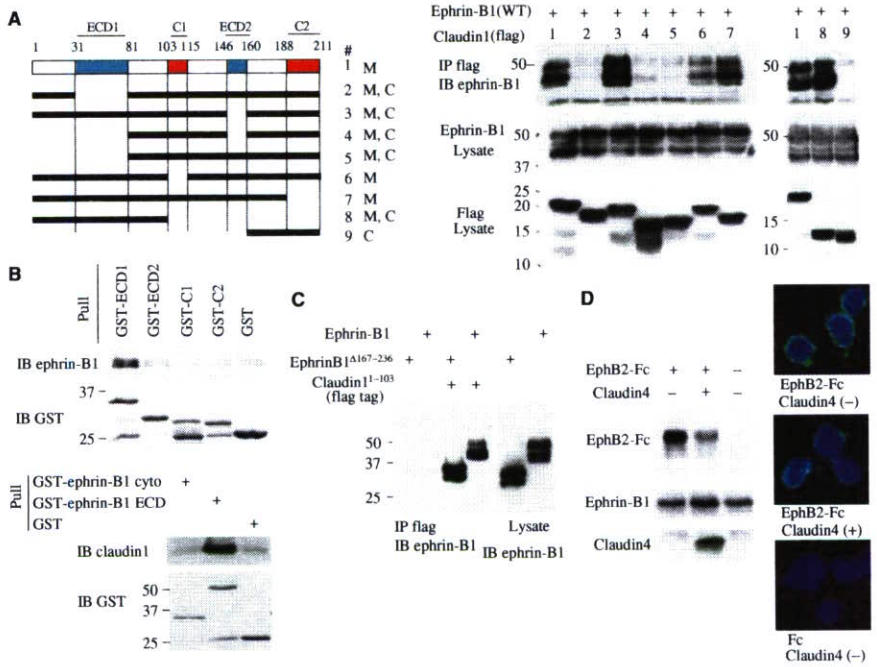

Figure 2 ECD of ephrin-B1 and claudins are required for their association: (**A**) A schematic diagram of the wild-type and deletion mutants of CLD1 used in this study. Proteins are depicted to scale: ECD1 and ECD2, the first and the second ECD; C1 and C2, the first and the second cytoplasmic domain. COS1 cells were transiently transfected with ephrin-B1, with flag-tagged deletion mutants of CLD1. The numbers indicated above the lanes correspond to those in the scheme. The cell lysates were immunoprecipitated (IP) with anti-flag and subjected to IB with anti ephrin-B1 (C18). The localization of each mutant in COS1 cells was examined by immunostaining, and depicted as M (cell membrane) and C (cytoplasm). The mutant #9 was mostly localized in the cytoplasm. (**B**) The lysates from COS1 cells transiently transfected with ephrin-B1 (top) or CLD1 (bottom) were incubated with GST-fusion protein of CLD1 or ephrin-B1 mutants described in Supplementary data 1. GST-fusion proteins were pulled with glutathione-sepharose beads, and the co-precipitated ephrin-B1 or CLD1 was detected by immunoblot. The input of GST-fusion proteins was shown by rehybridization of the filters with anti-GST antibody. The lower band at 25 kDa was observed in some GST-fusion proteins, which might be the degradated product. (**C**) COS1 cells were transiently transfected with flag-tagged $CLD1^{1-103}$ with a wild-type or deletion mutant of ephrin-B1. The cell lysates were immunoprecipitated with anti-flag and then immunoblotted with anti-ephrin-B1 (C18) antibody. (**D**) L ephrin-B1 were either infected with retrovirus containing recombinant CLD4 plasmid (CLD4 +) or mock plasmid (CLD4−), and treated with EphB2–Fc or control Fc at 10 μg/ml for 5 min as indicated. After washing, the cells were either lysed for subjecting to the IB with anti-mouse IgG to detect EphB2–Fc, or immunostained with anti-mouse Fc antibody and TOTO-3 iodide (left and right panels, respectively).

in Figure 2A), was not able to induce the phosphorylation of ephrin-B1 (Figure 3A, lane 3). Similarly, the corresponding mutant of CLD4 (CLD4 ΔECD1) did not affect the phosphorylation of ephrin-B1 (Figure 3A, lane 6). Moreover, the same result was also obtained using another cell line, HEK 293 cells (Figure 3B). The phosphorylation of ephrin-B1 through interaction with claudins was also confirmed by the reconstitution experiments using L cells, in which ephrin-B1 is endogenously expressed at a low level. The tyrosine phosphorylation of ephrin-B1 was clearly induced in L cells stably expressing CLD1 (L CLD1) or CLD4 (L CLD4) when compared to the parent L cells (Figure 3C). However, ephrin-B1 was not phosphorylated in L cells stably expressing claudins lacking in the first ECD (ΔECD1) or only the ECD1 of CLD1 or CLD4 (corresponding to #8 in Figure 2A). These results indicate that the association of claudin with ephrin-B1 is required for its phosphorylation, but the binding region located in the ECD1 of claudin was insufficient to induce the phosphorylation of ephrin-B1. The phosphorylation of ephrin-B1 by claudin took place on tyrosine residues in its cytoplasmic region, because the phosphorylation was almost completely abolished when four tyrosine residues within the cytoplasmic domain of ephrin-B1 were mutated (ephrin-B1 4YF; Figure 4A). Two tyrosine residues located at the carboxyl-terminus of ephrin-B1 (Tyr 343, 344) were not the major target of claudin-induced phosphorylation, because the phosphorylation level of ephrin-B1 remained almost unchanged following the mutation of these two tyrosines (data not shown).

We next examined whether the claudin-induced phosphorylation of ephrin-B1 was caused by Src family kinases (SFK), known to be responsible for the tyrosine phosphorylation of

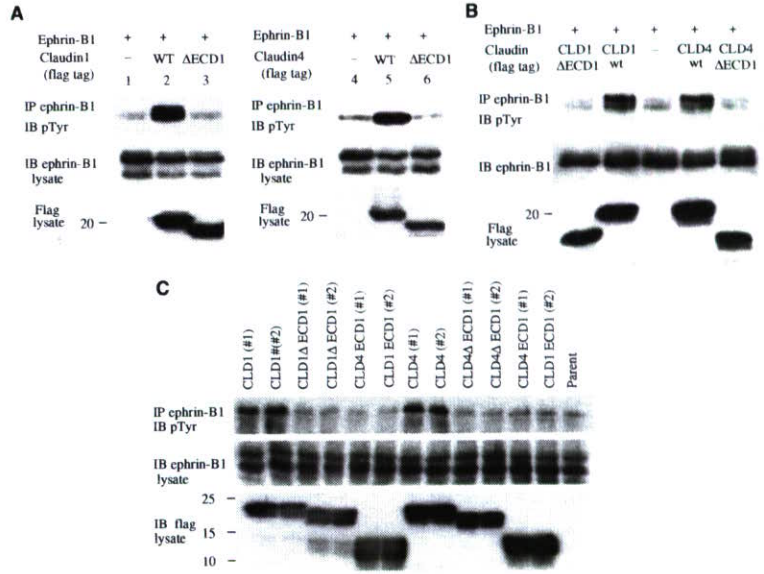

Figure 3 Ephrin-B1 is tyrosine phosphorylated by coexpression with claudins: (**A**) COS1 cells were transiently transfected with ephrin-B1 together with the wild type or mutant lacking the ΔECD1 of CLD1 (lanes 2, 3) or CLD4 (lanes 5, 6). Cell lysates were immunoprecipitated with anti-ephrin-B1 (goat) and subjected to IB with anti-phosphotyrosine (4G10). (**B**) HEK293 cells were transiently transfected with the plasmids as indicated. Cell lysates were subjected for the IP and IB as described in (A). (**C**) The cell lysates from either parent L cell, L cell lines stably expressing the wild type, ΔECD1 or the ECD1 of CLD1 or CLD4 were immunoprecipitated with anti-ephrin-B1 (goat) and subjected to IB with 4G10. Representative results of two independent clones (#1, 2) each are shown.

ephrin-B1 by the cognate Eph receptor stimulation. The treatment of the cells with 4-amino-5-(4-chlorophenyl)-7-(t-butyl)pyrazolo[3,4-d]pyrimidine (PP2), an inhibitor of the SFK, was seen to almost completely abolish the tyrosine phosphorylation of ephrin-B1 induced by the coexpression of CLD1 or CLD4 (Figure 4B). However, the control 4-amino-7-phenylpyrazol[3,4-d]pyrimidine (PP3) did not exhibit any effect on the tyrosine phosphorylation of ephrin-B1 in claudin-overexpressed cells (Figure 4B). Tyrosine phosphorylation of ephrin-B1 in stable lines of L CLD1 or L CLD4 was also inhibited by the treatment with PP2 (data not shown). These results suggest that ephrin-B1 is phosphorylated on tyrosine residues most probably via the activity of SFK following interaction with claudin. As interaction with EphB2 induces tyrosine phosphorylation of ephrin-B1, which in turn serves as the docking site for the Src homology 2 domain (SH2 domain) of Grb4 (Cowan and Henkemeyer, 2001), we examined whether claudin-induced phosphorylation of ephrin-B1 also induces association with Grb4. The GST fusion containing the SH2 domain of Grb4 was recruited to ephrin-B1 when ephrin-B1 was phosphorylated through coexpression with CLD1 or CLD4 (Supplementary data 2).

Phosphorylation of ephrin-B1 is significantly enhanced by cell–cell contact formation

The effect of cell–cell contacts on the phosphorylation of ephrin-B1 was then analyzed through the overlay coculture method using stable lines of L cells. L ephrin-B1 were overlaid on the parent cells or either CLD1- or CLD4-expressing cells, while, as a control, L ephrin-B1 cells were overlaid on the EphB2-expressing cells. Although ephrin-B1 was highly phosphorylated through the coculture with cells expressing EphB2, there was no significant phosphorylation of ephrin-B1 by the coculture with L CLD1 or L CLD4 (Supplementary data 3A). These results indicate that claudins do not stimulate the phosphorylation of ephrin-B1 through the mechanism of *trans*, intercellular association between the two proteins. On the other hand, ephrin-B1 was phosphorylated in L ephrin-B1 CLD1 when cocultured onto CLD1-expressing cells (Supplementary data 3B). Therefore, in response to the intercellular adhesion of claudins, ephrin-B1 may be phosphorylated through the interaction with adjacent claudins in the same cell membrane. We then tested the possibility of ephrin-B1 interacting with claudin *in cis* on the same cells. In L CLD4, ephrin-B1 associated with CLD4 even when they were plated as scattered single cells (Figure 5A, lane 4). The tyrosine phosphorylation of ephrin-B1 was seen to be greatly influenced by the cell density. Ephrin-B1 was highly phosphorylated when L CLD4 were plated at a high density, while it was reduced when the cells were plated as scattered single cells (Figure 5A, comparing lanes 4 and 6). On the other hand, the phosphorylation level of ephrin-B1 in the parent L cells was low and apparently unchanged by the cell density (Figure 5A, bottom, right). In order to examine the

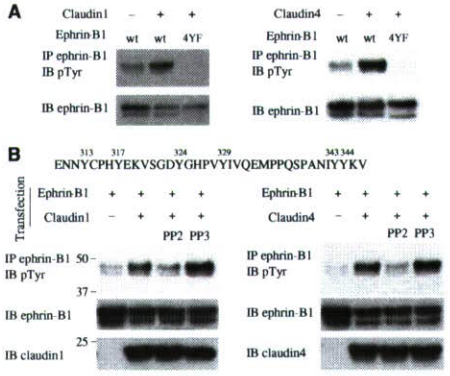

Figure 4 PP2 inhibits the phosphorylation of ephrin-B1 induced by claudins. (**A**) COS1 cells were transfected with the indicated plasmids. In (**B**), transfected cells were treated with PP2 or PP3 as described in Materials and methods. Ephrin-B1 was immunoprecipitated from individual cell lysate, and subjected to IB with 4G10. The amino-acid sequence of the carboxyl-tail of human ephrin-B1 is shown at the bottom of (A). The cell lysates were immunoblotted with anti-ephrin-B1 (goat) or anti-claudin antibodies to detect the expression level (bottom).

effect of the claudin–claudin *trans* adhesion accompanied by the cellular contact on the phosphorylation of ephrin-B1, the phosphorylation level of ephrin-B1 was evaluated during the dynamic change of the intercellular adhesion. When cell–cell interaction was completely disrupted by the depletion of calcium in the medium, the tyrosine phosphorylation of ephrin-B1 was also abolished (Figure 5B). Similar results were obtained in L CLD1 (data not shown). On the other hand, the cell dissociation did not modify the phosphorylation level of ephrin-B1 in the parent L cells (Figure 5B, bottom). In order to exclude the possibility that intracellular concentration of calcium may also have been decreased by the cell incubation with ethylene glycol bis (β-aminoethyl ether) *N,N,N′,N′*-tetraacetic acid (EGTA) and have affected the phosphorylation of ephrin-B1, we performed a control experiment where cells were treated with nifedipine, a blocker of the calcium channel. The decrease in the level of intracellular calcium caused by nifedipine did not affect the status of the association of ephrin-B1 with claudin, nor the phosphorylation of ephrin-B1 (data not shown). Therefore, these results suggest that the phosphorylation of ephrin-B1 through the interaction of claudin was significantly induced by cell–cell contact.

The previous conclusion was further supported by the examination of the intracellular localization of tyrosine-

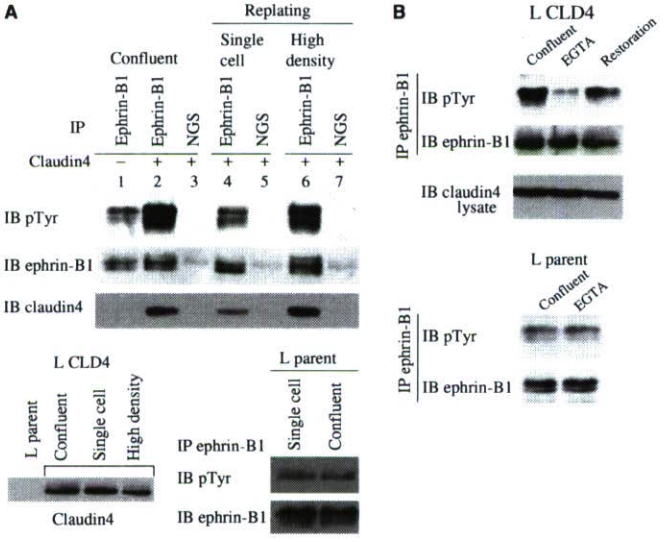

Figure 5 The phosphorylation of ephrin-B1 correlates with the cell–cell interactions. (**A**) Parent L cells (lane 1) or L cells stably expressing CLD4 (L CLD4, lanes 2–7), which were indicated as CLD4 (–) or (+) above the lanes, were grown until confluent. The cells were detached by EGTA, and replated on new dishes either at a low density as scattered single cells or at a high density. Cells were lysed for IP with anti-ephrin-B1 or NGS) which were then subject to IB with 4G10 (pTyr). The membrane was re-hybridized with anti-ephrin-B1 (goat) or anti-CLD4 antibody. The expression of CLD4 in each cell lysate was confirmed by IB (bottom, left). Bottom, right: The tyrosine phosphorylation of ephrin-B1 in parent L cells was examined when the cells were plated as single cells or at a high cell density. (**B**) L CLD4 (top) or parent L cells (bottom) were grown until confluent. The cells were incubated in $HBSS^{-}$ containing 2 mM EGTA until the majority of the cell–cell contacts were lost, but not detached from the substrate. After washing, monolayers were incubated in the cell culture medium for 4 h. The cells were lysed before (confluent) and after calcium depletion (EGTA), and after changing to the normal cell culture medium for 4 h (restoration) to analyze the phosphorylation of ephrin-B1 as described in (A).

phosphorylated ephrin-B1, with the phospho-specific antibody generated against Tyr317 of ephrin-B1. Tyr317 of ephrin-B1 (corresponding to Tyr305 of mouse ephrin-B1) is phosphorylated when stimulated with EphB2, and is a critical requirement for interaction with Grb4 (Bong *et al*, 2004). In the L ephrin-B1, tyrosine phosphorylation of ephrin-B1 was not observed, regardless of the cell density involved (Figure 6, columns A and C). On the other hand, the L ephrin-B1 CLD1 showed the tyrosine phosphorylation of ephrin-B1 clearly at the cell–cell contact sites, although it was not detected in single isolated cells (Figure 6, columns B and D). The same results were obtained when L CLD4 were used (data not shown), while these observations were further supported by the same analysis using MDCK ephrin-B1 Tet-ON cells, where CLD1 and CLD4 were endogenously expressed (Supplementary data 4).

In the L and MDCK cell lines used in this study, there was no detectable expression of EphB2 exposed through immunoblot analysis (data not shown). The enhancement of the tyrosine phosphorylation of EphB2 was not detected after these cells were treated with ephrin-B1–Fc (Supplementary data 5A). Moreover, when L or MDCK cells were incubated with ephrin-B1–Fc, the membrane-bound ephrin-B1–Fc was not detected following staining with anti-Fc antibody (Supplementary data 5B). The treatment of the cells with an excess volume of soluble ephrin-B1 blocks receptors to interact with membrane-bound ephrin-B1 *in trans*, thereby shutting off the reverse signaling. On the other hand, the ephrin-B1 phosphorylation level was not attenuated in the L and MDCK cell lines through the addition of ephrin-B1–Fc (Supplementary data 5C), indicating that receptors stimulating ephrin-B1 are not detected in these cells.

Phosphorylation of ephrin-B1 is enhanced by ECD of CLD1

In order to evaluate the possibility that claudin–claudin *trans* interaction enhances the tyrosine phosphorylation of ephrin-B1, CLD1–Fc fusion protein was prepared. For mimicking the *trans* interaction between claudins mediated by the intercell contacts, the first and the second ECDs of CLD1, which were linked by flag-epitope tag, were fused to the Fc region of immunoglobulin. Preclustered CLD1–Fc attached to HT29 cell membrane, and at least a part of CLD1 in the cell membrane was colocalized with the CLD1–Fc (Figure 7A). Moreover, the endogenous CLD1 protein was co-precipitated with CLD1–Fc (Figure 7B, top). These results indicate that the CLD1–Fc fusion protein effectively binds to the cellular CLD1 at the cell surface. The induction of ephrin-B1 phosphorylation was not evident by adding the preclustered soluble CLD1–Fc in the culture medium of L ephrin-B1 CLD1 (data not shown). On the other hand, when the cells were plated on preclustered CLD1–Fc-coated plates, ephrin-B1 was phosphorylated on tyrosine residues (Figure 7B, bottom). Although the enhanced phosphorylation of ephrin-B1 was detected within 30 min after the cells were attached on the CLD1–Fc precoated plates (data not shown), we noticed faster attachment of CLD1-expressing L cells on CLD1–Fc-coated plate compared to that on albumin-coated plate. On the other hand, no significant difference was observed in cell attachment and spreading between these two plates at 3 h after plating, when our biochemical analyses were performed. To further confirm this result, we examined the induction of ephrin-B1 phosphorylation using CLD1–Fc-coated microbeads. When clustered CLD1–Fc beads were added on L ephrin-B1 CLD1, phosphorylation of ephrin-B1

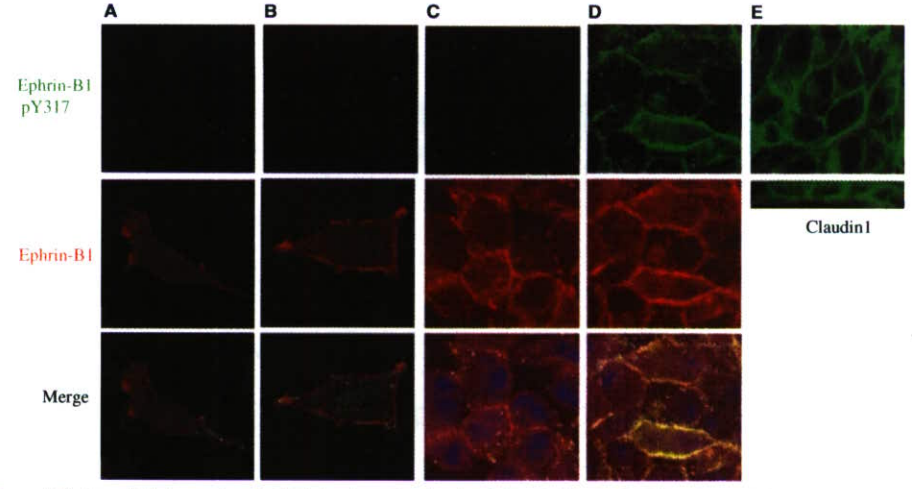

Figure 6 The intercellular interaction of L CLD induced tyrosine phosphorylation of ephrin-B1. (**A–D**) L ephrin-B1 (columns A, C) or L ephrin-B1 CLD1 (columns B, D) were plated either at a low (columns A, B) or high (columns C, D) cell density. The cells were immunostained with anti-ephrin-B1 (red) and anti-pTyr ephrin-B1 (green) antibodies while the nucleus was stained with TOTO-3 iodide. (**E**) The expression of cludin1 in L ephrin-B1 CLD1 cells is shown.